Quantum Reactive Scattering Dynamics of D + H_2 reaction: From Ultracold to Thermal Regime

THESIS

Submitted in partial fulfilment
Of the requirements for the degree of
DOCTOR OF PHILOSOPHY

By

Ranga Santosh
ID. No. 2012PHXF0528H

Under the Supervision of
Dr. Subhas Ghosal

BIRLA INSTITUTE OF TECHNOLOGY AND SCIENCE, PILANI
2018

BIRLA INSTITUTE OF TECHNOLOGY AND SCIENCE, PILANI

CERTIFICATE

This is to certify that the thesis entitled **"Quantum Reactive Scattering Dynamics of D + H_2 reaction: From Ultracold to Thermal Regime"** submitted by Ranga Santosh, ID No 2012PHXF0528H for the award of Ph. D of the institute embodies original work done by him under my supervision.

Signature of the Supervisor:

Name: Dr. Subhas Ghosal

Designation: Assistant Professor
Department of Chemistry
BITS-Pilani Hyderabad Campus.

Date:

Acknowledgements

It is a pride moment to show the gratification with a sense of contentment at the long travelled Journey, to be able to recapture some of the fine moments and to be able to thank some of whom were with me from the beginning, some who joined me at some stage during the journey, whose rally round kindness, love, and blessings have brought me to this day. I wish to thank each and every one of them with all my heart.

Foremost, I owe thanks to a very special person, my supervisor, ***Dr. Subhas Ghosal*** *for his continuous friendly support of my Ph.D. study and research, for his enormous patience, motivation, enthusiasm, and immense knowledge. His valuable guidance helped me in all the time of my research and writing of this thesis.*

I would like to thank many people who helped me in this entire tenure of my Ph.D. with their valuable time, suggestions and encouragement. I will start with my doctoral advisory committee (DAC) members, I am thankful to acknowledge ***Prof. Sumithra*** *and* ***Dr. AmitNag*** *for their support and encouragement during this period. I thank DRC convener* ***Prof. J.Subbalakshmi*** *for her importamt suggestions and encouragement.*

I am thankful to Head of the Department (HOD), ***Prof. Manab Chakravarty****, entire Chemistry department faculty members specially* ***Prof. N Rajesh****, for his valuable interaction and discussions throughout the journey.*

I am grateful to former vice-chancellor ***Prof. Bijendra Nath Jain****, vice-chancellor* ***Prof. Souvik Bhattacharyya*** *of BITS Pilani, former director* ***Prof. V. S. Rao*** *and* ***Prof. G Sundar****, present director of BITS Pilani Hyderabad Campus for giving me an opportunity to pursue and to carry out my Doctoral research work.*

I would like to express my sincere thanks to ***Prof. Vidya Rajesh****, Dean, Academic Research Division (Ph.D. Programme), for their continuous support and encouragement during my research work. And I extend my thanks to Mr. Praveen, ARD for his help and information to complete the course formalities in time.*

It's my great pleasure to thank ***Prof. D.A.Padmavathi****, University College of Science (Chemistry), Osmania University for her inspiring words and valuable suggestions.*

*My Sincere Thanks to Department of Science and technology (****DST****) and Council of Scientific & Industrial Research (****CSIR****), for their financial support without which it would have been very difficult to carry out my research work.*

I would like to thank my friends, Dr. Gangaram, Ravikiran, Saisudhakar Mukka, Nagendraprasad (DNP), Krishna, Dr.Sathish Mukka, Swaraj Pal, Srinivasrao and Swapna for their encouragement and support.

I thank my department non-teaching staff (Mr. Ashok, Mr.Sudhir & Mrs. Shanthakumari) for their support and encouragement throughout my Ph.D. journey.

*My heart felt regards goes to my parents (**Surender** & **Bharathi**) and grandparents (Sankaraiah & late Kalavathi) for their love and moral support. Special thanks to my brother **Mr.Manoj** and cute sister **Mrs.RadhikaHanish** who standing beside me with their love and unconditional support. I really consider myself the luckiest in the world to have such a lovely and caring family.*

*I thank the Almighty, **The Lord Krishna** for giving me the strength and patience to work through all these years.*

(Santosh Ranga)

Abstract

The early age of universe was dominated by high energy radiations and subatomic particles. Due to very high temperature in the surroundings, interaction between radiation and the subatomic particles were instantaneous and led to the formation of atoms, molecules and respective ions. This process is commonly known as nucleosynthesis. Due to inelastic collisions between the high energy atoms/ions with molecules, the internal energy of the system got converted into radiation which is dissipated in the background medium in random direction (interstellar cooling). The overall energy of the system is reduced through many cycles of excitation de-excitation of the molecular rovibrational levels. In order to understand the process of interstellar cooling, one needs the rate coefficients for the collision processes between the species of more abundant in the early universe. It has been found that the H_2 molecule and its isotopic variants such as HD, D_2 *etc* were the most abundant in the early universe.

Thus, it is important to know the accurate rate coefficients for the reactions involving all these species for wide range of temperatures. In this thesis, we have studied the chemical reaction dynamics of the D + H_2 reaction (and its isotopic substituted reactions) from very low to high temperature limit where the atoms and molecules can be treated classically. In the ultralow temperatures (~ 10^{-6} K), due to the quantum behavior of atoms and molecules, general Arrhenius type temperature dependence of the rate coefficient is not obeyed, instead the Wigner's threshold laws can be applied to various dynamical observables.

In the first chapter, we have discussed in brief introduction about the cold and ultracold atoms and molecules. A review on classical theories of the atomic collisions such as transition state theory, collision theory, Arrhenius theory for the temperature dependence of the rate coefficients *etc*. have been presented. Classical collision theories consider all atoms and molecules as hard spheres to estimate the rate coefficients, but the effect of initial rovibrational quantum states on the dynamical outcomes and the effect of short lived resonances could not be properly explained. Therefore, the quantum mechanical approach of the collision dynamics considering the atoms and molecules as waves is more appropriate.

Reactive scattering dynamics of atom-molecule collisions in the ultracold regime has been investigated using time-independent quantum close coupling approach. We have started with the quantum mechanical description for collisions between two atoms and extended it to the atom-diatom collisions using Delves hyperspherical coordinates. The derivation of scattering matrix (*S-matrix*) from which we can calculate the dynamical observables such as reaction probability, cross-sections and rate coefficients has been described in detail in the chapter 2.

In order to perform the numerical calculations, we have modified the *ABC* reactive scattering code originally developed by Skouteris *et al* for atom-diatom collisions at high temperatures. To perform scattering calculations in the ultracold temperature limit, three main parameters should be optimized for numerical convergence: (i) if the diatomic basis large enough? (ii) the numerical integration step ($\Delta\rho$) is small enough? and (iii) if the asymptotic behavior of the potential is large enough?. In order to this, we have introduced new modules in the *ABC* reactive scattering code. This numerical convergence issues has been addressed in details for the D + H_2 reaction with respect to the size of the basis functions, extent of radial propagation and integration step *etc* in chapter 3.

Molecular hydrogen and its isotope HD acted as one of the most important interstellar coolants in the primordial gas medium, but the formation & destruction of these molecules are not well studied quantum mechanically for a wide range of temperatures. We present accurate time-independent quantum mechanical (TIQM) rate coefficients of formation of ultracold HD molecules by D + H_2 (v, j) $\rightarrow$ HD (v', j') +H reaction in the ultralow temperature regime in chapter 4. Different potential energy surfaces *e.g*. DMBE, LSTH, BKMP, BKMP2, Wu *et al* and Mielke *et al* are available in literature for this reaction. But the only PESdeveloped by Mielke *et al* includes the long range van der Waals interactions. Since the long range interactions very sensitive to the potential, in the ultracold temperature region, the BKMP2 and Mielke *et al* potential has been used to study this reaction.

The dynamical observables such as the state resolved integral cross sections between rotational (j) and vibrational (v) levels and corresponding rate coefficients are first computed for temperature T = 10^{-8} K – 10 K. We found that the exponential decrease of the rate coefficients with reducing temperature following Arrhenius empirical equation is not obeyed at ultracold temperature limit. At lower temperatures, the rate coefficients become

independent of temperature (constant) which is the consequence of enhanced quantum mechanical tunneling. Finally, we have calculated the rate coefficients of both inelastic and reactive processes using the calculated cross sections.

As temperature increases, the contribution from higher partial waves ($\ell > 0$) should be included. Generally, the *p-wave ($\ell = 1$)* would start contributing from 10^{-2} K and at T~150 K, we may need to consider up to $\ell = 35$ partial waves. Above T > 170 K, we have compared the calculated rate coefficients with available experimental data. We have observed that the reaction cross sections and rate coefficients are close to the experimental values and obey Arrhenius behavior at higher temperatures. While comparing the results using two different potential energy surfaces (BKMP2 and Mielke *et al*), there are significant difference in the ultracold temperature region (because of difference in the long range interactions in the potential), but high temperature rate coefficients converge for both the potentials.

Unlike H_2, HD molecule has permanent dipole moment and because of closely spaced rovibrational levels, HD molecule can act as more effective coolant in the interstellar medium. For this reason we have studied the H + HD reaction for all possible collisional outcomes: elastic, quenching, H exchange and formation of H_2 processes. All these processes have been treated separately in the scattering calculations and reported for a wide range of temperatures. We have also analyzed the effect of excited rovibrational initial states and found that the quenching processes dominate over the H exchange and the formation of H_2 processes.

We have found sharp resonance peaks near ~120K for all the vibrational states (v) for the H + HD (v, j) reaction. The energy gap between $j = 0$ and $j = 1$ for a particular vibrational state is found to be in the same order which might be the origin of these resonances. Previously, similar kind of resonances have been found for Cl + H_2 reaction by Balakrishnan *et al*. Since it is not due to the presence of any bound state, the signature of this resonance were not observed in the final rate coefficients. These findings have been presented in the chapter 5.

List of Symbols

Physical Constants

h	Plank Constant
c	Speed of light
k_B	Boltzmann Constant
$\hbar$	Plank Constant divided by 2π

Special Symbols

i	The imaginary quantity
J	Total angular momentum quantum number
j	A rotational quantum number of a diatomic molecule
$j_\ell(kr)$	A Spherical Bessel function
$\widehat{j_\ell}(kr)$	A Riccati-Bessel function
k	Wave vector of a particle
$k(T)$	Rate constant or Rate Coefficient
$K(T)$	Equilibrium constant
ℓ	An Orbital angular momentum quantum number
M	Mass of the system
m	Mass of an atom
$\eta_\ell(kr)$	A Spherical Bessel function of the second kind (Neumann)
$\widehat{\eta_\ell}(kr)$	A Riccati-Bessel function of the second kind
$P_\ell(cos\theta)$	The $\ell - th$ Legendre Polynomials
$\widehat{R}$	Unit vector in the direction of the interparticle separation
$\tilde{R}_\alpha$	A mass-scaled Jacobi coordinate for arrangement α
r	Distance between two atoms of a diatomic
$\tilde{r}_\alpha$	Mass-scaled Jacobi diatomic coordinate for arrangement α
S	A Scattering matrix
T	The transformation matrix
V	Potential energy of a system
v	A vibrational quantum number
$Y_{lm}(\theta, \phi)$	The $l, m - th$ spherical harmonics

$\mathcal{Y}_{j\ell}^{JM}(\hat{R},\hat{r})$	Angular function which is an Eigen function of the total angular momentum and its space fixed Z – component
Z	Z-coordinate of a center of mass, also a direction in a cartesian coordinate system.

List of Figures

Table of Contents

Chapter 1

An Introduction to the cold, ultracold atoms and molecules

1.1 Nucleosynthesis: Big Bang theory

The Big Bang theory is a widely accepted cosmological model which offers a comprehensive explanation to the evolution process of the early universe [1]. According to Big Bang theory, the universe was created with an instantaneous explosion and then started expanding from infinite density of matter at very high temperature [2, 3]. The radiations resulted from the big bang contained mainly high energy photons and only infinitesimal amount of matter (electron, positron) were present [4, 5]. Those high energy photons were soon converted to matter (atoms or ions) through the process commonly known as nucleosynthesis [6].

General theory of relativity by Einstein ($E = \Delta mc^2$) is one of the most important scientific observations of the last century. It predicts that, under proper conditions energy can be converted to matter, or *vice versa*. This mass-energy conversion was a common phenomenon in the universe with its high temperature and density in the early stage. Photons were converted to electrons and positrons and subsequently the formation of the protons and neutrons took place. The protons and neutrons are made up of subatomic particles of varying mass and charge (Hardons, Leptons, meson, quarks *etc*). For example, a proton has two up quarks whose charge is +2/3 and one down quark with its charge of -1/3. A neutron has zero charge as it has one up and two down quarks, respectively [7].

Because of the high energy density, initially the number of protons and neutrons were same due to high temperatures. But, as the universe expanded with time and the overall temperature decreased, the proton forming reactions were favored. According to the predictions made by several astrophysical observations, by 13.82 seconds of the Big Bang the temperature had dropped to 3×10^9 K [2, 4]. It has been observed that the simple atomic nuclei formed within first three minutes and more than thousand have been passed for the formation of the first electrically neutral atoms. The major elements/atoms produced from the Big Bang were hydrogen, helium and a little amount of lithium. The Giant clouds of these primordial gases later merge through gravity in order to form interstellar medium such as Stars and Galaxies *etc*.

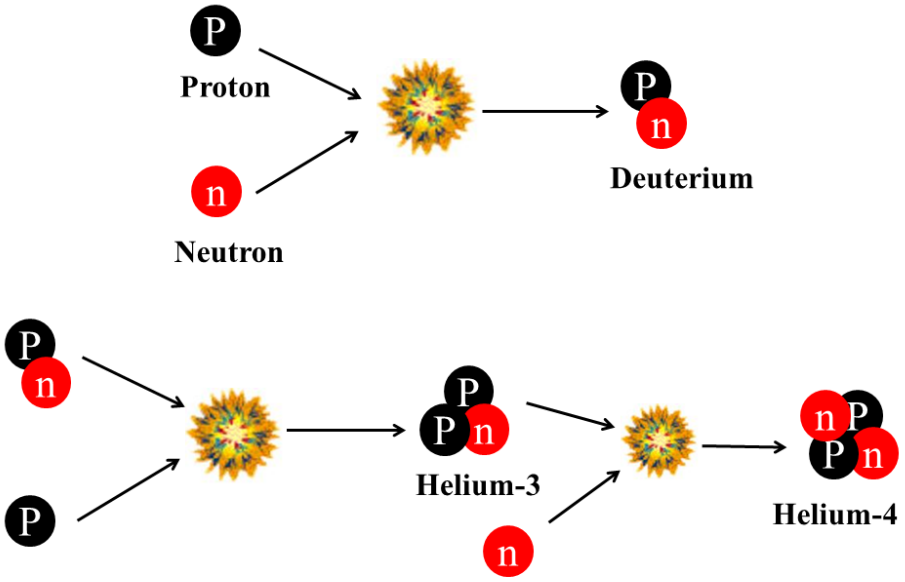

Figure 1: Schematic representation of the formation of lighter elements such as Deuterium (D), Helium (He) through Nucleosynthesis.

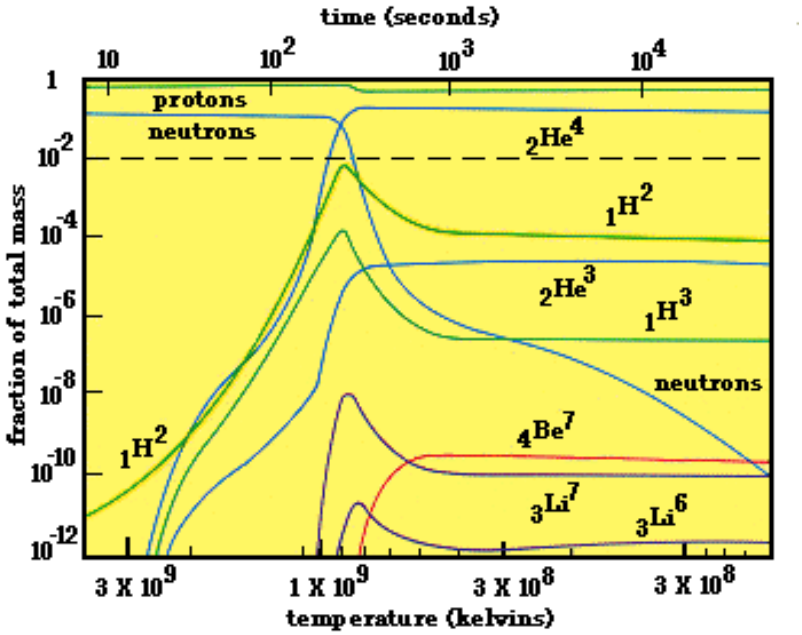

Figure 2: Density of matter with time at different temperatures reproduced from the Refs [8, 9].

In the early universe, the ions or atoms thus produced from nucleosynthesis started colliding themselves with very high collision energies resulting the formation of new atoms and molecules or molecular ions those species. Formation of Deuterium (a heavier isotope of hydrogen) through the collision between a proton and a neutron. According to George F. Smoot, as shown in Figure 2, depicts how the density of different atoms and their isotopes changed as functions of time and temperature [8, 9]. Initially, there were only protons, neutrons and as time progressed, hydrogen, deuterium, tritium, helium *etc*. have been formed. For Helium (He) atom, the numbers of protons are equal to number neutrons therefore it is more stable compared to the other nuclei. It can be noted from Figure 2 that the neutrons and protons were produced at higher temperatures, the synthesis of other atoms like Deuterium (D), Helium (He), Beryllium (Be) *etc* have been started as the temperature slightly reduced.

1.2 Interstellar Cooling

After the formation of lighter elements, small molecules and the molecular ions such as H_2, H_2^+, Li_2, Li_2^+, CO, OH, H_2O *etc* were started forming from the atomic species [10-13]. When fast moving atoms or ions collided with the molecules most of the kinetic energy of the atoms was absorbed by the molecules leading to either formation of a new species or excitation of the molecules to high energy quantum states. The excited species generally have shorter lifetimes. As they spontaneously relax to the ground state, excitation energy is generally released in the form of electromagnetic radiation. Most of the energy released from the excited molecules are emitted in random directions which gets dissipated in the surroundings. This absorption of collision energy and emission in the form of electromagnetic radiation happened in a cyclic manner in the early universe and significant amount of energy has been converted into background radiation leading to slowing down of the atoms and molecules of the system. This resulted in an overall slowing down of the colliding species and temperature of the interstellar medium gradually decreased [14, 15]. Atoms have only few quantum states where the electrons can be excited/de-excited through absorption/emission of radiation, on the other hand, molecules having additional vibrational and rotational degrees of freedom can have plenty of ro-vibrational levels where electronic transition can take place. For this reason, interstellar cooling process only initiated after the formation of molecules in the interstellar medium [16-18].

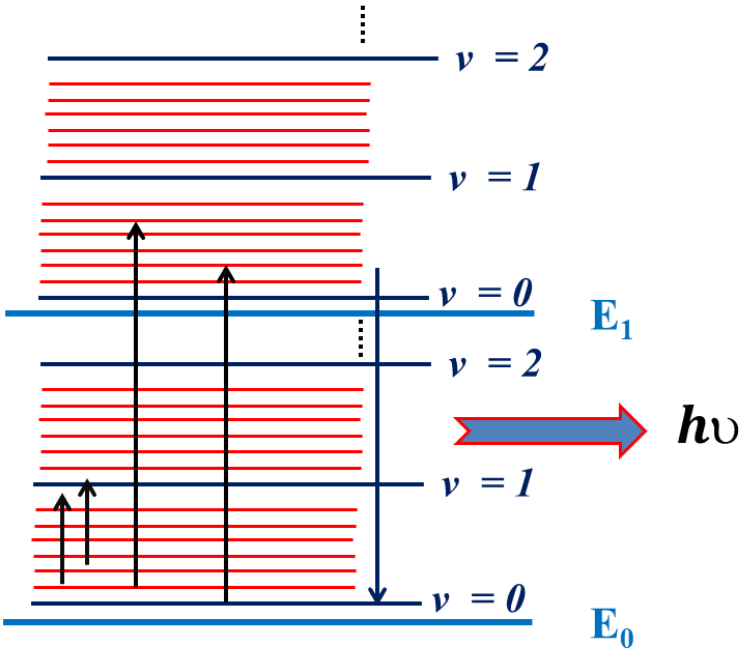

Figure 3: Mechanism of interstellar cooling: Excitation and de-excitation of molecules resulted in reducing their overall energy which dissipated in the background of the interstellar medium.

Over many billion years, due to interstellar cooling through inelastic collisions, some parts of the interstellar medium became very cold. But, owing to low density of elements, the overall interstellar space remained highly inhomogeneous in temperature due to lack of thermal equilibrium. In other words, although some part of the universe remained very hot, parts of it became very cold. It has been found that the average temperature of the universe is ~3 K [19, 20].

Molecular hydrogen (H_2) is the most abundant species (~ 75% by mass) in the interstellar medium [21]. Thus H_2 and its isotopic variant HD have served as the most important coolant molecules for the reduction of interstellar temperature.

Few important reactions of astrophysical interest involving atomic hydrogen are:

$$H + e^- \rightarrow H^- + h\nu$$

$$H^- + H \rightarrow H_2 + e^-$$

$$H + H^+ \rightarrow H_2^+ + h\nu$$

$$H + e^- \rightarrow H^- + h\nu$$

$$H^- + H \rightarrow H_2 + e^-$$

$$H + H^+ \rightarrow H_2^+ + h\nu$$

and few important reactions involving molecular hydrogen and its isotopes which contributed to the interstellar cooling are:

$$H + H_2 \rightarrow H_2 + H$$

$$H + H_2^+ \rightarrow H_2 + H^+$$

$$H + D_2 \rightarrow HD + H$$

$$D + H_2 \rightarrow HD + H$$

$$H + HD^+ \rightarrow HD + H^+$$

$$D^+ + H_2 \rightarrow HD + H^+$$

$$H_2^+ + D^- \rightarrow H_2 + D \text{ } etc.$$

In order to understand the evolution process, we need to study all these reactions (and many more) for wide range of temperatures. Thus information of the accurate rate coefficients from very low temperature (μ K or m K range) to thousands of Kelvin is required for modeling the evolution process.

The efficiency of cooling, *i.e*. how much energy is lost per second at a particular temperature, is defined as cooling functions for a particular species [22]. To calculate the cooling functions, the knowledge of state-to-state rate coefficients is required from very high to very low temperatures for several chemical reactions leading to formation and destruction of that species. The radiative cooling functions are later coupled with the fractional abundance of that particular species to obtain the overall evolution of the interstellar medium.

1.3 Quantum scattering of ultracold collisions

Classically, light or electromagnetic radiation is believed to be waves and atoms, molecules, sub-atomic species are described as particles. But, it was realized in the beginning of the twentieth century that both mater and electromagnetic waves can interchange their properties and wave-particle duality is expected to be significant for sub-atomic particles. This was first demonstrated theoretically by de Broglie and later verified experimentally through electron diffraction experiments [23, 24]. The properties of matter waves can be determined from its de Broglie wavelength as $\lambda = h/mv$, where m is the mass, v is the velocity of the particle, rand h is the Planck's constant. In extremely low temperature conditions, the average kinetic energy of the colliding pairs is very small and the wave behavior of the particles are manifested so much that the quantum mechanical wave behavior cannot be neglected [25].

For example, the de Broglie wavelength of H_2 molecule is 0.7123 Å at room temperature, whereas at 25 μK, it is 22500 Å, which is much larger than the molecular dimension and thus needs to be represented accurately. Since the de Broglie wavelength is much larger, the particles can interact from very far internuclear separations [26]. Thereby, to study atomic/molecular collisions at ultralow temperatures accurate description of the long range interaction potential is very important. Inclusion of the long range interaction potentials change the conventional dynamical outcome of the colliding pairs as it is majorly governed by quantum mechanical tunneling [27].

At very low collision energies, the centrifugal potential creates an impenetrable barrier for quantum states with orbital angular momentum quantum numbers $\ell > 0$. Because of this, in the limit of ultracold temperatures, collisions are dominated only by the ground rotational *i.e.* $\ell = 0$ $(s-wave)$ state of the molecule and reactions mostly happen through quantum mechanical tunneling. In 1948, Wigner reviewed general theory of quantum collisions and derived the expression for the energy dependence of the cross sections for elastic and inelastic collisions at the zero collision energy limit [28]. These expressions are referred to as Wigner's threshold laws. These laws apply to collisions starting from a state (*n*) with a given orbital angular momentum ℓ, three processes can be distinguished.

- Elastic collision $n\ell \rightarrow n\ell$ where the angular momentum ℓ and the internal energy has been conserved. *n* denotes the quantum numbers describing the rovibrational energy state.
- Elastic collision $n\ell \rightarrow n\ell'$ that means the internal energy is converged but not the angular momentum.
- Inelastic collisions or chemical reactions $n\ell \rightarrow n'\ell'$, in which the internal energy of the reacting particles and their angular momentum were changed.

According to Wigner's threshold law, the relationship between the collision velocity and the cross section for different processes as the following [28, 29],

$$\sigma_{n\ell \rightarrow n\ell} \sim v_n^{4\ell}$$

$$\sigma_{n\ell \rightarrow n\ell'} \sim v_n^{2\ell+2\ell'}$$

$$\sigma_{n\ell \rightarrow n'\ell'} \sim v_n^{2\ell-1}$$

Where, υ is the collision velocity, σ is the cross section, ℓ and ℓ' are the respective angular momentums. For bimolecular reactions, if we write these equations in terms of the collision energy, this relationship would behave as [30].

$$\sigma(E) \propto (E - \epsilon)^{p/2};\ p = 0, \pm 1/2$$

Where $\sigma(E)$ is the collision energy dependent reaction cross section, E is the collision energy, ϵ is the threshold energy of state *n*. p is a number which is determined according to the nature of the reaction: p = 1 for endothermic and -1 for exothermic reaction. It is clear that the inelastic cross sections are inversely proportional to the collision energy. Similarly in the ultralow collision energy limit, elastic cross section will be constant in the ultracold regime.

Collisions between atoms and molecules are highly dependent on the relative velocity of colliding pairs. Especially with low relative velocities, the formation of long-lived collision complexes (van der Waal's complex) is possible. As the collision energy of the colliding particles match with that of the van der Waal's complexes, they form resonances. It is evident from previous theoretical and experimental studies that these resonances can change the dynamics of chemical reactions drastically at low temperature limit [31-33]. Because of the sudden phase change of the corresponding wave function, the collision cross sections undergo large changes in its amplitude which leads to huge increase in the rate coefficients for certain situations [34-36]. Most of these resonances at ultralow collision energies are experimentally realized for ultracold atomic systems (Rb_2, RbCs, LiRb *etc*) under the influence of external magnetic and electric fields [37]. However, for atom-molecule ultracold collisions, the study of resonances is still challenging because of experimental limitations.

As it has been observed the long-range part of the potential energy surfaces (PESs) plays an important role in reaction dynamics at the ultracold temperature limit. Any quasi-bound states in the van der Waals region of the potential energy surface may undergo pre-reaction. These regions of the PES which are not in the vicinity of the transition state may influence the outcome of the overall reaction. There are different kinds of scattering resonances [36] that can influence the rate coefficients at ultracold temperature limit (*e.g.* threshold resonances [35, 38], shape resonances[34] and Feshbach resonances [39, 40] *etc*).

1.4 Recent advances of the ultracold atoms, molecules and their applications

In recent years, the availability of different cooling and trapping techniques for atoms and molecules allow the investigation of cold and ultracold collisions of a wide variety of systems. Apart from astrophysical interest, ultracold atoms and molecules have general importance in various applications like atomic clocks [41], quantum information sciences, precision measurement [37-41] and high resolution spectroscopy [42, 43] *etc*. The ability to cool, trap and manipulate the cold and ultracold atoms and molecules is challenging but has lot of promising applications in both fundamental science and technology.

The properties of the ultracold bosonic and fermionic species had been predicted in the beginning of the ninth century [44] , but it was realized experimentally only recently after the development of laser cooling techniques [33]. In Figure 4 we have depicted a general scheme of laser cooling technique that can be used to attend very low temperature ($T \sim 10^{-3}$ K) using multiple coherent laser beams. An atom initially in its ground state is allowed to move against the laser light. The frequency of the laser light is slightly red-detuned (the energy of laser beam is lower than the transition energy) so that only when the atoms are moving directly opposite towards the laser beam, due to Doppler effect the atom would be able to absorb the energy of the laser beam and promoted to the excited state. The excited atoms will spontaneously emit the absorbed energy as electromagnetic radiation in order to return to their ground state and thereby slow down the atoms before getting ready to start this cycle again. Thus, through this cyclic absorption and emission process in random direction, the energy of the system is dissipated in the background and eventually the overall system cools down [45].

When atomic gases are confined at sufficiently high density, the cold atoms tend to establish a thermodynamic equilibrium. The energy distributions of these atoms are usually given by Boltzmann distribution. The cold atoms thus prepared through laser cooling are confined under the influence of optical and magnetic field in magneto-optical traps (MOT) [46-48] . When the potential of the MOT is reduced gradually, certain atoms with larger collision energies escape from the trap. At this stage a new equilibrium is established and the overall temperature of the ensemble is further decreased. This technique is known as evaporate cooling [49-51]. Using evaporative cooling the atoms can be cooled down to ultracold (10^{-6} K) temperature limit.

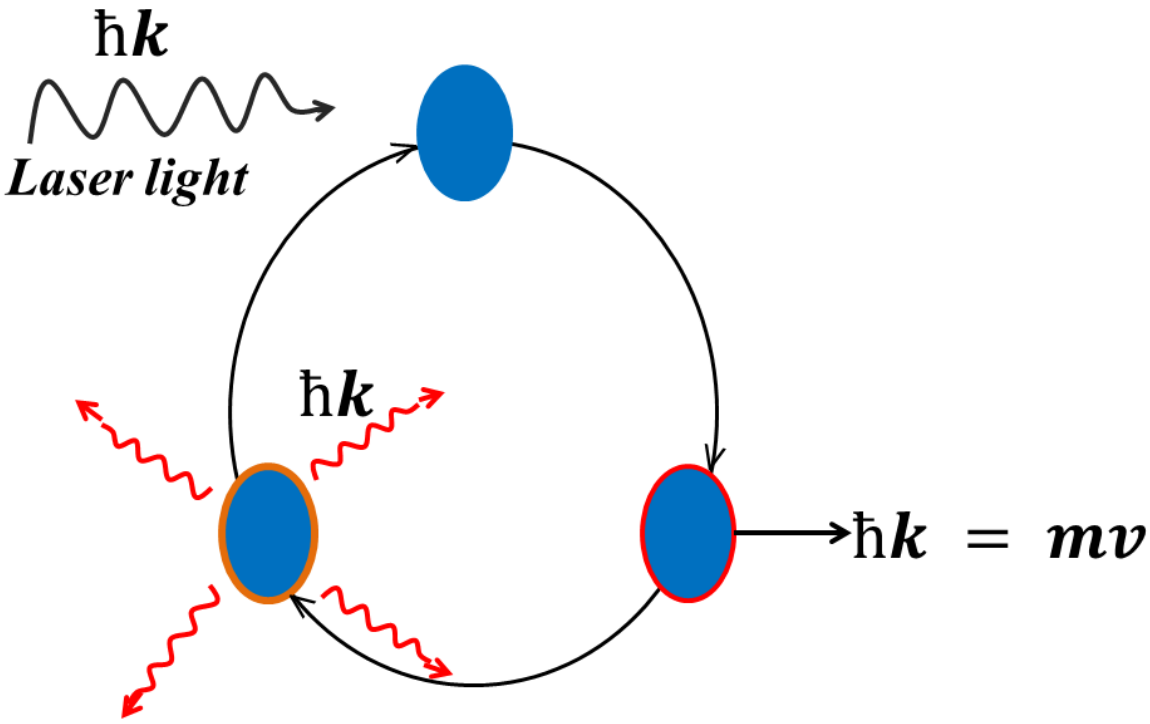

Figure 4: An atom absorbing a photon with momentum ***ħk***. The atom is now in the excited state and has increased its velocity by ***ħk/m*** in the direction of laser beam. The internal atomic energy is released by spontaneous emission which leads to the overall reduction in the kinetic energy of the system.

Evaporative cooling technique relies on removing the particles with higher kinetic energies and redistributing the residual energy among the remaining particles by elastic collisions so that temperature falls. Both elastic and inelastic (reactive) collision rates can be tuned by controlling the strength of the applied external fields and the trap depth. In this scenario, the ratio (branching ratios) of elastic and inelastic collisions play an important role to attain cold atoms/molecules remain inside the trap (MOT).

After the first realization of ultracold Rb atoms using laser cooling techniques [52-55], many other direct cooling techniques such as Stark decelaration [56, 57], Buffergas cooling [58], Sympathetic cooling [59] and Photoassociation [60-62], Magnetoassociation [63-65], Simulated Raman Adiabatic Passage (STIRAP) [66] have been used to attend very cold to ultralow temperature limit for a large number of atomic and molecular species. Main aim of cooling and trapping the atoms/molecules to ultracold temperatures was to realize quantum degeneracy, a new state of matter known as Bose-Einstein condensation [67]. Apart from

studying the exotic form of matter in the Bose-Einstein condensates, there are several other research areas that had emerged from the ultracold atoms. For example, high resolution spectroscopy under Doppler free conditions, time dependence of fundamental constants (the ratio of proton mass to that of the electron in the cosmological models), lifetime measurements up to micro-nano second range etc. Apart from these, ultracold atoms/molecules are used to build new atomic clocks, a system for quantum information processing and storage.

1.5 Gap in Existing research

Why are collisions so important in the mK (cold) and μK (ultracold) regime?

While initial studies on cold and ultracold atoms/molecules were focused on the creation of dense samples of ultracold matter, recent studies have been mostly on the ultracold collisions, controlling and the intermolecular interactions [68]. External control of chemical reactions using electric/magnetic fields is an active area of interest. In contrast to scattering at thermal energies, ultracold collisions offer unique opportunities in the extreme quantum regime where the scattering is mostly dominated by a single partial wave (*s-wave* only). One of the main goals is to create dense samples of ultracold molecules and retain them for sufficiently longer time in MOT to study chemical reactions close to absolute zero temperature.

After the successful realization of ultracold atoms, theoretical studies have been received an immense interest. It is also possible to calculate kinetic parameters such as reaction cross-sections and rate coefficients from the dynamical calculations and these would be immensely helpful to select suitable systems for experimental measurement.

How the energy of the atoms/molecules are lost in a trap is an important question for these experiments. In photoassociation technique, molecules were produced in highly excited vibrational levels. Whether the molecules decay by vibrational quenching or through a chemical reaction is the question. In this scenario, detailed investigation of different processes (elastic, inelastic and reactive) at very low temperatures using their dynamics is required to understand the stability of molecules.

Vibrational relaxation rate coefficients are often influenced by the presence of van der Waals complexes (bound states) formed during the collision process. The decay of these complexes leads to resonances in the energy dependence cross-sections [35]. It has been demonstrated that the vibrational pre-dissociation (quenching) lifetimes of resonances that lie close to the

threshold energy can be derived accurately from the value of zero temperature quenching rate coefficients [69, 70]. Further, this formalism was extended to describe the quenching of trapped molecules and proved that rate coefficients controlled by weakly bound states of the van der Waal complexes [71]. A larger value of rate coefficients in the zero-temperature limit is due to the wave behavior of atom which can tunnel through the narrow energy barrier and found to be efficient. The effect of tunneling can be studied for different processes using the magnitude of cross-section or the rate coefficient [27, 72].

Due to their application in quantum information sciences and precision measurements, getting cold molecules into a desired quantum regime is important [57, 73, 74]. But in practice, it is difficult because of the internal rovibrational structure of the molecules. Furthermore, due to very low collision energy, the collisional process would be suppressed as the reaction barrier is effectively raised. Therefore, the theoretical investigation of these interactions between atoms and molecules is important. It is worthwhile to mention that the exact treatment of collision processes is challenging considering all possible collision channels and number of possible outcomes of the collision event.

For atom-diatom system, there are few open source reactive scattering codes available such as, *MOLSCAT* [75], *ABC* [76] and a MATLAB based reactive scattering program [77] *etc.* They have been tested for different benchmark reactions such as H + H_2, D + H_2, H + D_2, F + H_2 in the thermal region. But in the ultracold temperature limit, the kinetic energy of reacting partners is very small, thus one has to modify and test these codes to make it suitable for all atom-diatom collisions in the ultralow collision energy limit. It has been found that there is no systematic study exist which connects both ultracold and thermal regimes. To address this issue we have adopted the *ABC* [76] reactive scattering code and modified suitably to study ultracold collisions of D + H_2 reaction and its isotopic substitutions.

Few major objectives of this thesis are listed as follows:

- The effect of rovibrational excited states of the target molecule for cold and ultracold collisions, on the behavior of reaction cross sections and the reaction probabilities.
- To investigate the origin of different resonances (Threshold, Shape and Feshbach) and their effect on the dynamics in the ultracold temperature limit.
- To calculate the accurate rate coefficients from ultracold (~ 1μ K) to thermal (~ 300 K) temperature limit.

In Chapter 2, a brief review on classical theories such as transition state theory (TST), Arrhenius theory of temperature dependence of the rate coefficients and collision theory have been presented. Classical theories consider all the atoms and molecules as billiard balls to estimate the rate coefficients at different temperatures. We have also described the quantum mechanical approach to molecular collisions where all the atoms and molecules will be treated as quantum waves. After briefly reviewing the atom-atom collisions, we have extended discussion on atom-diatom molecular collisions using Delves hyperspherical coordinates. The calculation of the Scattering matrix (*s-matrix*) and all the dynamical parameters such as reaction probability, cross-sections and reaction rate coefficients has been discussed at length.

In chapter 3, we have discussed the convergence scheme for some of the numerical parameters required to calculate low energy scattering matrix. Three major parameters that have been tested are (i) is the diatomic basis is large enough? (ii) is the integration step ($\Delta\rho$) is small enough? and (iii) if the asymptotic behavior of the potential is large enough? This numerical convergence issue has been addressed in a detailed manner with respect to the size of the basis functions, extent of radial propagation and integration step *etc*. In order to do this, new modules in the *ABC* reactive scattering code have been introduced and the code has been extensively modified for calculations reported in this thesis. The long range part of the potential energy surface is very sensitive for ultracold collisions. We have made a thorough review of the available PES for D + H_2 reaction and optimized the parameters for ultracold reactive scattering.

In the first part of chapter 4, we have presented accurate time-independent quantum mechanical (TIQM) rate coefficients for the formation of ultracold HD molecules by D + H_2 $(v, j) \rightarrow$ HD (v', j') +H reaction in the ultralow temperature regime. The dynamical parameters such as the state resolved integral cross sections, reaction probabilities and corresponding rate coefficients are computed between temperature T = 1μ K – 10 K. We have found that the exponential decrease of the rate coefficients with reducing temperature following Arrhenius' empirical equation is not valid at ultracold temperature limit. At lower temperatures, the rate coefficients become independent of temperature (constant) which is in accordance of the Wigner's threshold law [78]. We have observed a dynamical resonance near ~10^{-2} K and tried to understand their origin. Finally, we have calculated the rate coefficients of both inelastic and reactive processes which are important for the calculation of the cooling functions.

In the second and third part of the chapter 4, we have extended our calculations from the ultracold to the intermediate and thermal temperature limit. As the temperature increased, the contributions from higher partial waves are included. At T ~150 K, we may have to consider upto $\ell = 35$ partial waves. We have compared our findings with the available experimental values and observed that the reaction cross sections and rate coefficients are comparable in the thermal temperature range.

Quantum reaction dynamics of H + HD (v, j) reaction from ultracold to thermal regime has been discussed in chapter 5. Unlike H_2, HD molecule has some resultant dipole moment and higher reduced mass which makes it better interstellar coolant. For this reaction (H + HD), elastic, quenching, exchange and the formation of H_2 processes have been treated separately. The effect of higher rovibrational initial states on the dynamics is also analyzed. We have found that the quenching process is more dominant over H exchange and the formation of H_2 in the ultracold temperature limit.

We have also studied few organic reactions to understand the mechanism of the phospha Brook rearrangement, this work is presented separately as an Appendix.

1.6 References

[1] J. Silk, The Big Bang, W.H. Freeman 2001.

[2] J.D. Barrow, J. Silk, The left hand of creation: the origin and evolution of the expanding universe, Basic Books 1983.

[3] S. Singh, Big Bang: The Origin of the Universe, Harper Perennial; Reprint edition 2005.

[4] B. Povh, Particles and nuclei: an introduction to the physical concepts, Springer 1999.

[5] E.R. Hudson, H.J. Lewandowski, B.C. Sawyer, J. Ye, Cold Molecule Spectroscopy for Constraining the Evolution of the Fine Structure Constant, Physical Review Letters 96 (2006) 143004.

[6] D. Arnett, Supernovae and nucleosynthesis: an investigation of the history of matter, from the big bang to the present, Princeton University Press 1996.

[7] F. Halzen, A.D. Martin, Quarks and Leptons: An Introductory Course in Modern Particle Physics, Wiley 1984.

[8] S. Weinberg, R. Todd, The first three minutes, Blackstone Audio, Incorporated 2005.

[9] J.S. Trefil, The moment of creation: Big Bang physics from before the first millisecond to the present universe, Courier Corporation 2013.

[10] N.N. Greenwood, A. Earnshaw, Chemistry of the Elements, Butterworth-Heinemann 1995.

[11] J.W. Truran, Theories of nucleosynthesis, Space Science Reviews 15 (1973) 23-49.

[12] A. Frebel, W. Aoki, N. Christlieb, H. Ando, M. Asplund, P.S. Barklem, T.C. Beers, K. Eriksson, C. Fechner, M.Y. Fujimoto, S. Honda, T. Kajino, T. Minezaki, K.i. Nomoto, J.E. Norris, S.G. Ryan, M. Takada-Hidai, S. Tsangarides, Y. Yoshii, Nucleosynthetic signatures of the first stars, Nature 434 (2005) 871.

[13] J.J. Cowan, C. Sneden, Heavy element synthesis in the oldest stars and the early Universe, Nature 440 (2006) 1151.

[14] A.C. Fabian, P.E.J. Nulsen, C.R. Canizares, Star formation in a cooling flow, Monthly Notices of the Royal Astronomical Society 201 (1982) 933-938.

[15] I.W. Smith, Low temperatures and cold molecules, World Scientific 2008.

[16] R. McCray, M. Kafatos, Supershells and propagating star formation, The Astrophysical Journal 317 (1987) 190-196.

[17] N. Katz, Dissipational galaxy formation. II-Effects of star formation, The Astrophysical Journal 391 (1992) 502-517.

[18] W.Y. Harold, S. Cordula, On the Formation of Massive Stars, The Astrophysical Journal 569 (2002) 846.

[19] N. Strobel, Astronomy Notes, in: N. Strobel (Ed.), McGraw-Hill, US, 2013.

[20] I.W.M. Smith, Low Temperatures and Cold Molecules, Imperial College Press 2008.

[21] H.E. Suess, H.C. Urey, Abundances of the Elements, Reviews of Modern Physics 28 (1956) 53-74.

[22] T. Jonathan, H. Kelsey, K.N. Omree, N.Y. Sergei, Radiative lifetimes and cooling functions for astrophysically important molecules, Journal of Physics B: Atomic, Molecular and Optical Physics 49 (2016) 044002.

[23] G.P. Thomson, A. Reid, Diffraction of Cathode Rays by a Thin Film, Nature 119 (1927) 890.

[24] K. Hasselmann, On the non-linear energy transfer in a gravity wave spectrum Part 2. Conservation theorems; wave-particle analogy; irrevesibility, Journal of Fluid Mechanics 15 (1963) 273-281.

[25] A.B. Henson, S. Gersten, Y. Shagam, J. Narevicius, E. Narevicius, Observation of Resonances in Penning Ionization Reactions at Sub-Kelvin Temperatures in Merged Beams, Science 338 (2012) 234.

[26] P.F. Weck, N. Balakrishnan, Importance of long-range interactions in chemical reactions at cold and ultracold temperatures, International Reviews in Physical Chemistry 25 (2006) 283-311.

[27] A. Smerzi, S. Fantoni, S. Giovanazzi, S. Shenoy, Quantum coherent atomic tunneling between two trapped Bose-Einstein condensates, Physical Review Letters 79 (1997) 4950.

[28] E.P. Wigner, On the Behavior of Cross Sections Near Thresholds, Physical Review 73 (1948) 1002-1009.

[29] R. V Krems, Chemical reactions and inelastic collisions of atoms and molecules at cold and ultracold temperatures, 2002.

[30] T. Takayanagi, N. Masaki, K. Nakamura, M. Okamoto, S. Sato, G.C. Schatz, The rate constants for the H + H_2 reaction and its isotopic analogs at low temperatures: Wigner threshold law behavior, The Journal of Chemical Physics 86 (1987) 6133-6139.

[31] T. Wang, J. Chen, T. Yang, C. Xiao, Z. Sun, L. Huang, D. Dai, X. Yang, D.H. Zhang, Dynamical Resonances Accessible Only by Reagent Vibrational Excitation in the F + HD→HF + D Reaction, Science 342 (2013) 1499.

[32] T. Takayanagi, The effect of van der Waals resonances on reactive cross sections for the F+HD reaction, Chemical Physics Letters 433 (2006) 15-18.

[33] M. Schnell, G. Meijer, Cold molecules: preparation, applications, and challenges, Angewandte Chemie International Edition 48 (2009) 6010-6031.

[34] X. Wang, W. Dong, M. Qiu, Z. Ren, L. Che, D. Dai, X. Wang, X. Yang, Z. Sun, B. Fu, S.-Y. Lee, X. Xu, D.H. Zhang, HF(v' = 3) forward scattering in the F + H_2 reaction: Shape resonance and slow-down mechanism, Proceedings of the National Academy of Sciences 105 (2008) 6227.

[35] N. Balakrishnan, R.C. Forrey, A. Dalgarno, Threshold phenomena in ultracold atom–molecule collisions, Chemical Physics Letters 280 (1997) 1-4.

[36] R. Krems, B. Friedrich, W.C. Stwalley, Cold Molecules: Theory, Experiment, Applications, Taylor & Francis 2009.

[37] M. Marinescu, L. You, Controlling atom-atom interaction at ultralow temperatures by dc electric fields, Physical review letters 81 (1998) 4596.

[38] Threshold resonance effects in reactive processes, Phys. Rev. 89 (2014).

[39] P. Tangney, S. Scandolo, How well do Car–Parrinello simulations reproduce the Born–Oppenheimer surface? Theory and examples, The Journal of Chemical Physics 116 (2001) 14-24.

[40] M.H. Jeremy, Feshbach resonances in ultracold atomic and molecular collisions: threshold behaviour and suppression of poles in scattering lengths, New Journal of Physics 9 (2007) 152.

[41] A.D. Ludlow, M.M. Boyd, J. Ye, E. Peik, P.O. Schmidt, Optical atomic clocks, Reviews of Modern Physics 87 (2015) 637-701.

[42] A.E. Leanhardt, J.L. Bohn, H. Loh, P. Maletinsky, E.R. Meyer, L.C. Sinclair, R.P. Stutz, E.A. Cornell, High-resolution spectroscopy on trapped molecular ions in rotating electric fields: A new approach for measuring the electron electric dipole moment, Journal of Molecular Spectroscopy 270 (2011) 1-25.

[43] J.K. Webb, M.T. Murphy, V.V. Flambaum, V.A. Dzuba, J.D. Barrow, C.W. Churchill, J.X. Prochaska, A.M. Wolfe, Further Evidence for Cosmological Evolution of the Fine Structure Constant, Physical Review Letters 87 (2001) 091301.

[44] K. Levin, A.L. Fetter, D.M. Stamper-Kurn, Ultracold Bosonic and Fermionic Gases, Elsevier 2012.

[45] H. Metcalf, P. van der Straten, Cooling and trapping of neutral atoms, Physics Reports 244 (1994) 203-286.

[46] Z. Hu, H. Kimble, Observation of a single atom in a magneto-optical trap, Optics letters 19 (1994) 1888-1890.

[47] W. Petrich, M.H. Anderson, J.R. Ensher, E.A. Cornell, Behavior of atoms in a compressed magneto-optical trap, JOSA B 11 (1994) 1332-1335.

[48] C. Gabbanini, A. Fioretti, A. Lucchesini, S. Gozzini, M. Mazzoni, Cold rubidium molecules formed in a magneto-optical trap, Physical review letters 84 (2000) 2814.

[49] H.F. Hess, Evaporative cooling of magnetically trapped and compressed spin-polarized hydrogen, Physical Review B 34 (1986) 3476.

[50] N. Masuhara, J.M. Doyle, J.C. Sandberg, D. Kleppner, T.J. Greytak, H.F. Hess, G.P. Kochanski, Evaporative cooling of spin-polarized atomic hydrogen, Physical Review Letters 61 (1988) 935.

[51] W. Ketterle, N. Van Druten, Evaporative cooling of trapped atoms, Advances in atomic, molecular, and optical physics, Elsevier1996, 181-236.

[52] R. Côté, A. Dalgarno, Mechanism for the Production of $^{6}Li_2$ and $^{7}Li_2$ Ultracold Molecules, Journal of Molecular Spectroscopy 195 (1999) 236-245.

[53] A. Fioretti, D. Comparat, A. Crubellier, O. Dulieu, F. Masnou-Seeuws, P. Pillet, Formation of Cold Cs_2 Molecules through Photoassociation, Physical Review Letters 80 (1998) 4402-4405.

[54] T. Takekoshi, B.M. Patterson, R.J. Knize, Observation of Optically Trapped Cold Cesium Molecules, Physical Review Letters 81 (1998) 5105-5108.

[55] M.H. Anderson, J.R. Ensher, M.R. Matthews, C.E. Wieman, E.A. Cornell, Observation of Bose-Einstein condensation in a dilute atomic vapor, science 269 (1995) 198-201.

[56] H.L. Bethlem, G. Berden, G. Meijer, Decelerating Neutral Dipolar Molecules, Physical Review Letters 83 (1999) 1558-1561.

[57] H.L. Bethlem, G. Meijer, Production and application of translationally cold molecules, International Reviews in Physical Chemistry 22 (2003) 73-128.

[58] J.D. Weinstein, R. deCarvalho, T. Guillet, B. Friedrich, J.M. Doyle, Magnetic trapping of calcium monohydride molecules at millikelvin temperatures, Nature 395 (1998) 148.

[59] C.J. Myatt, E.A. Burt, R.W. Ghrist, E.A. Cornell, C.E. Wieman, Production of Two Overlapping Bose-Einstein Condensates by Sympathetic Cooling, Physical Review Letters 78 (1997) 586-589.

[60] Y.B. Band, P.S. Julienne, Ultracold-molecule production by laser-cooled atom photoassociation, Physical Review A 51 (1995) R4317-R4320.

[61] J. Weiner, V.S. Bagnato, S. Zilio, P.S. Julienne, Experiments and theory in cold and ultracold collisions, Reviews of Modern Physics 71 (1999) 1-85.

[62] D.J. Heinzen, R. Wynar, P.D. Drummond, K.V. Kheruntsyan, Superchemistry: Dynamics of Coupled Atomic and Molecular Bose-Einstein Condensates, Physical Review Letters 84 (2000) 5029-5033.

[63] S. Jochim, M. Bartenstein, A. Altmeyer, G. Hendl, C. Chin, J.H. Denschlag, R. Grimm, Pure Gas of Optically Trapped Molecules Created from Fermionic Atoms, Physical Review Letters 91 (2003) 240402.

[64] M.W. Zwierlein, C.A. Stan, C.H. Schunck, S.M.F. Raupach, S. Gupta, Z. Hadzibabic, W. Ketterle, Observation of Bose-Einstein Condensation of Molecules, Physical Review Letters 91 (2003) 250401.

[65] M. Greiner, C.A. Regal, D.S. Jin, Emergence of a molecular Bose–Einstein condensate from a Fermi gas, Nature 426 (2003) 537.

[66] R. Unanyan, M. Fleischhauer, B.W. Shore, K. Bergmann, Robust creation and phase-sensitive probing of superposition states via stimulated Raman adiabatic passage (STIRAP) with degenerate dark states, Optics Communications 155 (1998) 144-154.

[67] C.J. Pethick, H. Smith, Bose-Einstein condensation in dilute gases, Cambridge university press 2002.

[68] R.V. Krems, Cold controlled chemistry, Physical Chemistry Chemical Physics 10 (2008) 4079-4092.

[69] N. Balakrishnan, R.C. Forrey, A. Dalgarno, Quenching of H_2 Vibrations in Ultracold ^{3}He and ^{4}He Collisions, Physical Review Letters 80 (1998) 3224-3227.

[70] R.C. Forrey, N. Balakrishnan, V. Kharchenko, A. Dalgarno, Feshbach resonances in ultracold atom-diatom scattering, Physical Review A 58 (1998) R2645-R2647.

[71] R.C. Forrey, V. Kharchenko, N. Balakrishnan, A. Dalgarno, Vibrational relaxation of trapped molecules, Physical Review A 59 (1999) 2146-2152.

[72] R.T. Skodje, D. Skouteris, D.E. Manolopoulos, S.-H. Lee, F. Dong, K. Liu, Resonance-Mediated Chemical Reaction: F + HD $\rightarrow$ HF + D, Physical Review Letters 85 (2000) 1206-1209.

[73] W. Dong, N. Mukherjee, R.N. Zare, Optical preparation of H_2 rovibrational levels with almost complete population transfer, The Journal of Chemical Physics 139 (2013) 074204.

[74] W.E. Perreault, N. Mukherjee, R.N. Zare, Preparation of a selected high vibrational energy level of isolated molecules, The Journal of Chemical Physics 145 (2016) 154203.

[75] J. Hutson, S. Green, MOLSCAT computer code, version 14, Collaborative computational project (1994).

[76] D. Skouteris, J. Castillo, D. Manolopoulos, ABC: a quantum reactive scattering program, Computer Physics Communications 133 (2000) 128-135.

[77] M. Warehime, M.H. Alexander, A MATLAB-based finite-element visualization of quantum reactive scattering. I. Collinear atom-diatom reactions, The Journal of chemical physics 141 (2014) 024118.
[78] E.P. Wigner, On the behavior of cross sections near thresholds, Physical Review 73 (1948) 1002.

Chapter - 2

Theoretical Methodology

2.1 Introduction

The classical hard-sphere collision theory to estimate the rates of chemical reactions was used extensively, but has been found to be unsatisfactory for many elementary chemical reactions [1]. The crossed molecular beam experiments have recently been developed and it is now possible to obtain detailed experimental information about reaction mechanisms [2, 3] *e.g.,* one can measure the energy and angular distributions of the product molecules. Since the philosophy behind the crossed molecular beam experiments is based on quantum mechanics, classical reaction rate theories cannot interpret those results. These experiments have led to the formulation of alternative theories based on accurate quantum mechanical principles that can treat molecular collisions in more realistic manner**.**

In 1986, soon after the first successful experiments reported optical cooling and trapping in alkali gasses, scientists had started working more rigorously on the possible consequences of binary collisions in cold or ultracold gaseous medium [4]. At very low temperatures the wave nature of the translational motion become quite large and quantum mechanical treatment is essential to represent their collision. The theoretical methods applied for the analysis of ultracold scattering experiments is briefly described in this chapter. We restrict our discussion on the time-independent non-relativistic quantum treatment for multi-channel scattering experiments. In this chapter we intend to bridge the gap between scattering dynamics from ultracold to thermal temperature region, therefore we start with brief description of the classical theories of collision dynamics.

2.2 Classical theories of molecular collisions

Classical collision theory was first proposed by Max Trautz in 1916 and William Lewis independently in 1918 [5, 6]. This theory explains how chemical reactions take place and why reaction rate coefficients are different for different kind of reactions. According to collision theory, when reactant particles collide with each other, only a certain percentage of the collisions cause any significant chemical change; these successful collisions are called fruitful collisions. These fruitful collisions have enough energy to overcome the activation energy, at the time of collision. As a result, new chemical bonds form leading to new species

(products). Several factors such as the concentration of the reactants, temperature, pressure *etc.* can influence the collision events and thereby can change the rate of reaction.

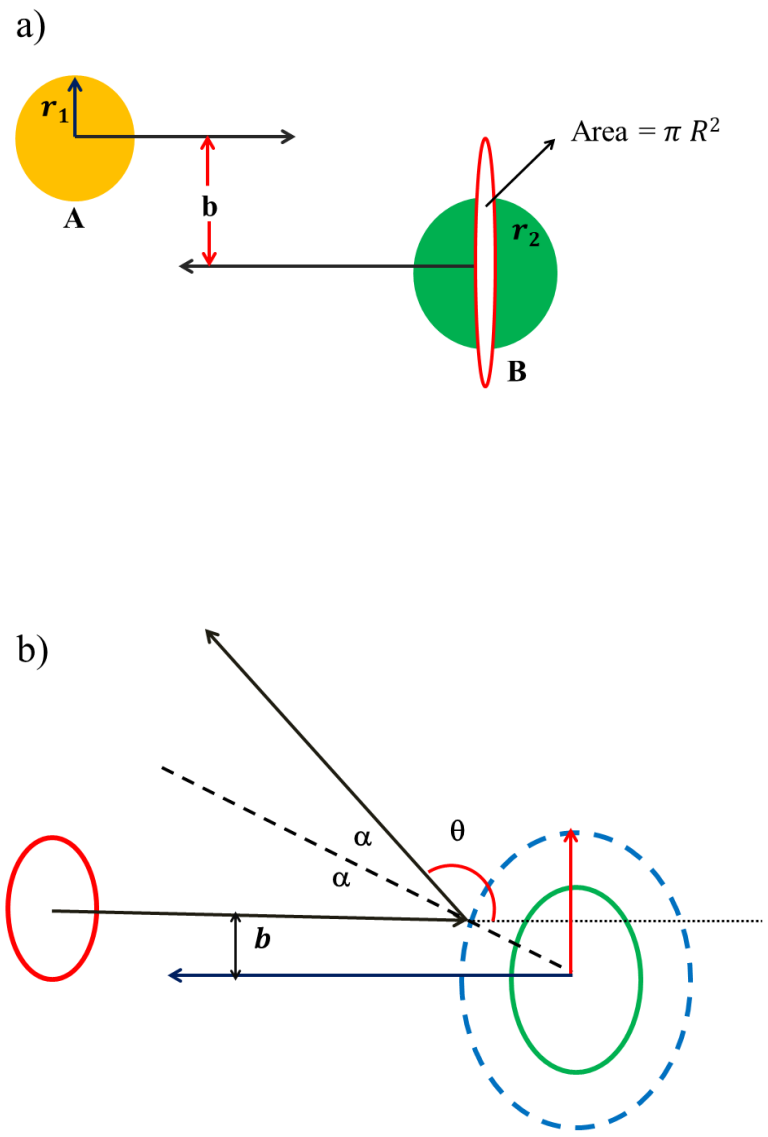

Figure 1: a) *b* is the impact parameter. b) Illustrative representation of atom-atom collisions and the concept of cross section.

In Figure 1 collision between two atoms is schematically shown. If the impact parameter (overall distance between the colliding pairs) is larger, the atoms miss out each other and there would be no collision. The maximum value of impact parameter for a collision to occur is the sum of the radii of the two atoms ($b = r_1 + r_2$). If atom A lies within the area of the circle (Area = πR^2), then collision can take place. This effective area which quantifies the collisional event when an incident atom strikes a target atom is classically called the collision

cross section ($\sigma = \pi R^2$, where $R = r_1 + r_2$). Another important parameter is the angle of scattering (α) after the collision. From the Figure 1, it can be calculated that the impact parameter

$$b = Rsin\alpha$$

$$\theta + 2\alpha = \pi$$

Thus,

$$b = Rsin\left(\frac{\pi - \theta}{2}\right) = Rcos\frac{\theta}{2}$$

Colliding atoms with an impact parameter b to $b + db$ are scattered within scattering angle θ to $\theta + d\theta$. Therefore, the scattering cross section in terms of polar angles $\theta + d\theta$ is

$$2\pi b|db| = 2\pi R\left(cos\frac{\theta}{2}\right)\left|Rsin\frac{\theta}{2}\frac{d\theta}{2}\right| = \frac{1}{2}\pi R^2 \sin\theta\, d\theta$$

The differential cross section is defined as the flux of atoms scattered into a solid angle ($d\Omega = \sin\theta d\theta\, d\phi$) over the flux of incident atoms. Since the azimuthal angle is not used in this case, the solid angle is integrated which becomes $2\pi \sin\theta d\theta$. Thus, In order to calculate the differential cross section, one needs to know the scattering angle.

The differential cross section can be written as [7],

$$\frac{d\sigma}{d\Omega} = \frac{R^2}{4}$$

Upon integration of the differential cross section over all angles, total cross section or integral cross section can be calculated as,

$$\int d\Omega \frac{d\sigma}{d\Omega} = \int_0^{\pi} \sin\theta d\theta \int_0^{2\pi} d\phi \frac{d\sigma}{d\Omega}$$

$$= \frac{R^2}{4}\int_0^{\pi} \sin\theta\, d\theta \int_0^{2\pi} d\phi$$

$$= \pi R^2$$

According to collision theory of gases, the rate constant for bimolecular gas-phase reactions is equal to the rate of successful collisions.

The rate of fruitful collisions known as the rate coefficient is proportional to the fraction of fruitful collisions multiplied by the overall collision frequency [7]

$$k(T) = Z\ exp(^{-E_a}/_{RT})$$

Where Z is the collision frequency of the reaction, T is the temperature, E_a is the activation energy and R is the gas constant.

From statistical thermodynamics, collision frequency $(Z) = N_A\sigma_{AB}\sqrt{\frac{8K_BT}{\pi\mu_{AB}}}$, where N_A is the Avogadro number, σ_{AB} is the reaction cross section $k_B$is the Boltzmann's constant and μ_{AB} is the reduced mass of the reactants. The above reaction rate constant resembles the Arrhenius equation in which Z becomes the pre-exponential factor. The rate coefficients of chemical reactions strongly depend upon the temperature. For many reactions, the temperature dependent rate constant is described by following Arrhenius formula [6]:

$$\frac{dlnk}{dT} = \frac{E_a}{RT^2}$$

Where E_a have units of energy. If E_a is independent of temperature, the above equation can be written as follows,

$$lnk = lnZ - \frac{E_a}{RT}$$

This empirical equation was derived from many experimental observations without any mechanistic considerations. One or more reactive intermediates are involved in the conversion from reactants to the products. Thus, further development was necessary to understand two key parameters present in this law *i.e.* the pre-exponential factor (Z) and the activation energy (E_a). Further, Transition State Theory (TST), which was developed later could able to relate the physical significance of these parameters.

Transition state theory represents how reactions generally take place at the molecular level [5, 6]. Considering a general reaction,

$$A + B \rightarrow P;\ \text{rate coefficient} = k$$

The rate law is given by

$$\frac{dP}{dt} = k\ [A][B]$$

According to this theory, the reaction coordinate from reactants to products passes through a transition state which has higher energy compared to the reactants and the corresponding products. It is represented as the highest point on the energy profile diagram as shown schematically in Figure 7.

$$\mathbf{A + B} \rightleftharpoons \mathbf{[AB]^{\#}} \longrightarrow \mathbf{P,\ (Rate\ coefficient = } k\mathbf{)}$$

TST assumes that pre-equilibrium is first established between the reactants and the transition state which then leads to the formation of the products. Here $K^{\#}$ is the equilibrium constant for the pre equilibrium.

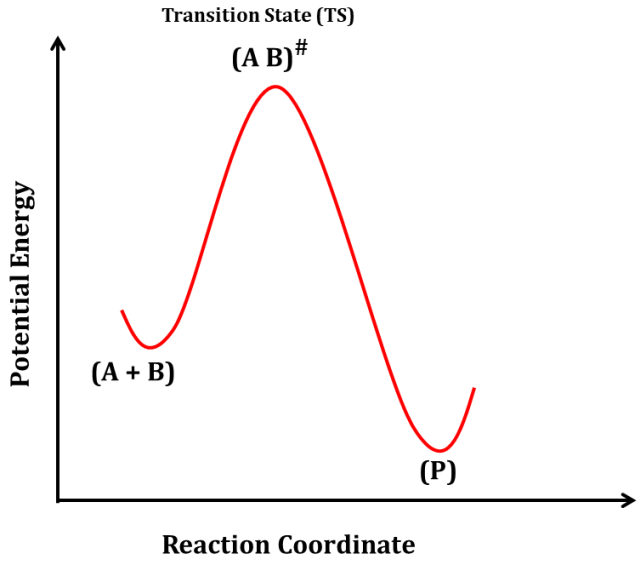

Figure 2: The general representation of the potential energy of the reactants, products and the transition state.

$AB^{\#}$ is the activated complex or the transition state. The equilibrium constant defined as $K_c^{\#} = \frac{[AB]^{\#}}{[A][B]}$. Now the rate coefficient $k = \frac{K_B T}{hc^o} K^{\#}$ and $\Delta G = -RT \ln K^{\#}$, thus the rate coefficient is $k = \frac{K_B T}{h} e^{\frac{-\Delta G}{RT}}$. But since ΔG = ΔH – TΔS, the expression of the rate coefficient can be modified as

$$k = \frac{K_B T}{hc^o} e^{\frac{\Delta S^{\#}}{R}} e^{\frac{-\Delta H^{\#}}{RT}}$$

This equation is very similar to the Arrhenius equation $k = Ae^{-E_a/RT}$. The factor $\frac{K_B T}{hc^o} e^{\frac{\Delta S^{\#}}{R}}$ relates to the pre-exponential factor A where, $\Delta S^{\#}$ is the entropy change for the bimolecular

reaction. The activation energy E_a resembles $-\Delta H^{\#}$ which can be estimated from the reaction profile.

Although, the Arrhenius equation had been used extensively to determine the activation energies of chemical reactions, the plot of lnk versus $1/T$ for some reactions is not linear [8]. This nonlinear behavior can be rationalized by considering temperature dependent of the frequency factor and accordingly the reaction rate constant would behave like

$$k = aT^m e^{-E'/RT}$$

Where a, E' and m (= 1, 1/2, -1/2) are temperature independent constants. But still this modified Arrhenius equation fails to explain the behavior of the rate coefficients as it becomes constant at the ultralow temperature limit.

Some literature reviews have suggested that the deviations from Arrhenius equation are due to (i) Quantum mechanical effects (ii) Reaction medium (iii) quasi-thermodynamic effects *etc*. [9, 10]. Apart from explosion reactions, reactions involving enzymes also do not follow Arrhenius theory of temperature dependence [6]. But none of these theories take into account of the energy distribution among the rovibrational states when two molecules collide with each other. At very low temperatures, colliding pairs will not have sufficient energy to cross over the barrier to form products but still the reaction can happen through quantum mechanical tunneling which does not have any classical analog [11, 12]. The temperature dependence of the rate coefficients differs significantly from the Arrhenius behavior at the ultracold temperature limit.

2.3 Atom-atom collisions: The wave picture of the scattering process

In quantum mechanical treatment, the relative motion of two colliding particles approaching each other is represented by a plane waves. Such a plane wave has well-defined linear momentum and following the Heisenberg's uncertainty principle, it is totally delocalized in coordinate space. Considering the incident particle as a plane wave approaching from the negative *Z* direction and the scattering center is located at the origin, its wave function can be written as [1, 7, 13]:

$$\psi_o(r, E) = \left(\frac{k\mu}{2\pi h^2}\right)^{1/2} e^{ik.r}, \qquad (2.1)$$

where, subscript *o* indicates the solution of the problem in absence of any interaction potential at collision energy *E*, *k* is the wavenumber or momentum $\left(k = \frac{\sqrt{2\mu E}}{\hbar}\right)$ and μ is the reduced mass.

If the interaction potential is taken to be spherically symmetric, the azimuthal angle ϕ plays no role in the collision processes. After the collision, the particle is scattered into different polar angles with a scattering amplitude of $f(\theta)$. At large distances from the scattering center the wave function therefore takes the form [7]

$$\Psi(r, E) = \left(\frac{k\mu}{2\pi h^2}\right)^{1/2} \left\{e^{ik.z} + f(\theta)\frac{e^{ik.r}}{r}\right\} \tag{2.2}$$

The term $e^{ik.z}$ is the incident wave, while $f(\theta)e^{ik.z}$ represents the scattered wave moving away from the scattering center. The number of atoms crossing a unit area per unit time (incident flux) of atoms corresponding to the plane wave $e^{ik.z}$ is $\frac{k\hbar}{\mu}\left|e^{ik.z}\right|^2 = \frac{\hbar k}{\mu}$. The solid angle $sin\theta d\theta d\phi$ subtends an area of $r^2 sin\theta d\theta d\phi$ on the surface of radius r located on the scattered center. As we consider the collision to be elastic, the radial momentum remains unchanged by the collision and equals to $k\hbar$. The flux of atoms passing through the small area $r^2 sin\theta d\theta d\phi$ on the surface of the sphere arising from the scattered wave $f(\theta)e^{ik.z}$ is therefore

$$\frac{k\hbar}{\mu}\left|f(\theta)\frac{e^{ik.r}}{r}\right|^2 r^2 sin\theta d\theta d\phi = \frac{\hbar k}{\mu}|f(\theta)|^2 sin\theta d\theta d\phi$$

Now, the differential cross section is defined as the flux of scattered atoms into a given solid angle divided by the incident flux of atoms.

Therefore,

$$\sigma(\Omega)\, d\Omega = \frac{\frac{\hbar k}{\mu}|f(\theta)|^2 sin\theta d\theta d\phi}{\frac{\hbar k}{\mu}} \tag{2.3}$$

So the differential cross section is given by

$$\sigma(\Omega) = |f(\theta)|^2 \tag{2.4}$$

The description for the reaction dynamics and the behavior of atoms/molecules near ultracold temperatures can be found in various text books, and discussed later in section 2.8 [1, 7, 11-14].

2.4 Solution of the Time-Independent Schrödinger Equation (TISE)

At the scattering center, the wave function can be found by solving the time independent Schrodinger equations.

$$\left\{-\frac{\hbar^2}{2\mu}\ \nabla^2 + V(r)\right\}\psi(r) = E\,\psi(r) \tag{2.5}$$

There are two linearly independent solutions to this equation; we focus in the regular solution which tends to be zero near the origin where the interaction potential becomes infinite. Introducing the spherical polar coordinates [15, 16] the $Eq.2.5$ becomes:

$$-\frac{\hbar^2}{2\mu}\left\{\frac{1}{r^2}\frac{\partial}{\partial r}r^2\frac{\partial\psi}{\partial r} + \frac{1}{r^2}\left[\frac{1}{sin\theta}\frac{\partial}{\partial\theta}\left(sin\theta\frac{\partial\psi}{\partial\theta}\right) + \frac{1}{sin^2\theta}\frac{\partial^2\psi}{\partial\phi^2}\right]\right\} + V(r)\psi = E\,\psi \tag{2.6}$$

The above equation (E$q.$ 2.6) is separable if we multiply with r^2. The angular wave functions are the Eigenfunctions of the orbital angular momentum operator

$$-\hbar^2\left[\frac{1}{sin\theta}\frac{\partial}{\partial\theta}\left(sin\theta\frac{\partial\psi}{\partial\theta}\right) + \frac{1}{sin^2\theta}\frac{\partial^2\psi}{\partial\phi}\right]Y_{lm}(\theta,\phi) = \ell\,(\ell+1)\hbar^2 Y_{lm}(\theta,\phi) \tag{2.7}$$

Where, $Y_{lm}(\theta,\phi)$ are the spherical harmonics [17]. Now the total wave function will be in the form of

$$\psi_{\ell,m}(r) = \frac{1}{r}\,\chi_\ell(r)Y_{\ell m}(\theta,\phi) \tag{2.8}$$

extra factor of $\frac{1}{r}$ is introduced so as to simplify the ensuing differential equation in the radial coordinate r. Substituting $Eq\ 2.8$ into $Eq\ 2.6$ we get,

$$\frac{\hbar^2}{2\mu}\left[\frac{\partial^2}{\partial r^2} + \frac{\ell(\ell+1)}{r^2}\right]\chi_\ell(r) + V(r)\chi_\ell(r) = E\,\chi_\ell(r) \tag{2.9}$$

this can be written as

$$-\frac{\hbar^2}{2\mu}\frac{\partial^2}{\partial r^2}\chi_\ell(r) + \left\{V(r) + \frac{\hbar^2}{2\mu}\frac{\ell(\ell+1)}{r^2}\right\}\chi_\ell(r) = E\,\chi_\ell(r) \tag{2.10}$$

The term in curly brackets in $Eq.2.10$ is called the effective potential. At large r both centrifugal potential $\left(\frac{\hbar^2}{2\mu}\frac{\ell(\ell+1)}{r^2}\right)$ and the interaction potential $V(r)$ tend to zero.

The general solution to the *Eq* 2.9 can be written in the form of *sines* and *cosines*:

$$\chi(r)\sim^{r\to\infty} A sin\left(kr-\frac{l\pi}{2}+\eta_\ell\right)$$

$$= A\frac{1}{2i}\left\{e^{i(kr-\frac{l\pi}{2}+\eta_\ell)} - e^{-i(kr-\frac{l\pi}{2}+\eta_\ell)}\right\}$$

$$= A\frac{i^{\ell+1}e^{-i\eta_\ell}}{2}\left\{e^{-ikr} + (-1)^{-(\ell+1)}e^{-i(kr+2\eta_\ell)}\right\} \quad (2.11)$$

Where, k is the wave number and η_ℓ is the phase shift which represents the difference in phase of the wave function compared to the solution in the absence of potential.

The radial equation (*Eq* 2.9) for free motion has two linearly independent solutions when *V(r)* = 0. These are called as Riccati-Bessel functions [18] $\widehat{j_\ell}(kr) = krj_\ell(kr)$ and $\widehat{\eta_\ell}(kr) = kr\,\eta_\ell(kr)$ where $j_\ell(kr)$ and $\eta_\ell(kr)$ are the closely related spherical Bessel functions [19]. The regular solution $\widehat{j_\ell}(kr)$ goes to zero at the origin where the centrifugal potential $\frac{\hbar^2}{2\mu}\frac{\ell(\ell+1)}{r^2}$ becomes infinite. The irregular solution $\widehat{\eta_\ell}(kr)$ becomes infinite as $r \to 0$. At large r values the solutions behave as below

$$\widehat{j_\ell}(kr) = krj_\ell(kr) \sim^{r\to\infty} \sin\left(kr - \frac{\ell\pi}{2}\right)$$

$$\widehat{\eta_\ell}(kr) = kr\,\eta_\ell(kr)\sim^{r\to\infty} -\cos\left(kr - \frac{\ell\pi}{2}\right) \quad (2.12)$$

2.5 Plane wave expanded in terms of partial waves.

The plane wave can be expanded in terms of regular Bessel functions which is travelling along the positive Z direction

$$e^{ikz} = \sum_{\ell=0}^{\infty}(2\ell+1)i^\ell j_\ell(kr)P_\ell(cos\theta)$$

(2.13)

where, $P_\ell(cos\theta)$ are the Legendre polynomials [20, 21], submitting Eq 2.12, Eq 2.13 in Eq 2.2 , we obtain the following equation.

$$\psi(r,E) \sim^{r\to\infty} \left(\frac{k\mu}{2\pi h^2}\right)^{\frac{1}{2}}\left\{\sum_{\ell=0}^{\infty}(2\ell+1)i^\ell \frac{1}{kr}\,\mathrm{x}\sin\left(kr-\frac{\ell\pi}{2}\right)P_\ell(cos\theta)+f(\theta)\frac{e^{ikr}}{r}\right\}$$

$$= \left(\frac{k\mu}{2\pi h^2}\right)^{\frac{1}{2}}\left\{\sum_{\ell=0}^{\infty}(2\ell+1)i^\ell \frac{1}{kr}\frac{1}{2i}\left(e^{i\left(kr-\frac{\ell\pi}{2}\right)}-e^{-i\left(kr-\frac{\ell\pi}{2}\right)}\right)\mathrm{x}\,P_\ell(cos\theta)+f(\theta)\frac{e^{ikr}}{r}\right\}$$

$$= \left(\frac{k\mu}{2\pi h^2}\right)^{\frac{1}{2}}\left\{\sum_{\ell=0}^{\infty}(2\ell+1)i^\ell \frac{1}{kr}\frac{1}{2i}\frac{(-1)^{\ell+1}}{2i}\left\{e^{-ikr}+(-1)^{-(\ell+1)}e^{ikr}\right\}\mathrm{x}\,P_\ell(cos\theta)\right.$$
$$\left.+\,f(\theta)\frac{e^{ikr}}{r}\right\} \qquad (2.14)$$

Again, it is required to expand the scattering amplitude $f(\theta)$ in terms of the Legendre polynomials in order to relate with the phase shift.

$$f(\theta)=\sum_{\ell=0}^{\infty} f_\ell\, P_\ell(cos\theta) \qquad (2.15)$$

This summation is known as the partial wave expansion where the number of partial waves contributing to the scattering dynamics determined from numerical convergence studies and f_ℓ constitutes the amplitude of the partial waves.

$$\psi(r,E) \sim^{r\to\infty} \left(\frac{k\mu}{2\pi h^2}\right)^{\frac{1}{2}}\left\{\sum_{\ell=0}^{\infty}(2\ell+1)i^\ell \frac{1}{kr}\frac{1}{2i}\frac{(-1)^{\ell+1}}{2i}\,\mathrm{x}\left\{e^{-ikr}\right.\right.$$
$$\left.\left.+(-1)^{-(\ell+1)}e^{ikr}\right\}\mathrm{x}\,P_\ell(cos\theta)\sum_{\ell=0}^{\infty} f_\ell\, P_\ell(cos\theta)\frac{e^{ikr}}{r}\right\}$$

$$=\left(\frac{k\mu}{2\pi h^2}\right)^{\frac{1}{2}}\frac{1}{r}\left\{\sum_{\ell=0}^{\infty}\left[(2\ell+1)\frac{(-1)^{\ell+1}}{2ik}e^{-ikr}+\left((2\ell+1)\frac{1}{2ik}+f_\ell\right)e^{ikr}\right]P_\ell(cos\theta)\right\}$$

$$= \left(\frac{k\mu}{2\pi h^2}\right)^{\frac{1}{2}} \frac{1}{2ik}\left\{\sum_{\ell=0}^{\infty}\left[(2\ell+1)(-1)^{\ell+1}e^{-ikr}\right.\right.$$

$$\left.\left.+\left((2\ell+1)+2ikf_\ell\right)e^{ikr}\right]P_\ell(cos\theta)\right\} \quad (2.16)$$

Comparing the relative coefficients of two waves Eq 2.16 and Eq 2.11

$$(-1)^{-(\ell+1)}e^{i(2\eta_\ell)} = \frac{((2\ell+1)+2ikf_\ell}{(2\ell+1)(-1)^{\ell+1}} \quad (2.17)$$

And thus,

$$f_\ell = \frac{(2\ell+1)}{k}e^{i\eta_\ell}\sin\eta_\ell \quad (2.18)$$

Now, combining *Eq.* (2.18) with (2.4) and (2.15), the elastic cross section is

$$\sigma(\Omega) = \left|\sum_{\ell=0}^{\infty}\frac{(2\ell+1)}{k}\, e^{i\eta_\ell}\sin\eta_\ell\, P_\ell(cos\theta)\right|^2 \quad (2.19)$$

The condition for normalization of Legendre polynomials considered here is

$$\int_0^{\pi} P_\ell(cos\theta)P_{\ell'}(cos\theta)\sin\theta\, d\theta = \frac{2\delta_{\ell\ell'}}{2\ell+1} \quad (2.20)$$

Therefore, the total integral cross-section is given by

$$\sigma = \int \sigma(\Omega)d\Omega$$

$$= \int_0^{2\pi} d\phi \int_0^{\pi}\left|\sum_{\ell=0}^{\infty}\frac{2\ell+1}{k}e^{i\eta_\ell}\sin\eta_\ell\, P_\ell(\cos\theta)\right|^2 \sin\theta\, d\theta$$

$$= 2\pi\int_0^{2\pi}\left|\sum_{\ell=0}^{\infty}\frac{2\ell+1}{k}e^{i\eta_\ell}\sin\eta_\ell\, P_\ell(\cos\theta)\right|^2 \sin\theta\, d\theta$$

$$= 2\pi\sum_{\ell=0,\ell'=0}^{\infty}\frac{(2\ell+1)}{k}\frac{2\ell'+1}{k}e^{i(\eta_\ell-\eta'_\ell)}\sin\eta_\ell\sin\eta'_\ell \text{ x } \int_0^{\pi}P_\ell(cos\theta)P_{\ell'}(cos\theta)\sin\theta\, d\theta$$

$$= \frac{4\pi}{k^2}\sum_{\ell=0}^{\infty}(2\ell+1)sin^2\eta_\ell \quad (2.21)$$

The integral cross section is represented as a sum of partial integral cross sections

$$\sigma = \sum_{\ell=0}^{\infty}\sigma_\ell \quad (2.22)$$

$$= \frac{4\pi}{k^2}(2\ell+1)sin^2\eta_\ell \quad (2.23)$$

Following correlation is observed between the partial wave quantum number ℓ and the classical impact parameter *b* which describes effective interaction between two particles.

$$b^2 \sim \frac{\ell(\ell+1)}{k^2}$$

The collision occurs when *b* less than the distance at which their interaction potential is negligible. Due to high angular momentum of interacting particles, we need to consider hundreds of partial waves at room temperature or above. But in the cold and ultracold regime, dynamics is dominated by single partial wave $\ell = 0$ (*s-wave*). Using electronic orbital terminology partial waves are often referred to as *s-wave*, *p-wave* and *d-wave* for $\ell = 0, 1, 2$ and so on.

2.6 Atom-molecule inelastic/reactive scattering dynamics

In order to understand the theory behind atom-molecule inelastic collision process, we start with an atom-diatom system. There are three possible inelastic outcomes/channels which can arise when an atom and a diatom collides as schematically shown in Figure 3. When an atom (A) approaches a molecule (BC), one of the atoms of the diatomic molecule will be exchanged with atom A leading to a scattering process or if there is no exchange then the scattering is non-reactive and this process is said to be either elastic or inelastic. There may be a chance of three body break up at higher energies.

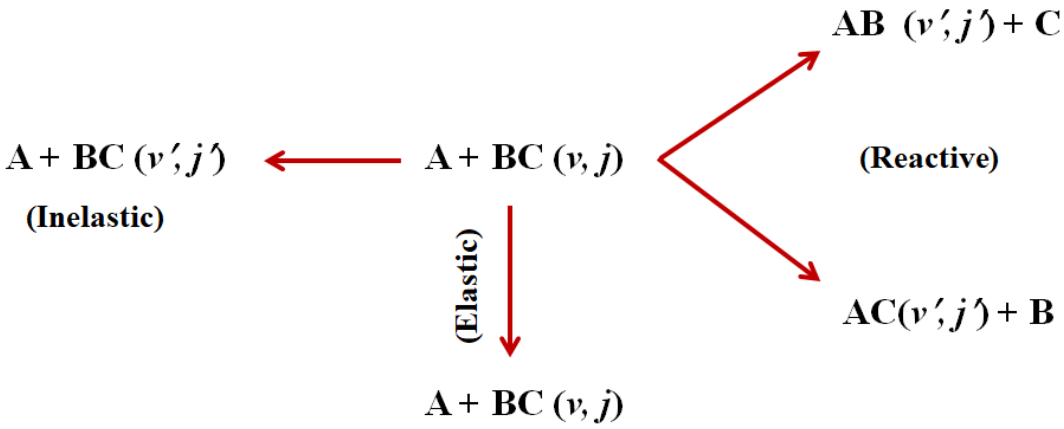

Figure 3: Representation of atom-diatom collision includes elastic, inelastic and reactive processes.

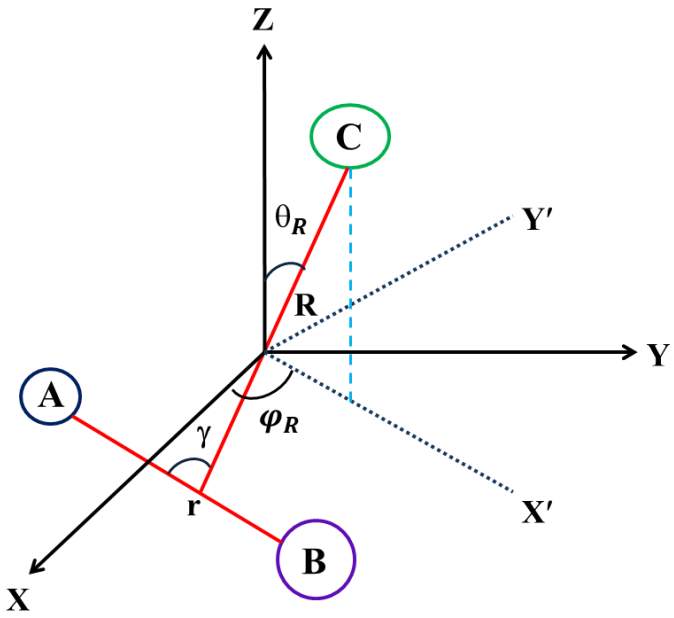

Figure 4: Schematic representation of atom-diatom collision in Jacobi Coordinates [7]. R is the distance from the incident atom (A) to the center of mass of the diatomic molecule (BC). The internuclear distance in the diatomic molecule is r and the angle between the two coordinates is γ.

Jacobi coordinates is the most commonly used coordinate system for inelastic scattering processes (Figure 4). Here *r*, is the diatomic internuclear distance, *R* is the distance for the isolated atom to the center of mass of the diatomic molecule and the γ is the angle between *R* and *r*. *r* is the separation coordinate of the two atoms of the diatomic molecule and consequently, the energy Eigenfunctions of the isolated diatomic molecule form a natural basis set for the expansion of the full wave function.

The Schrodinger equation for a system of atom-diatom in the center of mass reference frame is

$$\widehat{H}\psi(R,r,E) = \left\{-\frac{\hbar^2}{2\mu_R}\nabla_R^2 - \frac{\hbar^2}{2\mu_r}\nabla_r^2 + V(R,r\,\gamma)\right\}\psi(R,r,E)$$

$$= E\,\psi(R,r,E) \tag{2.24}$$

The kinetic energy operators in the above *Eq* can be expanded as,

$$-\frac{\hbar^2}{2\mu_R}\nabla_R^2 = -\frac{\hbar^2}{2\mu_R}\left\{\frac{1}{R^2}\frac{\partial}{\partial R}R^2\frac{\partial\psi}{\partial R} + \frac{1}{R^2}\left[\frac{1}{\sin\theta_R}\frac{\partial}{\partial\theta_R}\left(\sin\theta_R\frac{\partial\psi}{\partial\theta_R}\right) + \frac{1}{sin^2\,\theta_R}\frac{\partial^2\psi}{\partial\phi_R}\right]\right\}$$

$$= -\frac{\hbar^2}{2\mu_R}\left\{\frac{1}{R^2}\frac{\partial}{\partial R}\left(R^2\frac{\partial}{\partial R}\right)\right\} + \frac{\hat{\ell}^2}{2\mu_R R^2} \tag{2.25}$$

$$-\frac{\hbar^2}{2\mu_r}\nabla_r^2 = -\frac{\hbar^2}{2\mu_r}\left\{\frac{1}{r^2}\frac{\partial}{\partial r}r^2\frac{\partial\psi}{\partial r} + \frac{1}{r^2}\left[\frac{1}{\sin\theta_r}\frac{\partial}{\partial\theta_r}\left(\sin\theta_r\frac{\partial\psi}{\partial\theta_r}\right) + \frac{1}{sin^2\theta_r}\frac{\partial^2\psi}{\partial\phi_r}\right]\right\}$$

$$= -\frac{\hbar^2}{2\mu_r}\left\{\frac{1}{r^2}\frac{\partial}{\partial r}\left(r^2\frac{\partial}{\partial r}\right)\right\} + \frac{\hat{j}^2}{2\mu_r r^2} \tag{2.26}$$

Where ℓ is the angular momentum of atom with respect to the diatomic molecule and *j* is the angular momentum of the diatomic molecule. μ_R, μ_r are the reduced masses of the atom relative to the diatom and the reduced mass of the diatomic, θ_R, ϕ_R are the polar and azimuthal angles of the vector R, respectively, θ_r, ϕ_r are those for the diatom internuclear axis.

Let us now imagine that if collision partners are far apart each other (*i.e.* $R\rightarrow\infty$), the interaction potential $V(R\rightarrow\infty, r,\gamma)$ no longer depends on the distance between the diatomic molecule and it is governed by only the diatomic potential due the vibrational motion, $V_{\text{diatom}}(r)$. The Schrodinger equation for the system becomes:

$$\lim_{R\to\infty}\left\{-\frac{\hbar^2}{2\mu_R}\nabla_R^2-\frac{\hbar^2}{2\mu_r}\nabla_r^2+V(R,r\,\gamma)\right\}\psi_{\mathrm{O}}(R,r,E)$$
$$=\left\{-\frac{\hbar^2}{2\mu_R}\nabla_R^2-\frac{\hbar^2}{2\mu_r}\nabla_r^2+V(R,r\,\gamma)\right\}\psi_{\mathrm{O}}(R,r,E)\;=\;E\,\psi(R,r,E)\quad(2.27)$$

Where the subscript "o" indicates the solution to the problem considered as there is no interaction between atom-diatom i.e. in the absence of interaction potential. In the limit of large *R*, the Hamiltonian and the wavefunction can be written as the product of a wave function in two vector coordinates R and r. $\chi_{vj}(r)\mathrm{Y}_{j,m_j}(\theta_r\,,\phi_r)$ is the wavefunction for the diatomic molecule where $\mathrm{Y}_{j,m_j}(\theta_r\,,\phi_r)$ is the spherical harmonics. The Eigenfunction of angular momentum operator which obeys the following equation:

$$\hat{j}^2\,\mathrm{Y}_{j,m_j}(\theta_r\,,\phi_r)=j(j+1)\hbar^2\,\mathrm{Y}_{j,m_j}(\theta_r\,,\phi_r)\qquad(2.28)$$

And the vibrational wavefunction $\chi_{vj}(r)$ obeys the following equation

$$\left[-\frac{\hbar^2}{2\mu_r}\left\{\frac{1}{r^2}\frac{\partial}{\partial r}\left(r^2\frac{\partial}{\partial r}\right)\right\}+\frac{j(j+1)\hbar^2}{2\mu_r r^2}+V_{diatom}(r)\right]\chi_{vj}(r)=\varepsilon_{vj}\,\chi_{vj}(r)\qquad(2.29)$$

Therefore, the overall wavefunction in the absence of the interaction potential can be written as a plane wave corresponding to the motion of atom-diatom collision system multiplied by the vibrational-rotational wavefunction.

$$\psi_o(R,r,E)=\left(\frac{k_{vj}\mu}{2\pi h^2}\right)^{1/2}e^{ik.R}\,\chi_{vj}(r)\mathrm{Y}_{j,m_j}(\theta_r\,,\phi_r)\qquad(2.30)$$

Unlike atom-atom collisions, a diatomic molecule has internal wavefunction and also possesses angular momentum. So large no of partial wave contributes expansion as we have discussed before.

Now, let us consider the wavefunction at large separations of the scattering partners. Assume that the colliding partners approach along space-fixed *Z*-axis, then the plane wave $e^{ik.r}$ becomes $e^{ik.z}$ and in analogy to $Eq.\,2.2$, we can write the asymptotic form of wave function at large separation as

$$\psi(R,r,E)\ \widetilde{R\to\infty}\ \left(\frac{k_{vj}\mu}{2\pi h^2}\right)^2\left[e^{ik_{vj}Z}\,\chi_{vj}(r)\,\mathrm{Y}_{j,m_j}(\theta_r,\phi_r)\right.$$

$$\left.+\sum_{v'j'm'} f_{v'j'm_j'\leftarrow vjm}(\theta_R,\phi_R)\frac{e^{ik_{v'j'}R}}{R}\,\chi_{v'j'}(r)\mathrm{Y}_{j',m_{j'}}(\theta_r,\phi_r)\right] \qquad (2.31)$$

where E is the total energy, $k_{vj}=\sqrt{2\mu(E-\varepsilon_{vj})}/\hbar$ is the wavenumber associated with the vibrational-rotational level v,j whose energy ε_{vj}, $f_{v'j'm_j'\leftarrow vjm}(\theta_R,\phi_R)$ is the scattering amplitude.

In $Eq.2.31$, the first term corresponds to an incident plane wave representing the two collision partners in their initial rovibrational quantum states moving in the positive Z direction. The second term describes about the scattered wave radially outwards with the diatom in all the possible final rovibrational quantum states.

Now, the inelastic differential cross section as the flux of collision partners in states $v'j'm_{j'}$ can be written according to the Eq 2.3 as:

$$\sigma_{v'j'm_j'\leftarrow vjm}(\theta_R,\phi_R,E)=\frac{k_{v'j'}}{k_{vj}}\left|f_{v'j'm_j'\leftarrow vjm}(\theta_R,\phi_R)\right|^2 \qquad (2.32)$$

In the present context, we need to consider the two different angular momenta, the orbital angular momentum ℓ, and rotational angular momentum j, they are not independent to each other as they are coupled by the interaction potential. So while breaking up the problem into more manageable parts, we must remember that the total angular momentum J is a good quantum number and a conserved quantity. Thus, we can break the problem into many small problems, one for each value of J.

In the absence of interaction potential, the first term of the Eq 2.31 would represent the solution to the scattering problem. The plane wave corresponds to this term can be expanded as below (see Eq 2.13),

$$e^{ikZ}=\sum_{\ell=0}^{\infty}\{4\pi(2\ell+1)\}^{\frac{1}{2}}i^{\ell}\,j_{\ell}(kR)Y_{\ell,0}(\theta_R,\phi_R) \qquad (2.33)$$

Using $Y_{\ell,0} = \left(\frac{2\ell+1}{4\pi}\right)^{\frac{1}{2}} P_\ell(\cos\theta)$ relation, combing 2.30 and 2.33 Eqs, solution of the problem in the absence of any potential

$$\psi_o(R,r,E) = \left(\frac{k_{vj}\mu}{2\pi h^2}\right)^2 \sum_{\ell=0}^{\infty}\{4\pi(2\ell+1)\}^{\frac{1}{2}}\, i^\ell\, j_\ell\left(k_{vj}R\right)\, \chi_{vj}(r) Y_{\ell,0}(\theta_R\,,\phi_R)\mathrm{Y}_{j,m_j}(\theta_r\,,\phi_r). \tag{2.34}$$

Where, the $Y_{\ell,0}(\theta_R\,,\phi_R)\mathrm{Y}_{j,m_j}(\theta_r\,,\phi_r) = Y_{\ell,0}\left(\hat{R}\right)\mathrm{Y}_{j,m_j}(\hat{r})$ form a natural basis set in which to expand the scattering problem. In order to utilize the conservation of the total angular momentum, we need to take the linear combination of these functions so as to get the value of total angular momentum.

Recalling Eq. 2.30, the above equation can be modified as the follows,

$$\psi_o(R,r,E) = \left(\frac{k_{vj}\mu}{2\pi h^2}\right)^2 \sum_{JM\ell}\{4\pi(2\ell+1)\}^{\frac{1}{2}}\, i^\ell\; j_\ell\left(k_{vj}R\right)\, \chi_{vj}(r)\mathrm{x}\;\; Y_{j\ell}^{JM}(\hat{R},\hat{r})(j\ell JM \mid jm_j\ell\; 0) \tag{2.35}$$

The last part of this equation will take care of the conservation of total angular momentum where, $(j\ell JM \mid jm_j\ell\; 0)$ are the Clesbsch - Gordan coefficients [20, 21]. The equations corresponds to the above equation are known as the coupled equations.

We now consider the matrix elements of the Hamiltonian operator of $Eq.$ 2.24 in this basis, the matrix elements of the kinetic energy operator $-\frac{\hbar^2}{2\mu_R}\nabla_R^2$ are

$$\langle \chi_{vj}(r)\;\; Y_{j\ell}^{JM}(\hat{R},\hat{r}) \mid \left[-\frac{\hbar^2}{2\mu_R}\nabla_R^2\right] \mid\; \chi_{v'j'}(r)\;\; Y_{j'\ell'}^{JM}(\hat{R},\hat{r})\rangle$$

$$= \left[-\frac{\hbar^2}{2\mu_R}\left\{\frac{1}{R^2}\frac{\partial}{\partial R}\left(R^2\frac{\partial}{\partial R}\right)\right\} + \frac{\ell(\ell+1)\hbar^2}{2\mu_R R^2}\right]\delta_{v,v'}\,\delta_{j,j'}\,\delta_{\ell,\ell'} \tag{2.36}$$

The matrix elements corresponds to the diatomic molecular Hamiltonian is given by

$$\langle \chi_{vj}(r)\;\; Y_{j\ell}^{JM}(\hat{R},\hat{r}) \mid (-\frac{\hbar^2}{2\mu_r}\nabla_r^2 + V_{diatom}(r) \mid\; \chi_{v'j'}(r)\;\; Y_{j'\ell'}^{JM}(\hat{R},\hat{r})\rangle \;=\; \varepsilon_{vj}\;\delta_{v,v'}\,\delta_{j,j'}\,\delta_{\ell,\ell'} \tag{2.37}$$

Now, total wavefunction can be expanded in a form similar to the Eq 2.35 but replacing $j_\ell(k_{vj}R)$ by $\frac{\phi^{Jvj\ell}_{v'j'\ell'}(R,E)}{k_{vj}R}$,

$$\psi\,(R,r,E) = \left(\frac{k_{vj}\mu}{2\pi h^2}\right)^2 \sum_{JM\ell}\{4\pi(2\ell + 1)\}^{\frac{1}{2}}\; i^{\ell}\left(j\ell JM \mid jm_j\ell\,0\right) \mathrm{x} \sum_{v'j'\ell'} \frac{\phi^{Jvj\ell}_{v'j'\ell'}(R,E)}{k_{vj}R}\;\chi_{v'j'}(r)\;\; Y^{JM}_{j'\ell'}(\hat{R},\hat{r})$$

(2.38)

$\phi^{Jvj\ell}_{v'j'\ell'}(R,E)$ are solutions of the set of coupled second order radial Schrodinger equations.

The above equation must obey the following boundary conditions:

$$\phi^{Jvj\ell}_{v'j'\ell'}(R,E)\;\widetilde{R\to 0}\quad 0$$

$$\phi^{Jvj\ell}_{v'j'\ell'}(R,E)\widetilde{R\to\infty}\;\hat{\jmath}_{\ell'}\left(k_{v'j'}R\right)\delta_{v,\;v'}\,\delta_{j,\;j'}\,\delta_{\ell,\;\ell'} - T^{J}_{v'j'\ell',vj\ell}\;\frac{1}{2i}\frac{k_{vj}}{k_{v'j'}}e^{i\left(k_{v'j'}-\frac{\ell'\pi}{2}\right)}$$

(2.39)

The alternative form of Riccati-Bessel functions [18] (see Eq 2.12) can be rewritten for the second boundary condition as

$$\phi^{Jvj\ell}_{v'j'\ell'}(R,E)\widetilde{R\to\infty} - \frac{1}{2i}\left\{e^{-i\left(k_{v'j'}R-\frac{\ell'\pi}{2}\right)}\delta_{v,\;v'}\,\delta_{j,\;j'}\,\delta_{\ell,\;\ell'} - S^{J}_{v'j'\ell',vj\ell}\left(\frac{k_{v'j'}}{k_{vj}}\right)^{1/2} e^{i\left(k_{v'j'}R-\frac{\ell'\pi}{2}\right)}\right\}$$

(2.40)

Therefore the *S* and *T* matrices are related as

$$S^{J}_{v'j'\ell',vj\ell} = \delta_{v,\;v'}\,\delta_{j,\;j'}\,\delta_{\ell,\;\ell'} - T^{J}_{v'j'\ell',vj\ell} \qquad (2.41)$$

The asymptotic form of full wavefunction can be obtained by substituting Eq 2.39 and 2.40 in Eq. 2.38,

$$\psi\,(R,r,E) = \left(\frac{k_{vj}\mu}{2\pi h^2}\right)^2 \sum_{JM\ell} \{4\pi(2\ell+1)\}^{\frac{1}{2}}\;\; i^{\ell}\,\left(j\ell JM \mid jm_j \ell\; 0\right)$$

$$\text{x}\;\left\{\sum_{v'j'\ell'} \frac{1}{k_{vj}R}\widehat{J_{\ell}}\left(k_{v'j'}R\right)\delta_{v,\;v'}\,\delta_{j,\;j'}\,\delta_{\ell,\;\ell'}\right.$$

$$\left. -\;T^{J}_{v'j'\ell';vj\ell}\;\frac{1}{2i}\;\frac{1}{\sqrt{k_{vj}k_{v'j'}}}\;\frac{1}{R}\;e^{i\left(k_{v'j'}R-\frac{\ell'\pi}{2}\right)}\right\}\;\chi_{v'j'}(r)\;\;Y^{JM}_{j'\ell'}\left(\widehat{R},\hat{r}\right)$$

(2.42)

The integral cross section can be written in terms of *T* matrix as follows

$$\sigma_{v'j'\leftarrow vj}\,(E) = \int \sigma_{v'j'\leftarrow vj}\,(\theta_R,\;\phi_R,E)\sin\theta_R\;\;d\theta_R\;d\phi_R$$

$$= \frac{1}{(2j+1)}\frac{\pi}{k_{vj}^2}\sum_{\ell'=|J-j|}^{|J+j|}\sum_{\ell=|J-j|}^{|J+j|}(2J+1)\left|T^{J}_{v'j'\ell';vj\ell}\right|^2$$

(2.43)

2.7 Solution of TISE in terms of hyper spherical coodinates

In the previous section, we have considered space-fixed coordinate system. According to this formalism, we have chosen that the *Z* axis is the direction of initial relative velocity. This resulted that there is no angular momentum component about the Z axis ($m_{\ell} = 0$). In contrast, the final relative velocity is in the direction of $\hat{R}$ and final Z component of the orbital angular momentum ranges over all possible values. Therefore, there must be a marked difference in the treatment of initial and final states of collisional system.

In the Body fixed reference frame, this difference vanishes as the Jacobi coordinate $\hat{R}$ is aligned along the Z axis.

In the body fixed formalism, this equation (2.42) is written in simple form in terms of Ω', is the helicity quantum number.

$$\sigma_{v'j'\Omega'\leftarrow vjm_j}\,(E) \;=\; \frac{\pi}{k_{vj}^2}\sum_{J}(2J+1)\left|T^{J}_{v'j'\Omega';vjm_j}\right|^2 \qquad (2.44)$$

This equation is for the state-to-state integral cross sections and is lot simpler than the space fixed case.

Quantum reactive scattering problems are often solved using hyperspherical coordinates and these coordinates are preferred over the Jacobi coordinates as they treat both reactants products on equal basis. There are several hyperspherical coordinates in the literature but we will use the base definitions on those of Pack and Parker [22]. These coordinates are related to each other by following relationships $\tilde{r}_\alpha = \rho \sin \alpha_\alpha$, $\tilde{R}_\alpha = \rho \cos \alpha_\alpha$, where $0 \leq \rho \leq \infty$ and $0 \leq \alpha_\alpha \leq \pi/2$. The hyperradius ρ and the angle α_α are called Delves coordinates [23, 24].

These can be written as follows

$$\rho = \left(\tilde{R}_\alpha{}^2 + \tilde{r}_\alpha{}^2\right)^{1/2}$$

$$\alpha_\alpha = \tan^{-1}\left(\frac{\tilde{r}_\alpha}{\tilde{R}_\alpha}\right)$$

Here we note that, $\tilde{R}_\alpha$ and $\tilde{r}_\alpha$ represent the mass-scaled Jacobi coordinates [22, 25] written for the arrangement channel α.

$$\tilde{R}_\alpha = d_\alpha R_\alpha$$

$$d_\alpha = \left[\frac{m_A}{\mu}\left(1 - \frac{m_A}{M}\right)\right]^{1/2}$$

Where, $M = m_A + m_B + m_C$ is the total mass of the triatomic system and the three body reduced mass, μ is

$$\mu = \left(\frac{m_A m_B m_C}{M}\right)^{1/2}$$

The three body reduced is same for all the arrangements.

We can now expand the wavefunction in terms of vibrational wavefunctions, $\chi^{J}_{vj\Omega}(\alpha\,;\,\rho)$ in the angular value α. These basis functions depends on the hyperradius ρ.

$$\psi\left(\tilde{R}_{\alpha},\tilde{r}_{\alpha},E\right)=2\sum_{JM}\sum_{\alpha'v'j'\Omega'}\sum_{\Omega}\left\{\sum_{\ell}(2\ell+1)^{\frac{1}{2}}\,(j\ell JM \mid jm_j\ell 0)\,B_{\ell,\Omega}\right\}\mathrm{x}\;\frac{\Gamma^{J\alpha vj\Omega}_{\alpha'v'j'\Omega'}(\rho,E)}{\rho^{5/2}}\;\frac{\chi^{J}_{\alpha'v'j'\Omega'}(\alpha_{\alpha};\,\rho)}{\sin 2\alpha_{\alpha}}\;\Xi^{JM}_{j\Omega}\left(\hat{\tilde{R}},\,\hat{\tilde{r}}'\right)$$

The vibrational functions $\chi^{J}_{vj\Omega}(\alpha\,;\,\rho)$ are solutions of the equation

$$\left\{\frac{\hbar^2}{2\mu\rho_s^2}\left[-\frac{\partial^2}{\partial\alpha_{\alpha}}+\frac{j_{\alpha}(j_{\alpha}+1)}{sin^2\alpha_{\alpha}}+\frac{J(J+1)+j_{\alpha}(j_{\alpha}+1)-2\Omega^2}{cos^{\,2}\,\alpha_{\alpha}}\right]V_{\alpha}^{diatom}\,(\rho_s\sin\alpha_{\alpha})-\varepsilon_{vj}(\rho_s)\right\}\chi^{J}_{vj\Omega}(\alpha\,;\,\rho)=0 \qquad (2.45)$$

The numerical approach to solve the above problem is to divide ρ into different segments and use one of the standard methods to solve these coupled differential equations. ρ_s represents the particular value of ρ in the center of segment *s*. We have used the log-derivative method by Manopolous in the study [26]. The potential $V_{\alpha}^{diatom}\,(\rho_s\sin\alpha_{\alpha})=V_{\alpha}^{diatom}\,(r_{\alpha_{\alpha}})$ is the asymptotic diatomic potential at a large R_{α}. Vibrational (*v*), rotational (*j*) and angular quantum number (Ω) are always associated with arrangement channel subscript α but omitted for brevity.

Delves hyperspherical coordinates depends on a particular arrangement that has been chosen. They don't treat all the channels in an equal manner. If one would like to use these coordinates, complicated arrangements have to be made to transform the wavefunction from one arrangement channel to another to account for a chemical reaction and to maintain the continuity of the wave function and its first derivative. For this reason, we need a universal coordinate system which is independent of arrangement channel.

In the arrangement channels, the Euler angles were chosen to bring body-fixed Z axis into coincidence with the Jacobi coordinates. This requirement can be satisfied using principal axes of inertia of the system to determine the orientation of the body fixed axes. Due to this adjustment, for small values of hyperradius, orientation of body-fixed coordinate does not

coincide with the Jacobi coordinates of any channels. However, at large value of the hyperradius, one of the coordinates will point along the Jacobi *R* vector, depending on the hyperangle. To do this exercise, we use adiabatically adjusting, principal axes hyperspherical (APH) coordinates [22]. Now, the body-fixed *Z* axis points along the Jacobi *R* vector of one of the arrangement channels.

We obtain the final expansion of the wave function in the body-fixed reference frame as

$$\Psi^{JM\Omega n} = 4\sum_{n'\Omega'} \frac{\psi^{J\Omega n}_{\Omega' n'}}{\rho^{5/2}} \phi^{J}_{\phi' n'}(\theta, \chi; \rho) D^{J^*}_{M,\Omega'}(\alpha_Q, \beta_Q, \gamma_Q)$$

The hyperradius ρ is divided into segments. At the center of each such segment we solve for the two dimensional hyperspherical surface functions $\phi^{J}_{\phi' n'}(\theta, \chi; \rho)$ which are dependent on ρ and satisfy the following differential equations

$$\left\{-\frac{\hbar^2}{2\mu\rho_s^2}\left[\frac{4}{\sin 2\theta}\frac{\partial}{\partial\theta}\sin 2\theta\frac{\partial}{\partial\theta}+\frac{1}{sin^2\theta}\frac{\partial^2}{\partial\chi^2}\right]+\frac{A+B}{2}\hbar^2 J(J+1)+\frac{15\hbar^2}{8\mu\rho_s^2}\right.$$
$$\left.+\left[C-\frac{(A+B)}{2}\right]\hbar^2\Omega^2+V(\rho_s,\theta,\chi)-\varepsilon^{J}_{\Omega n}(\rho_s)\right\}\phi^{J}_{\phi' n'}(\theta,\chi;\rho)=0$$

These differential equations in terms of hyperradius ρ was solved using Log-derivative propagation method and transformed into scattering matrix using space fixed coordinates.

The total reaction probability can be obtained from the scattering matrix as

$$P_{\alpha' v' j' \leftarrow \alpha v j}(E) = \sum_{\alpha' v' j' \leftarrow \alpha v j} \left|S^{J}_{\alpha' v' j' \leftarrow \alpha v j}(E)\right|^2 \tag{2.46}$$

Similarly rate coefficients for the reactive, inelastic and elastic processes can be obtained from the scattering cross sections by averaging over the relative velocity of the colliding pairs [7].

$$R(T) = \frac{\sqrt{8k_BT/\pi\mu}}{(k_BT)^2}\int_0^\infty E_{\alpha v j} e^{-\frac{E_{\alpha v j}}{k_BT}} \sigma_{v' j' \leftarrow v j}(E) dE_{\alpha v j} \tag{2.47}$$

The exponential factor here represents the relative velocities which are calculated from the Maxwell-Boltzmann distribution [27].

2.8 Quantum behavior as collision energy approaches to zero

Collision among the atoms and molecules in the ultracold regime are quite different from the collisions at room temperatures. The description to the cross sections due to the larger de Broglie wavelength given by Bethe [28] in 1935 for the scattering of cold neutrons. Such quantum effects are manifested in collisions of neutral particles at very low temperature, typically, T << 1K. The outcome of the elastic & inelastic collision play important role in the experimental realization of laser cooling and evaporative cooling techniques [29, 30].

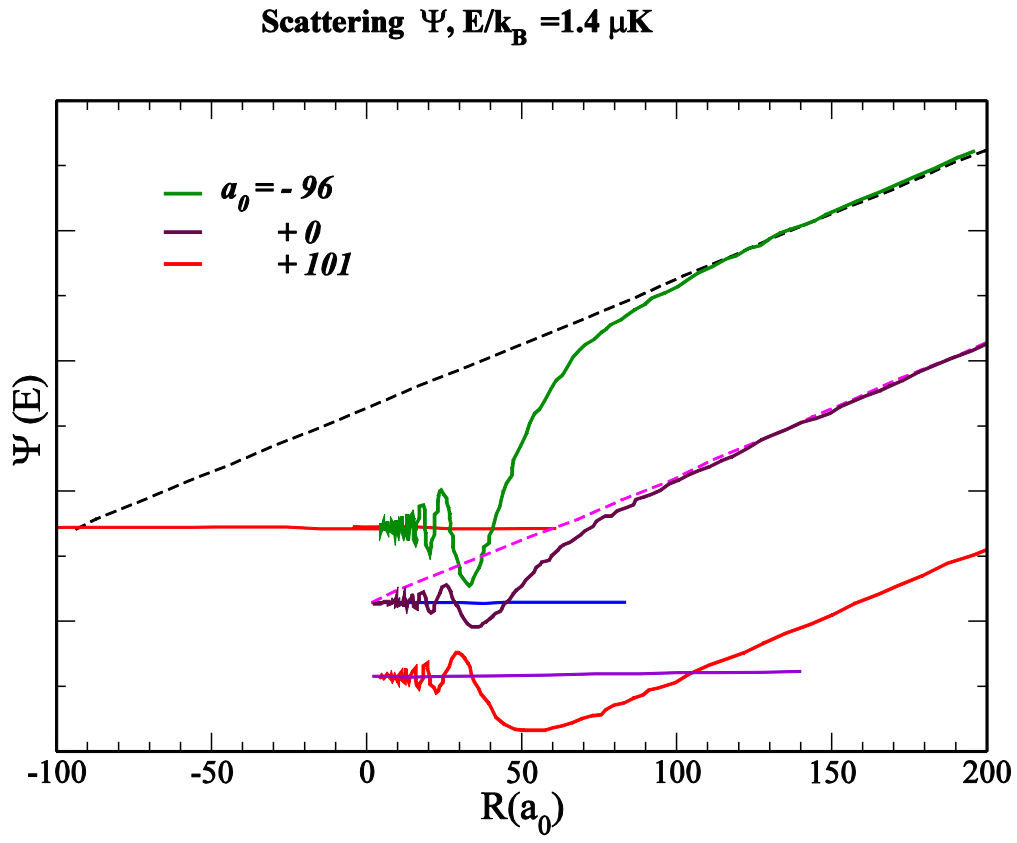

Figure 5: The short range wavefunction for three different potentials with three different scattering lengths (a_0)reproduced from the Ref. [14]

In the ultracold temperature limit the de Broglie wave length is much larger than the typical lengths associated with chemical bonds. The delocalization of collision wavefunction leads to have a behavior as $k = \sqrt{2\mu E} = {}^{\lambda}/_{2\pi}$ as $k \to 0$, depending on the long range potential which varies as R^{-n}.

According to Mott and Massey [31], *Eq* 2.23 the phase shift η_ℓ has the following property as $k \to 0$: if $2\ell < n - 3$,

$$\lim_{k\to 0} k^{2\ell+1} \cot \eta_\ell = \frac{-1}{a_\ell},$$

(2.47)

Where, a_ℓ is a constant and if $2\ell > n - 3$, this *Eq* would be

$$\lim_{k\to 0} k^{n-2} \cot \eta_\ell = constant \quad (2.48)$$

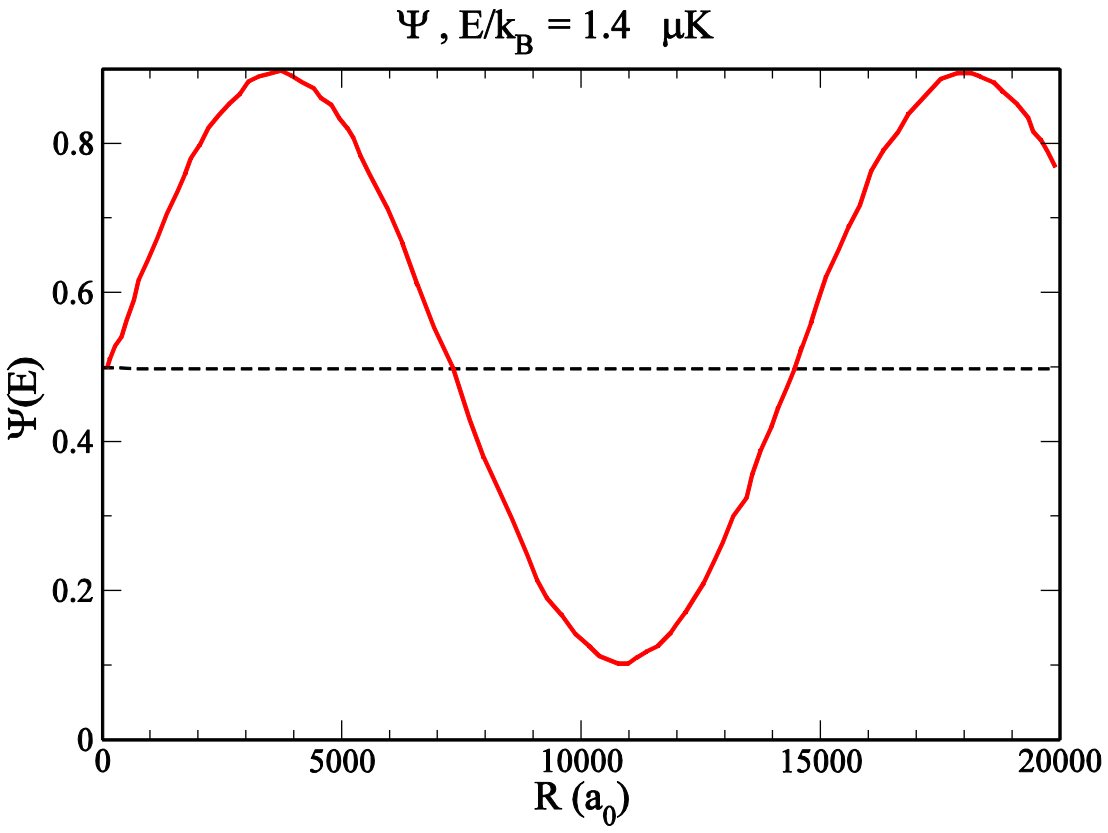

Figure 6: Asymptotic behavior of longrange part of the potential in the ultracold regime reproduced from the Ref the ref [14] .

This ensures that the phase shift vanishes as fast as k^3 for all $\ell \geq 1$ in case of neutral ground state atoms. Therefore, all the contributions to the cross section vanish when k becomes sufficiently small except the contribution from the *s-wave* i.e. $\ell = 0$. In this case the phase shift varies as $-ka_0$ as $k \to 0$. From the *Eq* 2.23, elastic cross section for identical particles as following [14],

$$\sigma(E) = 8\pi\, a_0^2 \quad (2.49)$$

Thus, the cross section for the elastic cross section is a constant quantity in the ulracold temperature limit. The quantity a_0 is the scattering length for the *s-wave* which is an important factor in the context of ultracold collisions. The rate coefficient for elastic process vanishes as $T^{1/2}$ in the limit of ultralow temperature ($K = \langle \sigma . v \rangle$).

Unlike elastic processes, inelastic process has different threshold properties. For exothermic reactions, i.e. the internal energy of separated atoms/molecules in the outgoing channel is lower than the entrance channel; the energy is released in the collision. The transformation matrix changes as [28, 32], $T(E) \propto k^{\ell+\frac{1}{2}}$, where ℓ is the individual partial wave index of the entrance channel. From the *Eq* 2.23, cross section vanishes as fast as k for all $\ell > 0$, but it varies as $1/k$ for the *s-wave*. This law sometimes called as inverse law of velocity [28, 32] . However, the cross section for inelastic process would become arbitrarily large as $k \to 0$.The rate coefficient K remains finite and approaches a non-vanishing constant.

2.9 Conclusions

A brief review of classical and quantum theories of atom-molecule collision theory have been presented. Classical theories consider all the atoms and molecules as billiard balls to estimate the rate coefficients at different temperatures. In quantum mechanical approach, all the atoms and molecules are treated as quantum mechanical waves. After briefly reviewing the atom-atom collisions we have extended discussion on atom-diatom molecular collisions using Delves hyperspherical coordinates. The calculation of the Scattering matrix (*s - matrix*) and all the dynamical parameters such as reaction probability, cross-sections and reaction rate coefficients has been discussed for ultra-low energy collisions.

2.10 References

[1] M.S. Child, Molecular collision theory, Courier Corporation 1996.

[2] W.R. Gentry, C.F. Giese, Ten-microsecond pulsed molecular beam source and a fast ionization detector, Review of Scientific instruments 49 (1978) 595-600.

[3] J.J. Lin, J. Zhou, W. Shiu, K. Liu, Application of time-sliced ion velocity imaging to crossed molecular beam experiments, Review of scientific instruments 74 (2003) 2495-2500.

[4] J. Vigué, Possibility of applying laser-cooling techniques to the observation of collective quantum effects, Physical Review A 34 (1986) 4476.

[5] A.D. McQuarrie, J.D. Simon, Physical Chemistry: a molecular approach, University Science Books 1997.

[6] K.J. Laidler, Chemical kinetics, Harper & Row, New York, 1987.

[7] G.G. Balint-Kurti, A. Palov, Theory of Molecular collisions, Royal Society of Chemistry 2015.

[8] P.T.M.e.T. Miyazaki, Atom Tunneling Phenomena in Physics, Chemistry and Biology, Springer-Verlag Berlin Heidelberg 2004.

[9] J.R. Hulett, Deviations from the Arrhenius equation, Quarterly Reviews, Chemical Society 18 (1964) 227-242.

[10] I. Simbotin, S. Ghosal, R. Cote, A case study in ultracold reactive scattering: D + H_2, Physical Chemistry Chemical Physics 13 (2011) 19148-19155.

[11] I.W. Smith, Low temperatures and cold molecules, World Scientific2008.

[12] R. Krems, B. Friedrich, W.C. Stwalley, Cold molecules: theory, experiment, applications, CRC press 2009.

[13] D.C. Clary, The theory of chemical reaction dynamics, Springer Science & Business Media 2012.

[14] J. Weiner, Cold and Ultracold Collisions in Quantum Microscopic and Mesoscopic Systems, Cambridge University Press 2003.

[15] L.I. Schiff, Quantum Mechanics 3rd, New York: M cGraw-Hill (1968) 61-62.

[16] L. Pauling, E.B. Wilson, Introduction to quantum mechanics with applications to chemistry, Courier Corporation 2012.

[17] I.N. Levine, D.H. Busch, H. Shull, Quantum chemistry, Prentice Hall Upper Saddle River, NJ 2000.

[18] M. Abramowitz, I.A. Stegun, Handbook of mathematical functions: with formulas, graphs, and mathematical tables, Courier Corporation 1964.

[19] P.M. Morse, H. Feshbach, Methods of theoretical physics, Technology Press 1946.

[20] R.N. Zare, Angular momentum: understanding spatial aspects in chemistry and physics, New York 1988.

[21] A.R. Edmonds, Angular momentum in quantum mechanics, Princeton University Press 2016.

[22] R.T. Pack, G.A. Parker, Quantum reactive scattering in three dimensions using hyperspherical (APH) coordinates. Theory, The Journal of chemical physics 87 (1987) 3888-3921.

[23] L.M. Delves, Tertiary and general-order collisions, Nuclear Physics 9 (1958) 391-399.

[24] L.M. Delves, Tertiary and general-order collisions (II), Nuclear Physics 20 (1960) 275-308.

[25] B. Johnson, On hyperspherical coordinates and mapping the internal configurations of a three body system, The Journal of Chemical Physics 73 (1980) 5051-5058.

[26] D. Manolopoulos, An improved log derivative method for inelastic scattering, The Journal of chemical physics 85 (1986) 6425-6429.

[27] McQuarrie, Physical Chemistry: A Molecular Approach, University Science Books; 1 edition 1997.

[28] H.A. Bethe, Theory of disintegration of nuclei by neutrons, Physical Review 47 (1935) 747.

[29] P.S. Julienne, F.H. Mies, Collisions of ultracold trapped atoms, JOSA B 6 (1989) 2257-2269.

[30] P.S. Julienne, A. Smith, K. Burnett, Theory of collisions between laser cooled atoms, Advances in atomic, molecular, and optical physics, Elsevier 1992, pp. 141-198.

[31] N.F. Mott, H.S.W. Massey, The theory of atomic collisions, Clarendon Press Oxford 1965.

[32] E.P. Wigner, On the behavior of cross sections near thresholds, Physical Review 73 (1948) 1002.

Chapter 3

Convergence studies of numerical parameters on D + H_2 (*v, j*) reaction in the ultracold temperature limit

3.1 Introduction

In the ultracold temperature limit, the translational kinetic energy between the colliding species becomes vanishingly small and the corresponding de Broglie wave length becomes extremely large. Thus, due to predominating quantum mechanical wave behavior, the colliding species can interact from very large internuclear distance. This leads to the crucial dependence of the reaction kinematics on the long range part of the interaction potential which can be manipulated using external electric, magnetic and optical fields. Though many dynamical observables can be estimated from the long range van der Waals coefficients of the interaction potentials, (*e. g.* using quantum defect theory [1, 2], accurate quantum mechanical treatment is required, particularly, at short internuclear distances where chemistry predominates in these extreme conditions.

The choice of time-independent quantum mechanical treatment is best suited to study ultracold collisions. Time-dependent wave packet methods become inefficient at ultra-low collision energies since it lacks required momentum to propagate the wave packet over the large special grid required to represent such systems. Several research groups have developed methods to solve multi-channel time-independent Schrödinger equation to carry out exact quantum mechanical calculations [3-6]. But, for most of them, obtaining numerical convergence still remains as the major issue for ultracold collisions. First, the nearly vanishing kinetic energy requires the solutions of the coupled equations to be propagated to very large asymptotic distances. Second, and more importantly, despite the fact that inelastic cross sections increase at low energy according to Wigner's threshold law [7], the scattering amplitudes themselves tend to vanish in the ultracold limit.

In order to obtain reliable results for these very small quantities, one needs a high level of numerical precision, which can be achieved mostly by drastically increasing the length of the radial propagation. Fulfillment of these two requirements will require an extremely large number of propagation steps. Moreover, in presence of any dynamical resonances, the scattering amplitudes abruptly changes to large values leading to divergence in numerical solutions. Though numerical convergence is routinely checked for reliable theoretical predictions, in this chapter, we will explicitly discuss some of the major numerical challenges

to study ultracold chemical reactions using quantum close coupling (CC) approach so that computational time can be minimized and optimum convergence is obtained.

In order to understand the various issues regarding convergence of the results obtained, we have performed numerous tests on several ultracold collisions, which were rather expensive, despite the current advances in computational power. We discuss our findings on the benchmark D + H_2 (v, j) $\rightarrow$ HD (v=0, j=0) + H ultracold collisions and its isotopic variations. Among these reactions of astrophysical interest, D + H_2 is particularly important, because it leads to the formation of most abundant interstellar coolant HD molecules [8, 9]. Thus, to model the interstellar cooling process, it is necessary to consider accurate temperature dependence of the rate coefficients for a wide range temperature. All possible initial rovibrational states of the reactant molecules are considered for this current study.

The convergence criteria strongly depend on the accuracy and long range part of the PES. Since H_3 system has been a subject of both experimental, theoretical research, studies on this reaction have led to significant advances in our understanding of gas-phase reaction dynamics. In the following, we have briefly reviewed the development of the potential energy of the H + H_2 (and its isotopic substitutions) over several decades. In 1973, Liu *et al* [10] have constructed the first *ab initio* studies of collinear H + H_2 potential energy surface (PES). Since then another four global analytic PESs of this system (namely the LSTH [10-13], DMBE [14], BKMP [15] and BKMP2 [16]) have been reported and used extensively in the field of chemical reaction dynamics. Each of these potential energy surfaces are partly build upon Liu's initial calculations. One of the disagreements with BKMP [15] and BKMP2 [16] PESs concerns the thermal rate coefficients for D + H_2 reaction at 200K. It has been found that at this low temperature, theoretical rate coefficients are higher than the experimental values by a factor of 2 [17-20]. After BKMP2 [16], Wu *et al* [21] constructed a new PES consisting of spline fitting of Extensive Quantum Monte Carlo Simulations (EQMS) of H_3 but is not as accurate as was originally believed.

In order to improve the longrange part of the potential, Mielke *et al* [22] in 2002 had reported a new PES which is believed to be more accurate for low energy collisions. This PES is based on multi-reference configuration interaction (MRCI) calculations using aug-cc-pVDZ, aug-cc-pVTZ and aug-cc-pVQZ basis sets for a set of 4067 H_3 configurations and convenient to use at any temperature.

3.2 Numerical calculations using modified reactive scattering program *ABC*:

The *ABC* reactive scattering code developed by Skouteris *et. al.* [3] has been used for a number of benchmark systems to study collisions at higher temperatures [23-28] and in the low temperature limit [29-34]. In order to use this program for ultra-low collision energies more efficiently, we have made substantial modifications in its structure, by including a new module which allows us to follow the convergence of the $S-matrix$ elements with respect to ρ_{max}. Given the fact that the ultracold calculations are quite time consuming, automated monitoring of the ρ_{max} convergence is extremely convenient, as we can study a series of collision energies and for a number of initial states H_2 (v, j) in a single run. Such a run, however, can take more than a week of CPU time repeated for different values of the other convergence parameters. We have also included a new module to stop and re-start the *ABC* program during propagation. This gives us the opportunity to stop the program at certain ρ if convergence is achieved or to propagate further if required for better convergence.

3.3 Convergence tests

We have used both BKMP2 [16] and the Mielke *et al* [22] PES for the various convergence tests, but extensive discussion obtained from the BKMP2 potential has been presented in this chapter. Comparison between the two PESs has been highlighted wherever the difference is significant.

Generally speaking, the main questions regarding convergence are: (i) if the target basis is large enough (ii) the integration step $\Delta\rho$ is small enough and (iii) if ρ_{max} large enough? The last question stems from simple considerations of energy scales; namely, we need to satisfy $\left|V_{nn'}(\rho)\right| \ll E_{kin}$ in the asymptotic region ($\rho \to \infty$). For scattering at high energy, these asymptotic conditions are easily fulfilled when ρ_{max} corresponds to separations of roughly 15–20 Bohr radii. However, in ultracold collisions, the initial kinetic energy in the entrance channel can be of the order of 1mK (10^{-7} eV) or even much smaller, and it required to propagate the numerical solutions far into the asymptotic region. For D + H_2 reaction, the convergence is obtained at $\rho_{max} = 50\ a.u.$ (atomic units, a_0), since the reduced mass of this system is small and the long range van der Waals forces are fairly weak for this reaction. Note that for other systems, *e.g.*, atom–atom scattering with heavy alkali species, the long

range interactions are much stronger and radial propagation needs to be calculated for distance of a few hundred Bohr radii. Also, the reduced mass of the binary collision has a compounding effect; indeed, when $E_{kin} \to 0$, the local momentum in the entrance channel is approximately given by $k_{loc}(\rho) \approx \sqrt{2\mu V(\rho)}$, and the enhancement coming from a large reduced mass needs to be compensated by the decrease of the diagonal potential $V(\rho)$ at larger distances.

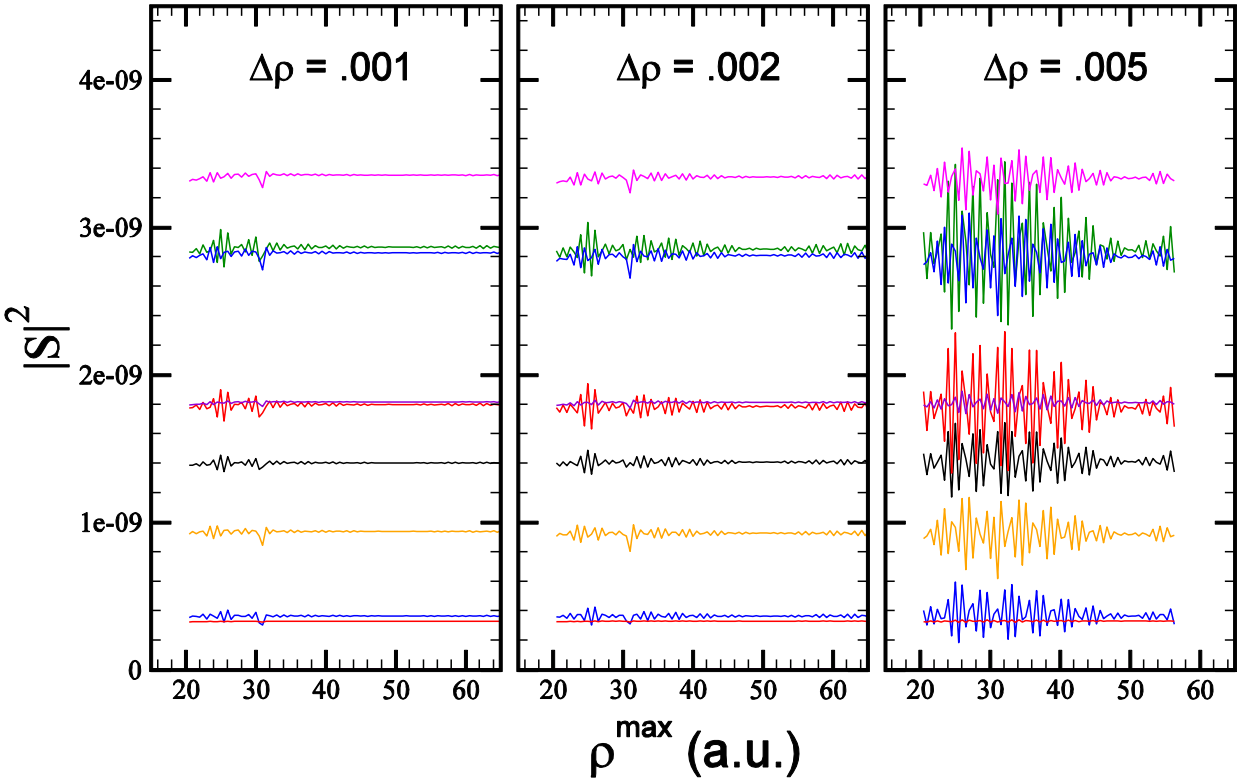

Figure 1: Convergence of $\Delta\rho$ with respect to ρ_{max} for different values of $\Delta\rho$.

We also need to pay special attention to the size of the integration step $\Delta\rho$. Indeed, in the ultracold regime, the amplitudes of the inelastic components of the scattering solution follow a simple scaling law, $\psi_n \sim k\,\psi$, assuming the normalization is such that the entrance (elastic) channel component oscillates with unit amplitude at $\rho \to \infty$.

Thus, relative to the asymptotic amplitude of the entrance channel component, all other components become vanishingly small when $k \to 0$. To ensure that we obtain reliable results, we have several test calculations which shows gradual improvement when the step size $\Delta\rho$ is reduced (see Figure 1).

Note that the propagation step has to be quite small (~ 0.002 a.u.) to reach full convergence. The results obtained with a slightly larger step size seem to oscillate around the converged values; however, care is needed, as the oscillations can have large amplitudes. Variable step size for the short and long-range of the potential could lead to better computational efficiency but we did not peruse this issue in the present study. We now consider the difficult question regarding the size of the target basis. Note that, in general, apart from the degrees of freedom of the target itself (*i.e.*, rovibrational motion of H_2 and DH), the so called target basis also includes one degree of freedom for the rotational part of the relative motion. As we mentioned, the approach employed in *ABC* uses Delves hyperspherical coordinates, in which different arrangements are treated separately with regards to the internal motion coordinates. For each arrangement, a basis is constructed depending mainly on two truncation parameters: E_{max}, and j_{max}. For a given initial dimer state [35] with channel energy ε_{vj}, the total collision energy is $E = \varepsilon_{vj} + E_{kin}$. In the ultracold regime E_{kin} is vanishingly small and all channels above the initial one are closed; indeed, there is no sufficient energy for their excitation, and the collision is completely exoergic. However, many of the closed channels play an important role, and we need to find out how many of them to include; hence, we repeat the computation for increased values of E_{max}, in order to obtain converged results. The truncation of channels is straightforward; namely, all channels with dimer eigenenergies bellow E_{max} are included, and all channels above E_{max} are ignored. In a similar fashion, the cutoff parameter j_{max} can be used to control the truncation of the number of rotational eigenstates of both dimers; however, in order to ensure that our computation is very nearly exact, we have eliminated the need for j_{max} by always including all j states that are energetically relevant (*i.e.*, all open and closed channels bellow E_{max} are included, no matter how large their quantum number j is).

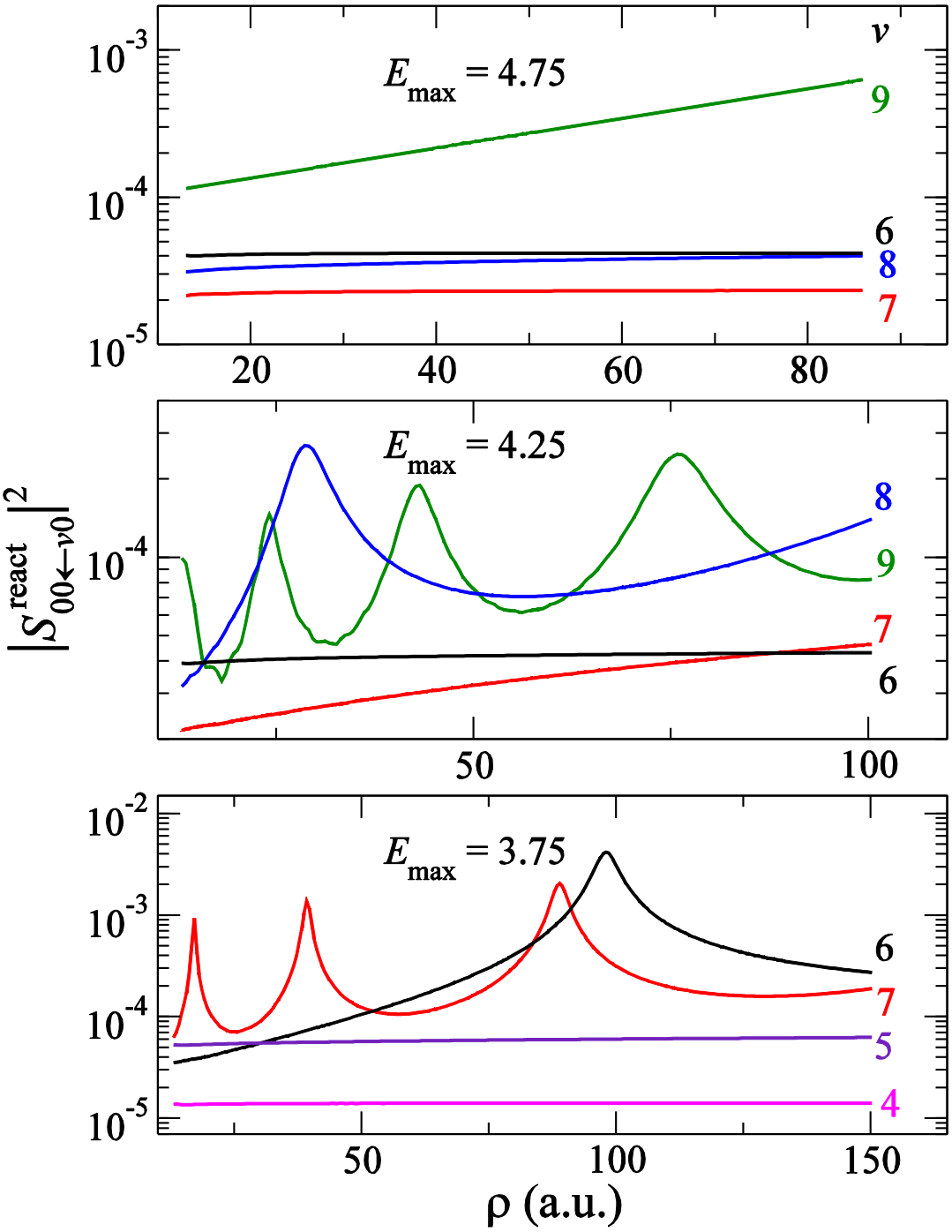

Figure 2: Convergence of S -matrix (squared) with respect to ρ_{max} for different values of E_{max}. we show results for a particular final state, namely DH ($v^{'}$ = 0, j$^{'}$ = 0) at a fixed collision energy E_{coll} = 1 μK; the state-to-state results for all other final states are similar. The different curves are for different initial states H_2 (v; j = 0) and each value of v is shown next to the corresponding curve.

Note that the dimer energy eigenbases are constructed from primitive particle-in-a-box bases, which depend on the size of the box in the radial-like coordinate for each dimer; also, there are additional parameters controlling the quadratures used in computing matrix elements, and we performed separate tests in which we varied these parameters. As expected, care is needed to ensure convergence with respect to the number of closed channels. This is especially

difficult for high vibrational states; not only does the size of the problem increase as we approach the threshold from $v = 0$, but we eventually need to include the dimer continuum (in a discretized fashion). We did attempt such a computation, but we obtained incorrect results; we speculate that this failure stems from an over completeness issue; in other words, there is too much linear dependence in the combined dimer bases of the separate arrangements. This obstacle could be circumvented, at least in principle, but we have not pursued this issue. The problem simply becomes prohibitively expensive when a significant part of the continuum needs to be included, and we decided to stop just shy of the threshold. With this elaborate caveat, we are now ready to present the concrete technical details of our results for $E_{\max}$ convergence.

In Figure 2, we show results from our convergence study for high vibrational initial states of H_2. It is readily apparent that the gradual improvement is rather slow when $E_{\max}$ is increased; *e.g.*, if we follow $v = 7$ in Figure 1, from the bottom panel to the top one, we see that its ρ_{max} behavior only shows stabilization for the highest cutoff energy used ($E_{\max} = 4.75$ eV, which was roughly at the dissociation threshold of the dimer). Note that we only obtained converged results for initial vibrational states $v \leq 8$. Regarding the difficulty of obtaining converged results for high v, we emphasize the strong connection between the $E_{\max}$ convergence and the ρ_{max} convergence, which is apparent in Figure 1. Strictly speaking, the stabilization of the results at large ρ_{max} does not guarantee convergence, but when the results remain unchanged for increased values of $E_{\max}$, we consider that we achieved convergence. As we see in Figure 1, the radial integration only needs to be propagated out to modest values of ρ_{max}, because the results stabilize rather quickly if $E_{\max}$ is sufficiently high. Conversely, if the results are not converged at these moderate distances, they cannot be improved by extending the propagation to larger distances, and it is very likely that $E_{\max}$ is simply too low. There is one exception to this empirical rule: if there is a resonance near the threshold, then it will amplify the long range sensitivity, and ρ_{max} will need to be much larger. Also, special attention needs to be paid to the diagonal matrix element for the entrance channel, as its complex phase $\varphi = \arg(S_{ee})$ is very sensitive to ρ_{max} even in the absence of dynamical resonances; this is well known from the simpler case of purely elastic (single channel) scattering.

In the pursuit of understanding the various aspects of convergence, we have amassed a substantial amount of numerical results, which we summarize in Figure 3. This graph contains another unpleasant surprise, this time regarding initial states with low v. In the

bottom right corner, we see that the results for $v = 0$ and $v = 1$ show a wild variation for large values of the truncation energy E_{max}.

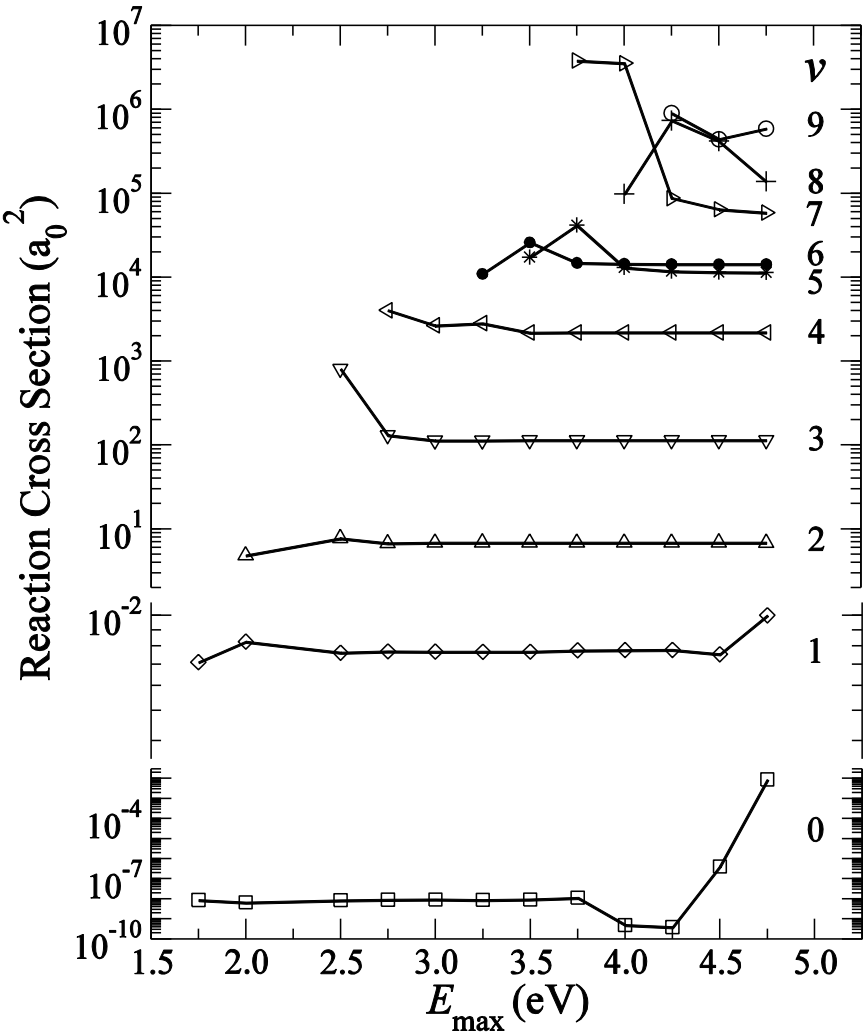

Figure 3: Variation of reaction cross sections of D + H_2 (v, j) reaction at fixed collision energy E_{kin} = 1 μK when increasing E_{max} up to 4.75 eV (near the continuum threshold of H2). The vibrational number of the initial dimer state is specified next to each curve. Note that the vertical axis is broken twice (below and above v = 1). Based on the convergence results shown in this graph, we determined which value of E_{max} is optimal for different initial v. Thus, we extracted our final results (shown in the Figures and table of Sec. 4) according to the following choices: E_{max} = 3:5 eV for $v \leq 2$, E_{max} = 4.25 eV for $3 \leq v \leq 6$, and E_{max} = 4.75 eV for $v \leq 7$.

This instability stems from the fact that the cross sections for the lowest vibrational states have extremely small values, and are thus very sensitive with respect to changing certain parameters of the numerical problem; specifically, those $S - matrix$ elements are very small become corrupted when the number of channels is increased above a certain value. With the benefit of hindsight, we can say that this anomaly should have been expected, especially for v = 0, however, despite this instability, there is still a plateau of converged results for E_{max} between 2.5 eV and 3.5 eV. Next, for intermediate values of the initial vibrational number (v = 2, 3, ….,7), we obtain converged results when the number of channels included

is sufficiently large, i.e., the results become stable when E_{max} is increased; as seen in Figure 3, they are much more robust than v = 0 and v = 1. For v = 8, the results barely begin to converge at E_{max} = 4.75 eV, judging by the ρ_{max} behavior in the top panel of Figure 2. We also obtained results for v = 9 (shown in Figures. 2 and 3) and v = 10, 11 (not shown), but they are not fully converged.

3.3 Conclusions

In this chapter, we have performed accurate close coupling calculations for numerical convergence of key parameters, *e.g.* extent of propagation along hyperradius, integration steps during propagation and size of the target basis functions *etc*. We have found to achieve convergence; large number of close collision channel needs to be included along with all open collision channels. This criterion sets an upper limit for the initial rovibrational levels of the colliding molecule that can be studied using this method. We have also developed a new module which allows us to monitor the convergence of the $S-matrix$ elements along hyperradius during propagation of the coupled-channel solutions. Using this new module, we can stop the program at certain value of hyper radius and restart to propagate further if required for better convergence. Given the fact, quantum close coupling calculations at ultra-low collision energies are very expensive due to very small integration steps required to achieve convergence, reduction in the extent of propagation alone can save significant amount of computational time.

3.4 References

[1] J.F.E. Croft, A.O.G. Wallis, J.M. Hutson, P.S. Julienne, Multichannel quantum defect theory for cold molecular collisions, Physical Review A 84 (2011) 042703.

[2] B. Gao, Universal Properties in Ultracold Ion-Atom Interactions, Physical Review Letters 104 (2010) 213201.

[3] D. Skouteris, J. Castillo, D. Manolopoulos, ABC: a quantum reactive scattering program, Computer Physics Communications 133 (2000) 128-135.

[4] T. González-Lezana, O. Roncero, P. Honvault, J.-M. Launay, N. Bulut, F. Javier Aoiz, L. Bañares, A detailed quantum mechanical and quasiclassical trajectory study on the dynamics of the H+ + $H_2 \rightarrow H_2$ + H+ exchange reaction, The Journal of Chemical Physics 125 (2006) 094314.

[5] T.V. Tscherbul, R.V. Krems, Quantum theory of chemical reactions in the presence of electromagnetic fields, The Journal of Chemical Physics 129 (2008) 034112.

[6] M. Warehime, M.H. Alexander, A MATLAB-based finite-element visualization of quantum reactive scattering. I. Collinear atom-diatom reactions, The Journal of Chemical Physics 141 (2014) 024118.

[7] E.P. Wigner, On the Behavior of Cross Sections Near Thresholds, Physical Review 73 (1948) 1002-1009.

[8] S. Glover, T. Abel, Uncertainties in H_2 and HD chemistry and cooling and their role in early structure formation, Monthly Notices of the Royal Astronomical Society 388 (2008) 1627-1651.

[9] P. Stancil, S. Lepp, A. Dalgarno, The deuterium chemistry of the early Universe, The Astrophysical Journal 509 (1998) 1.

[10] B. Liu, Ab initio potential energy surface for linear H_3, The Journal of Chemical Physics 58 (1973) 1925-1937.

[11] P. Siegbahn, B. Liu, An accurate three-dimensional potential energy surface for H3, The Journal of Chemical Physics 68 (1978) 2457-2465.

[12] D.G. Truhlar, C.J. Horowitz, Functional representation of Liu and Siegbahn's accurate abinitio potential energy calculations for H + H_2, The Journal of Chemical Physics 68 (1978) 2466-2476.

[13] D.G. Truhlar, C.J. Horowitz, Erratum: Functional representation of Liu and Siegbahn's accurate abinitio potential energy calculations for H + H_2, The Journal of Chemical Physics 71 (1979) 1514-1514.

[14] A.J. Varandas, F.B. Brown, C.A. Mead, D.G. Truhlar, N.C. Blais, A double many-body expansion of the two lowest-energy potential surfaces and nonadiabatic coupling for H_3, The Journal of Chemical Physics 86 (1987) 6258-6269.

[15] A.I. Boothroyd, W.J. Keogh, P.G. Martin, M.R. Peterson, An improved H3 potential energy surface, The Journal of chemical physics 95 (1991) 4343-4359.

[16] A.I. Boothroyd, W.J. Keogh, P.G. Martin, M.R. Peterson, A refined H_3 potential energy surface, The Journal of chemical physics 104 (1996) 7139-7152.

[17] B. Ridley, W. Schulz, D. Le Roy, Kinetics of the Reaction D + $H_2 \rightarrow$ HD + H, The Journal of Chemical Physics 44 (1966) 3344-3347.

[18] A. Westenberg, N. De Haas, Atom—Molecule Kinetics Using ESR Detection. II. Results for D + $H_2 \rightarrow$ HD + H and H + $D_2 \rightarrow$ HD + D, The Journal of Chemical Physics 47 (1967) 1393-1405.

[19] D. Mitchell, D.L. Roy, Rate Constants for the Reaction D + $H_2 \rightarrow$ DH + H at Low temperatures using ESR Detection, The Journal of Chemical Physics 58 (1973) 3449-3453.

[20] J. Michael, J. Fisher, Rate constants for the reaction D + H_2 yields HD + H, over the temperature range 655-1979 K, by the flash photolysis-shock tube technique, Journal of Physical Chemistry;(USA) 94 (1990).

[21] Y.-S. Wu, J. Anderson, A very high accuracy potential energy surface for H_3, Physical Chemistry Chemical Physics 1 (1999) 929-937.

[22] S.L. Mielke, B.C. Garrett, K.A. Peterson, A hierarchical family of global analytic Born–Oppenheimer potential energy surfaces for the H + H_2 reaction ranging in quality from double-zeta to the complete basis set limit, The Journal of chemical physics 116 (2002) 4142-4161.

[23] M.P. de Miranda, D.C. Clary, J.F. Castillo, D.E. Manolopoulos, Using quantum rotational polarization moments to describe the stereodynamics of the H + D_2 (v = 0, j = 0) → HD (v', j')+ D reaction, The Journal of chemical physics 108 (1998) 3142-3153.

[24] J. Aldegunde, P. Jambrina, V. Sáez-Rábanos, M.P. de Miranda, F. Aoiz, Quantum mechanical mechanisms of inelastic and reactive H + D_2 (v = 0, j = 2) collisions, Physical Chemistry Chemical Physics 12 (2010) 13626-13636.

[25] J.F. Castillo, D.E. Manolopoulos, K. Stark, H.J. Werner, Quantum mechanical angular distributions for the F + H_2 reaction, The Journal of chemical physics 104 (1996) 6531-6546.

[26] J. Castillo, D. Manolopoulos, Quantum mechanical angular distributions for the F + HD reaction, Faraday Discussions 110 (1998) 119-138.

[27] D. Skouteris, D.E. Manolopoulos, W. Bian, H.-J. Werner, L.-H. Lai, K. Liu, van der Waals Interactions in the Cl + HD Reaction, Science 286 (1999) 1713-1716.

[28] T. Yang, J. Chen, L. Huang, T. Wang, C. Xiao, Z. Sun, D. Dai, X. Yang, D.H. Zhang, Extremely short-lived reaction resonances in Cl + HD (v = 1)→ DCl + H due to chemical bond softening, Science 347 (2015) 60-63.

[29] N. Balakrishnan, A. Dalgarno, Chemistry at ultracold temperatures, Chemical physics letters 341 (2001) 652-656.

[30] N. Balakrishnan, On the role of van der Waals interaction in chemical reactions at low temperatures, The Journal of chemical physics 121 (2004) 5563-5566.

[31] E. Bodo, F.A. Gianturco, A. Dalgarno, The reaction of F + D_2 at ultra-low temperatures: the effect of rotational excitation, Journal of Physics B: Atomic, Molecular and Optical Physics 35 (2002) 2391.

[32] G. Quéméner, N. Balakrishnan, Cold and ultracold chemical reactions of F + H Cl and F + D Cl, The Journal of chemical physics 128 (2008) 224304.

[33] J. Aldegunde, J. Alvarino, M. de Miranda, V. Sáez Rabanos, F. Aoiz, Mechanism and control of the F + H_2 reaction at low and ultralow collision energies, The Journal of chemical physics 125 (2006) 133104.

[34] T. Roy, S. Mahapatra, H + LiH^+ collision dynamics at ultracold temperature conditions, Chemical Physics 448 (2015) 34-42.

[35] S.L. Mielke, G.C. Lynch, D.G. Truhlar, D.W. Schwenke, Ab initio chemical kinetics: Converged quantal reaction rate constants for the D + H_2 system, The Journal of Physical Chemistry 98 (1994) 8000-8008.

Chapter 4

Dynamics of D + H_2 ($v = 0, j = 0$) → H + HD ($v = v', j = j'$) reaction from ultracold to thermal temperature limit

4.1 Introduction

The reaction of Deuterium (D) with H_2 is one of the most important processes of the early universe [1-4]. Therefore, the knowledge of accurate rate coefficients for a wide range of temperature is of interest for modeling many astrophysical processes, such as, interstellar cooling and star formation. This reaction is exothermic (by ~ 0.035 eV) with a potential barrier of 9.6 kcal/mol (0.4 eV) [5]. Because of this high energy barrier, at low temperature ($T \leq 1K$) the reaction mainly goes through quantum mechanical tunneling. While experimental studies on thermal rate coefficients of this reaction have been reported at higher temperatures [6-8], no measurements have been carried out below T ~ 170 K. Accurate quantum mechanical studies have been performed for extremely low temperatures (at ~ lμ K) [9-11] and also, at higher temperatures [9, 12, 13], but no reports have been found to estimate accurate rate coefficients in the intermediate temperature range where deviation from usual Arrhenius behavior is observed and quantum mechanical tunneling effect starts to dominate.

In the view of interstellar processes in the early universe, reactions involving the formation of H_2 and destruction of H_2 molecule have lot of importance due to its simple electronic structure and abundance. Reactions involving molecular H_2 and its isotopic variants have contributed the most to interstellar cooling. The cooling efficiency, *i.e.* how much energy is lost per second at a particular temperature, is defined as cooling functions for a particular species [14]. To calculate the cooling functions, the knowledge of state-to-state rate coefficients is needed from for a wide range of temperatures *i.e.* very high to low temperature range for several chemical reactions leading to formation and destruction of those species. The radiative cooling functions are later coupled with the fractional abundance of that particular species in order to obtain the overall evolution of the interstellar medium. In this chapter, the results are presented in three parts; the first part describes our new finding in the ultracold regime ($1\mu K - 1K$) followed by the intermediate low temperature region ($1 - 20K$) and later the dynamics of D + H_2 in thermal temperature regime (20-500K). The reaction probability, cross sections and accurate rate coefficients of the D + H_2 reaction connecting all three temperature range have been presented in the following.

4.2 The reactive scattering dynamics of D+H_2 reaction in the ultracold temperature limit ($< mK$)

Owing to its simplicity, D + H_2 ($v = 0, j = 0$) → HD ($v = v', j = j'$) reaction has become the bechmark system to study the dynamics at higher energy regime. But in the subkelvin (~10^{-6}K) region, it is extremely sensitive to the interaction potential energy surface of this reaction. In the view of electronic structure calculations, this system is smaller which made the computations feasible for an accurate potential energy surfaces [5, 15]. The results presented here are using the theoretical formalism developed in chapter-2.

The role of initial rovibrational states of reactant molecule (H_2) in the ultralow energies is significant and important to understand. As discussed in the previous chapter, we have optimized all the numerical parameters and it has been found that the results are not converged for higher vibrational levels ($8 \leq v \leq 14$). Since the problem becomes computationally too expensive beyond $v \geq 7$, we restrict our calculations to v = 0-7, $j = 0$ initial states of H_2. Only single partial wave ($\ell = 0$, *s-wave*) is dominant in the subkelvin temperature regime, thus, the contribuion form the total angular momentum $J = j = 0$ only needed to be included.

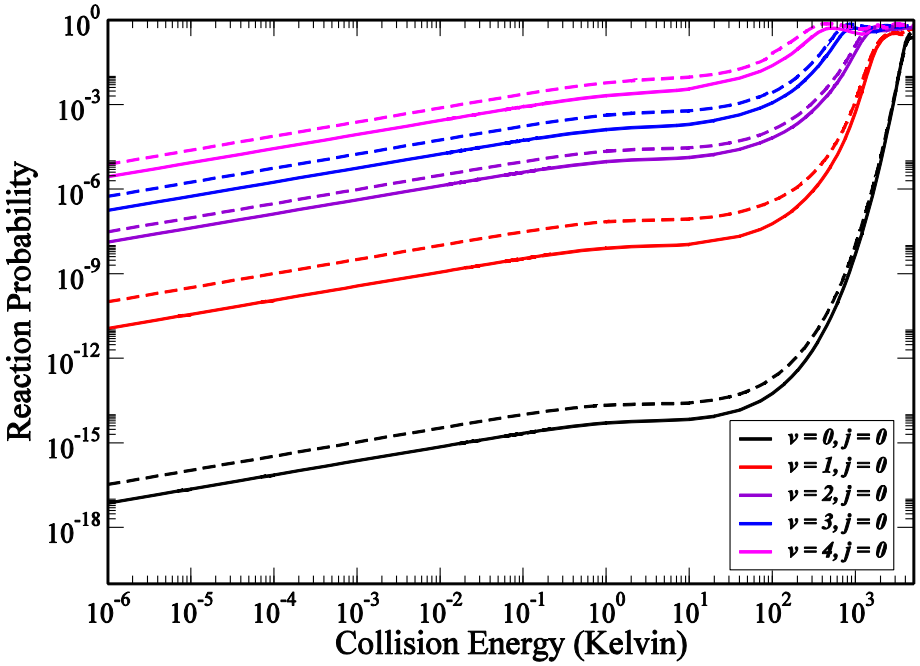

Figure 1 : Reaction probability is plotted against collision energy (Kelvin) of initial vibrational states ($v = 0$ *to* $v = 4$) of H_2 molecule. (Solidline is for Mielke *et al* [15] and dotted lines for BKMP2 [16])

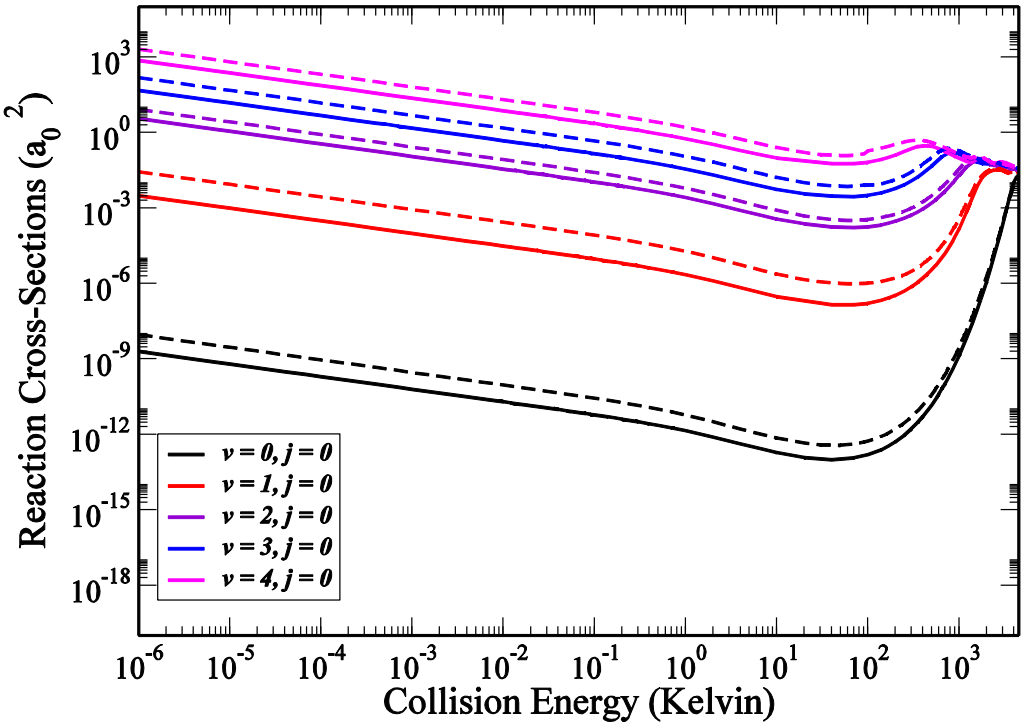

Figure 2: Reaction cross section is plotted as a function of collision energy (Kelvin) for different vibrational states (v = *0 to* v = *4*) of H_2 molecule calculated using Eq 2.2.43.

In Figure 1, the probabilities for the reactive process *i.e.* the formation of HD molecule as a function of collision energy of the respective initial states has been presented. The corresponding initial rovibrational levels of H_2 molecule have been shown in the legend. We have used both BKMP2 [16] and potential reported by Mielke *et al* [15] for our calculations and show as dashed and solid lines, respectively. The reaction probabilities are calculated from the respective *S*-matrix elements as

$$P = \sum_{k=-\min(J,j)}^{\min(J,j)} \left(\frac{2\ell+1}{2J+1}\right)^{\frac{1}{2}} \sum_{J,v'j'} \left|S^J_{\alpha vj\to\alpha' v' j'}E(\alpha vj)\right|^2$$

where, the sum is extended over all the inelastic and reactive channels for the final states of H_2 (j', $v' < v$) and HD (v', j') of a particular arrangement (α v j). We have chosen the initial rotational state of H_2 to be j = 0 only, while v represents its initial vibrational state.

For low values of v, we distinguish two very different regimes in Figure 1; at very low collision energy ($E_{coll} < 100\ mK$), where Wigner's threshold laws are applicable followed

by a transition into the barrier dominated regime ($E_{coll} \approx 0.1 - 100K$). The thermal temperature regime can be considered above $100K$. The reaction probabilities behave as $E_{kin}^{1/2}$ in the log-log plot at very low energies; this power law behavior is the manifestation of the Wigner threshold laws which produced straight lines in the log-log plot with a slope of ½ in Figure 1. This consequence stems from the simple energy scaling of a wave function at vanishing collision energy.

It is evident that, even with vanishingly small collision energies, the reaction can proceed through quantum mechanical tunneling. But due to the large energy barrier of reaction, the reaction probabilities are greatly reduced for the rovibrationally ground state of H_2 molecule. For collisions with D + H_2 (v = 0, j = 0), only three channels in the product arrangement HD (v' = 0, j' = 0, 1, 2) are open, thus the curve corresponding to v = 0, j = 0 represent the total inelastic probabilities. Reaction starting from all other initial states of H_2, quenching to states of D + H_2 ($v \neq v', j'$) should be included to estimate the total inelastic probabilities, but we focus here mainly on reaction probabilities as quenching probabilities are extremely low at ultra-low collision energies and thus, not shown here.

In Figure 2, we have shown the collision energy dependence reaction cross sections for the initial vibrational states of H_2 molecule. According to Wigner's threshold law, cross section depends on the kinetic energy as $\sigma_{inel} \propto 1/\sqrt{E_{coll}}$ for the inelastic and reactive collisions. As shown in the reaction probabilities, the reaction cross sections also have two different regimes: (i) Wigner's regime (ii) Barrier dominated regime and they are distinguished clearly. In the Wigner's regime at very low collision energies, reaction happens through quantum mechanical tunneling. Unlike the reaction probabilities, the reaction cross section behave $E_{Coll}^{-1/2}$ according to Wigner's threshold laws and thus produce a straight line with slope of -1/2 in the log-log plot as shown in Figure 2. As the internal collision energy of interacting particles increase the reaction proceeds through crossing over the potential barrier.

Using the inelastic cross sections in the ultracold regime, we have calculated the rate coefficients of this reaction in the ultracold temperature limit. As the rate coefficient is expressed as the average of the corresponding cross section multiplied by the relative velocity of the collision fragments: $K = \langle v_{rel}.\sigma \rangle$. If the temperature is low enough (T ≤ 0.1K), the velocity distribution of the colliding particles will be confined to a narrow collision energy range and in the Wigner's regime the product of $v_{rel}\,\sigma$ would become independent of the

relative velocity. Thus, in the Wigner regime, the rate coefficients would become independent of temperature and attains a constant value.

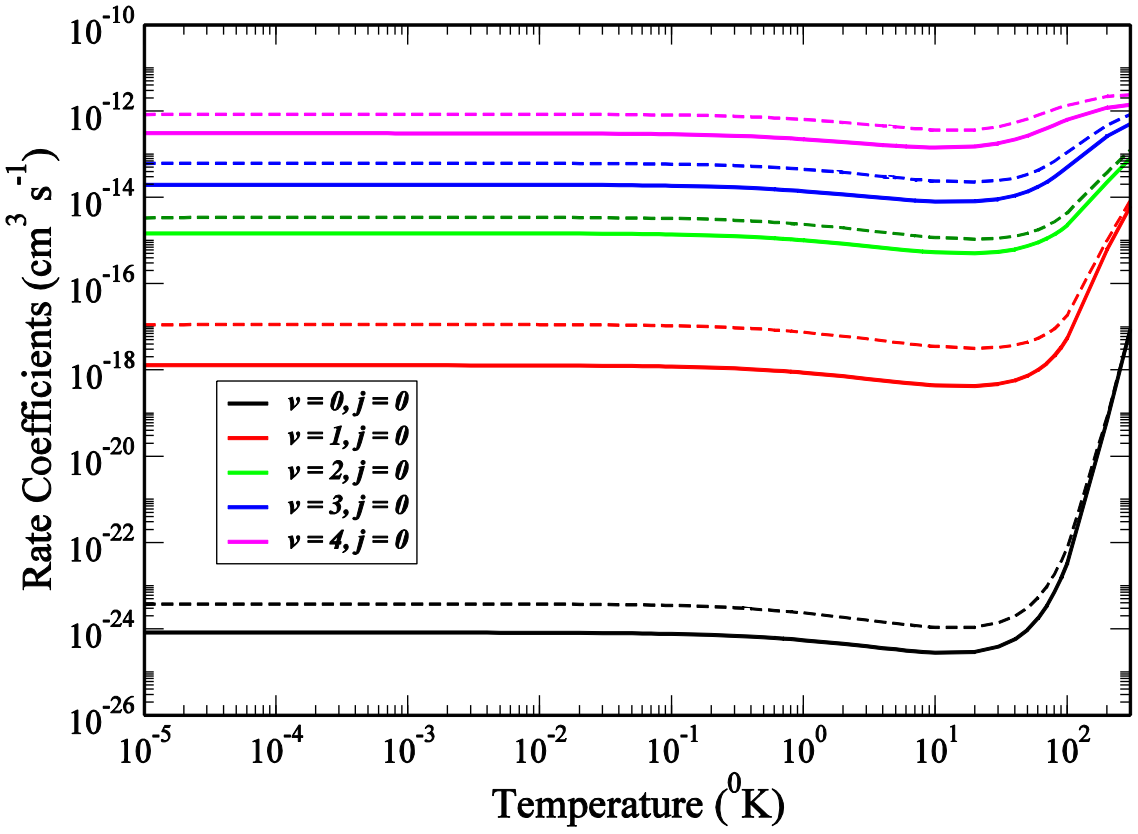

Figure 3: Rate coefficients for D + H_2 reactionobtained by multiplying the cross section with the average velocity obtained from the Boltzmann distribution function. (Solidline is for Mielke *et al* [15] and dotted lines for BKMP2 [16] potentials)

In Figure 3**,** we have plotted rate coefficients against temperature for different initial vibrational channels of H_2 molecule in the Wigner's regime. They have been calculated using following formula.

$$R(T) = \frac{\sqrt{8k_BT/\pi\mu}}{(k_BT)^2}\int_0^\infty E_{\alpha vj}\, e^{\frac{-E_{\alpha vj}}{k_BT}}\, \sigma_{\alpha vj\to\alpha' v' j'}(E_{\alpha vj})\, dE_{\alpha vj}$$

It can be seen that the rate coefficients become temperature independent in the Wigner's regime. For v = 0, the rate coefficient is extremely small because of the presence of reaction barrier as discussed in case of Figure 2. For $v \geq 5$, barrier height diminishes gradually and it would behave as barrier less reaction from v = 6 and above. We note that the increase in ultracold rate coefficients due to vibrational excitation is more than ten orders of magnitude

which may significantly influence the modeling outcome of the interstellar cooling process if included.

4.3 Dynamics of D + H_2 (v, j = 0) → HD (v', j') + H reaction in the intermediate low temperature (~1K- 10K) region

To study the state-to-state reactive scattering dynamics at higher temperatures, we have followed the time-independent quantum mechanical close coupling (CC) approach as described in Chapter 2. At higher temperatures, (T $\geq$ 100 mK), available kinetic energy can overcome the centrifugal barriers, thus contributions from higher partial waves needs to be considered. In *ABC* reactive scattering code, the angular momentum basis functions are used in terms of helicity quantum numbers (k) rather than the orbital angular momentum quantum number (ℓ). Thus, for $\ell > 0$ calculations, angular momentum basis functions are regenerated from helicity basis through othrogonal transformation [25]

$$\Psi_{j\ell}^{JM} = \sum_{k=-\min(J,j)}^{\min(J,j)} \left(\frac{2\ell+1}{2J+1}\right)^{\frac{1}{2}} C(j\ell J; k0k)\, \Psi_{jk}^{JM}$$

Where the notations carry the usual meaning. Note that, for large values of J, to keep the total number of collision channels within computational limit, k is truncated such that $k \leq \min(J, j, k_{max})$, where, k_{max} is another parameter (usually within 4–6) as numerically tested for convergence in Chapter 3.

To ensure convergence the cut-off energy (E_{max}) for the rovibrational basis sets is chosen to be 3.0 eV and all rovibrational channels below E_{max} in the reactant and product arrangement are included in the dynamical calculations. Contributions from higher partial waves are extended to total angular momentum $J_{max} \geq 35$ with helicity truncation at $k_{max} \geq 6$. This leads to inclusion of maximum 1039 channels for each full dimensional CC calculations.

The coupled equations are propagated up to maximum hyperradius (ρ_{max}) ~ 50 a_0 using small integration steps $d\rho = 0.02\, a_0$ for collision energy $E_{coll} \geq 20$ K and $d\rho = 0.002\, a_0$ for $E_{coll}^{vj} < 20\, K$. For Mielke *et al* PES [15], the solution needs to be propagated until ρ_{max} ~100 a_0 with $d\rho = 0.002\, a_0$

According to our numerous test calculations, these parameters are sufficient to achieve numerical convergence for studying reactive collisions for D + H_2 (v = 0 – 1, j) up to collision energy E_{coll}^{vj} ~ 11000 K (~1 eV).

We have also calculated the reaction cross sections for rotationally excited stat j = *1*. Rotational excitation requires additional partial waves (ℓ = 1) and thus computationally more expensive. There are no significant changes in the overall behavior of the reaction cross sections with rotationally excited states (see Figure 4). Contribution from higher rotational states are discussed in detail in the next section.

The reaction probabilities and cross sections for vibrationally excited states are shown in Figure 5 and 6 respectively. Inclusion of higher partial waves leads to increased reaction cross section (and reaction probabilities) near collision energies $E_{coll} \sim 10^{-3} - 10^{-1}\ K$. This is due to possible $p - wave$ resonances which is more prominent for reaction initatiated from D + H_2 (v = *1*, j = *0*).

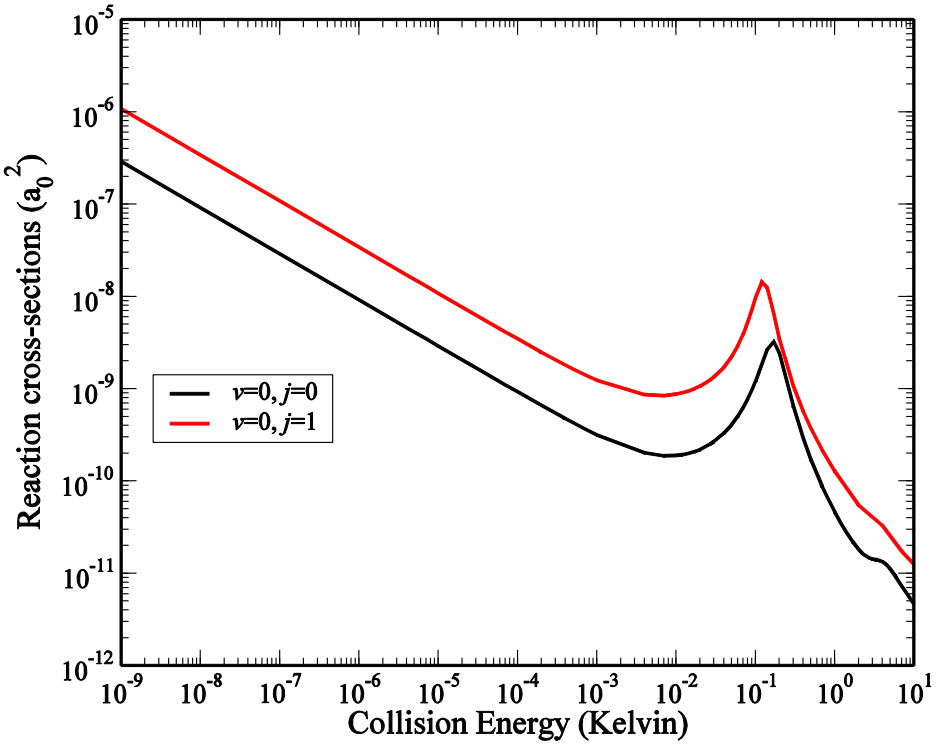

Figure 4: Collision energy dependence of reaction cross sections of D + H_2 (v, j) collisions. Initial rovibrational states are indicated in the legend. Note that for v =0 , j = 0, all open channels leads to the formation of product HD (v', j') + H, whereas, for v = 0, j = 1, quenching cross sections to D+H_2 (v =*0*, j = *0*) state is also included.

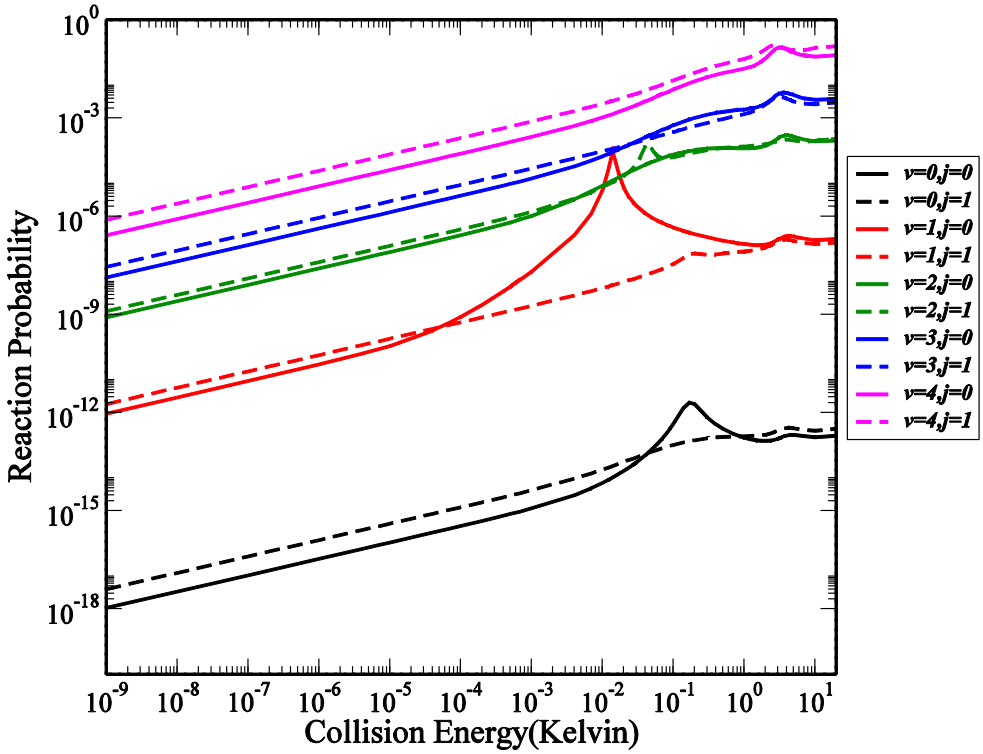

Figure 5: Reaction probability is plotted against collision energy (Kelvin) for the different initial rovibrational ($v, j = 1$) quantum states of HD molecule.

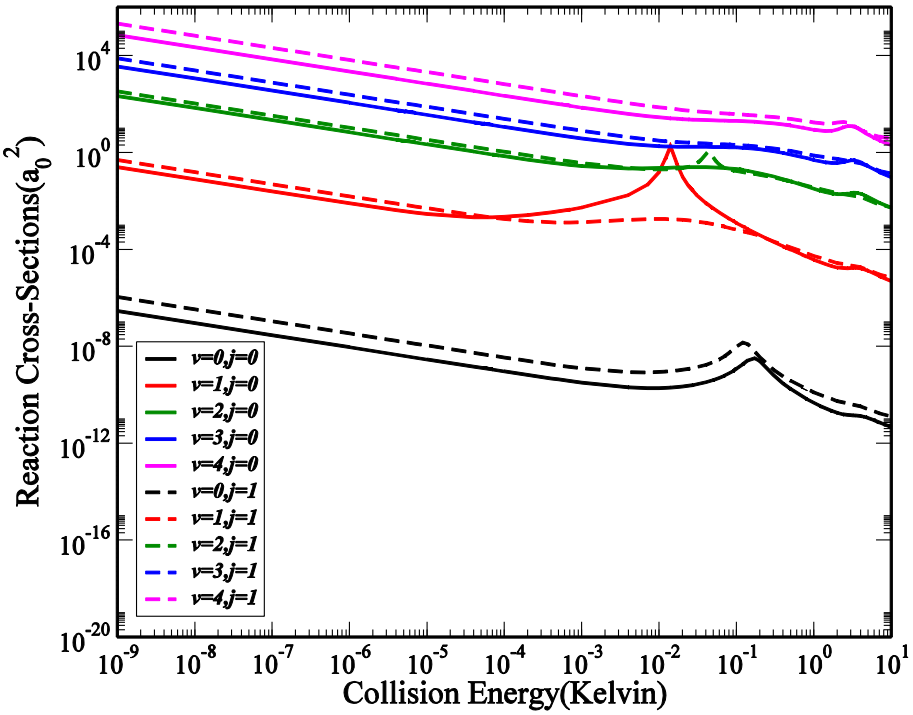

Figure 6: Reaction cross section is shown as the function of Collision energy(Kelvin) for the different initial rovibrational ($v, j = 1$) quantum states of HD molecule. (Solidline is for Mielke *et al* [15] and dotted lines for BKMP2 [16])

To understand the origin of the observed resonance, we analyze the individual from the *s*, *p* and *d* waves to the inelastic cross sections of D + H_2 ($v = 1, j = 0$) collisions in Figure 7. The contribution to the resonance is primarily from the *p*-wave ($\ell = 1$) collisions. Close to the reactant asymptotic, there is no open channel in the product arrangement in the collision energy range we have considered, thus possibility of observing a Feshbach resonance is ruled out. We understand that the resonance is observed primarily due to the presence of a quasi-bound level below the *p-wave* ($\ell = 1$) centrifugal barrier in the D + H_2 ($v = 1, j = 0$) arrangement. The energy of the quasi-bound level is much closer to the initial reactant asymptote (~ 1mK) thus a pronounced enhancement in the *p–wave* reaction probability (cross section and rate coefficients also) is observed. The quasi-bound state within centrifugal barrier of the D + H_2 ($v = 0, j = 0$) asymptote is relatively far from the threshold (~ 0.001 K), which leads to reduced effect due to the *p - wave* collisions [17].

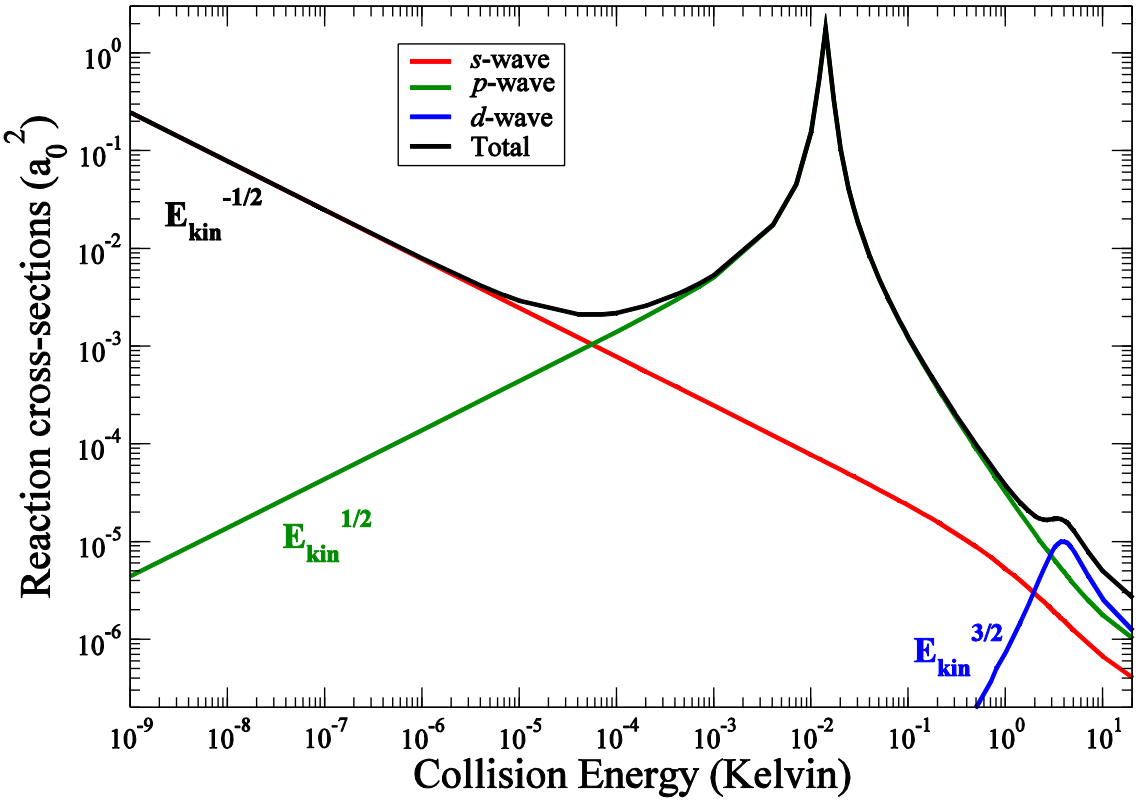

Figure 7: *s, p* and *d* wave contribution to the total reaction cross section of D + H_2 ($v = 1$, $j = 0$) collisions. Low collision energy behavior for individual partial waves follows Wigner's threshold laws [18] are verified.

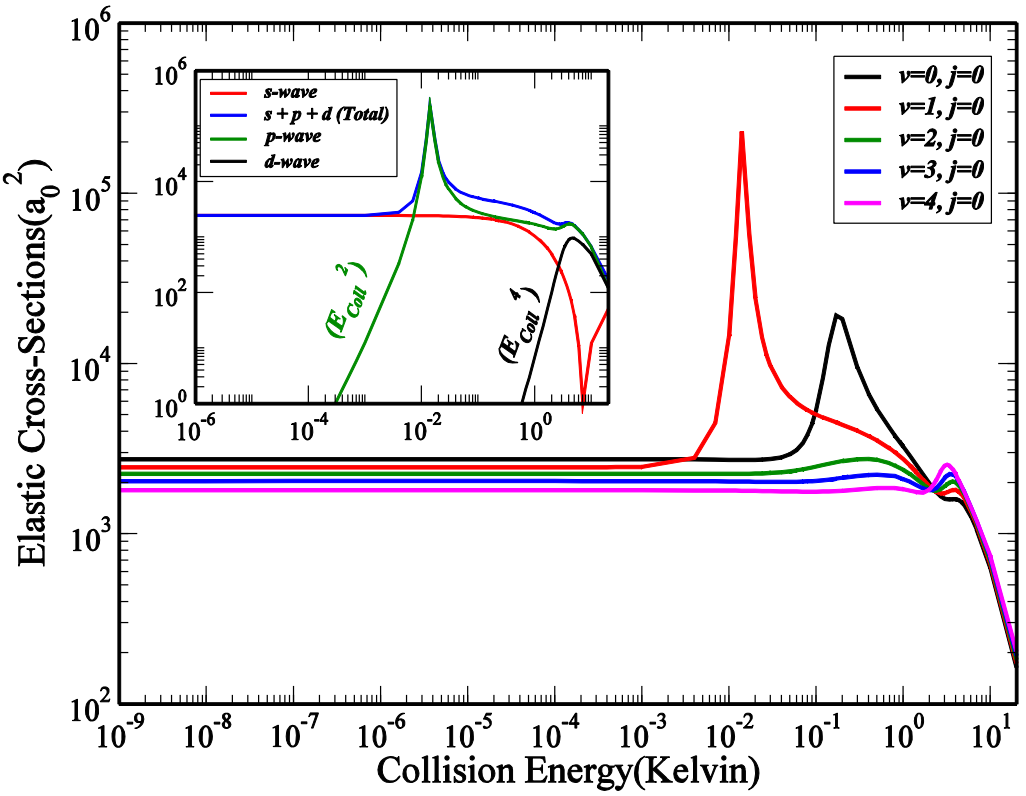

Figure 8: Same as Figure 1, collision energy dependence of elastic cross sections. Initial ro-vibrational levels of H_2 are indicated in the legend. Note that, at low collision energy, the elastic cross sections behaves as: $\sigma_{el} \propto E_{coll}^{2\ell}$, thus becomes constant for *s*-wave collisions.

For the initial state with rotational excitation (*e.g.* j = 1), the reaction cross section increases with the collision energy which means that first excited rotational states were populated enough and can easily penetrate through the barrier. Since ℓ = 1 is for *p-wave* and ℓ = 2 is for *d-wave*, cross sections were directly proportional to $E_{coll}^{\ell-1/2}$ and it is $E_{coll}^{1/2}$ for *p* wave and $E_{coll}^{3/2}$ for *d* wave.

To further confirm the origin of the shape resonances, we have calculated the elastic cross sections as shown in Figure 8. Similar enhancement in the elastic cross sections observed for v = 0, j = 0 and v = 1, j = 0 initial states of H_2. According to Wigner's threshold laws [18], elastic cross section becomes constant at ultra-low collision energies and is generally insensitive to vibrational and rotational excitations of the target molecule. Thus the sharp increase in the elastic cross section clearly indicates the contribution from the *p-wave* to the shape resonance (as shown in the inset of Figure 8).

Finally, we present the state-selected rate coefficients in Figure 9 (a-b) for the reactive and elastic processes. Rate Coefficients were obtained by averaging the corresponding cross

sections over Boltzmann velocity distribution of the colliding species at a particular temperature T (see *Eq*.2.2.45).

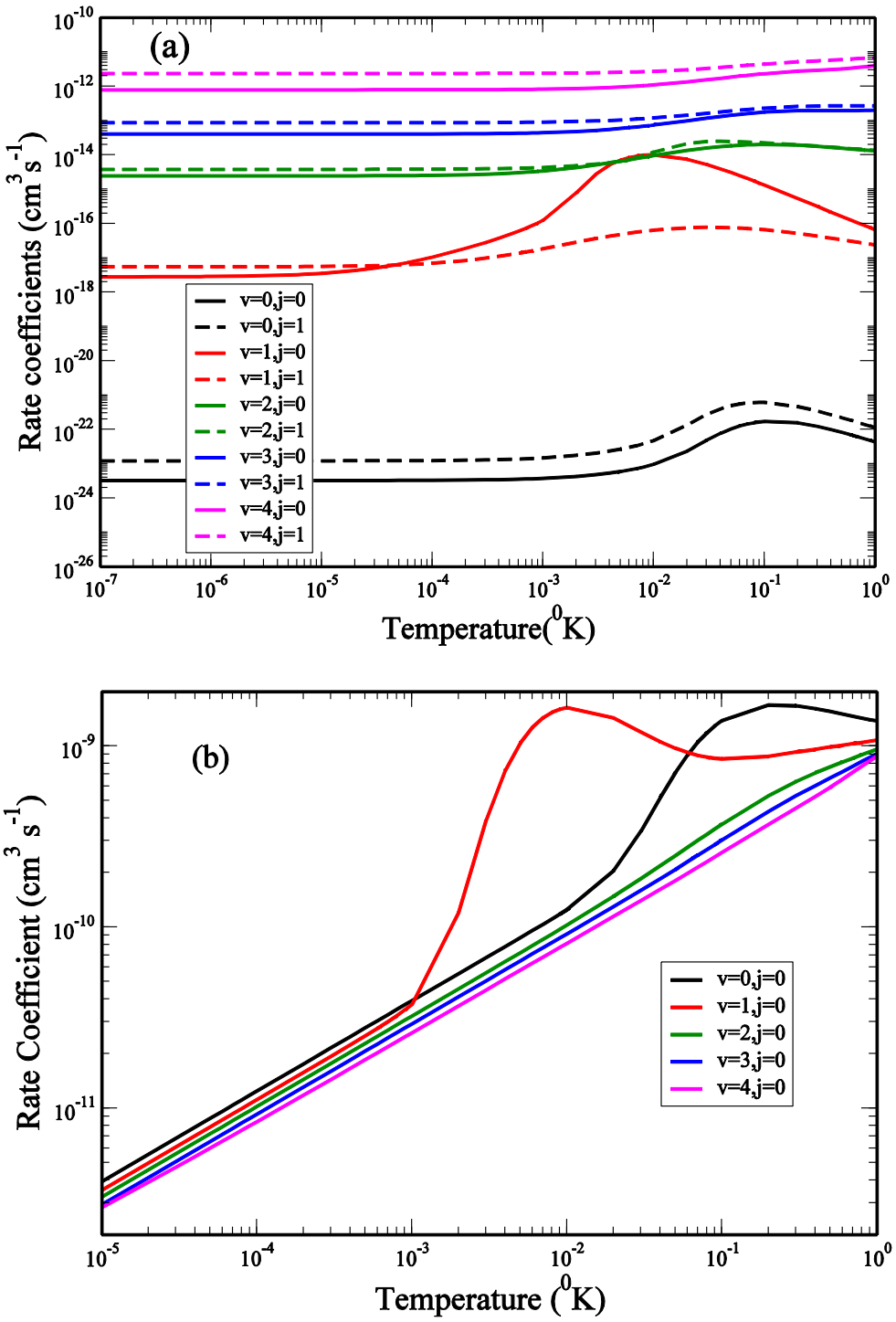

Figure 9: Temperature dependence of the rate coefficients (a) reactive and (b) elastic processes of D + H_2 $(v, j) \rightarrow$ HD + H reaction. Initial ro-vibrational states of H_2 in panel (a) and (b) are shown in the legend.

On averaging the reaction cross section over the narrow velocity distribution at ultracold temperature limit, the rate coefficients attain a constant value according to Wigner's threshold laws [18]. Thus, the temperature dependence of the rate coefficients at ultracold temperature limit behaves in complete disagreement with the familiar Arrhenius law [19]. On the other hand, at ultracold temperature limit, according to Wigner's threshold laws, the elastic rate coefficients is directly proportional to the temperature as shown in Figure 9 (b). The elastic rate coefficients don't change much with vibrational excitation as the tunneling probability of the elastic process is hardly affected by diminishing barrier suppression.

The sharp increase in the cross section for v = 0, 1 and j = 0 initial state leads to an increase in the reactive and elastic rate coefficients by two orders of magnitude around T = 0.001-0.1K. This can be used to design new experiments on ultracold D + H_2 (*0, 1*) collisions. In this regard, we note that, these resonances are very difficult to identify experimentally, though similar short lived resonances are recently observed for Cl + HD collisions [20].

4.4 Temperature dependence of the rate coefficients in the ultracold and low temperature regime

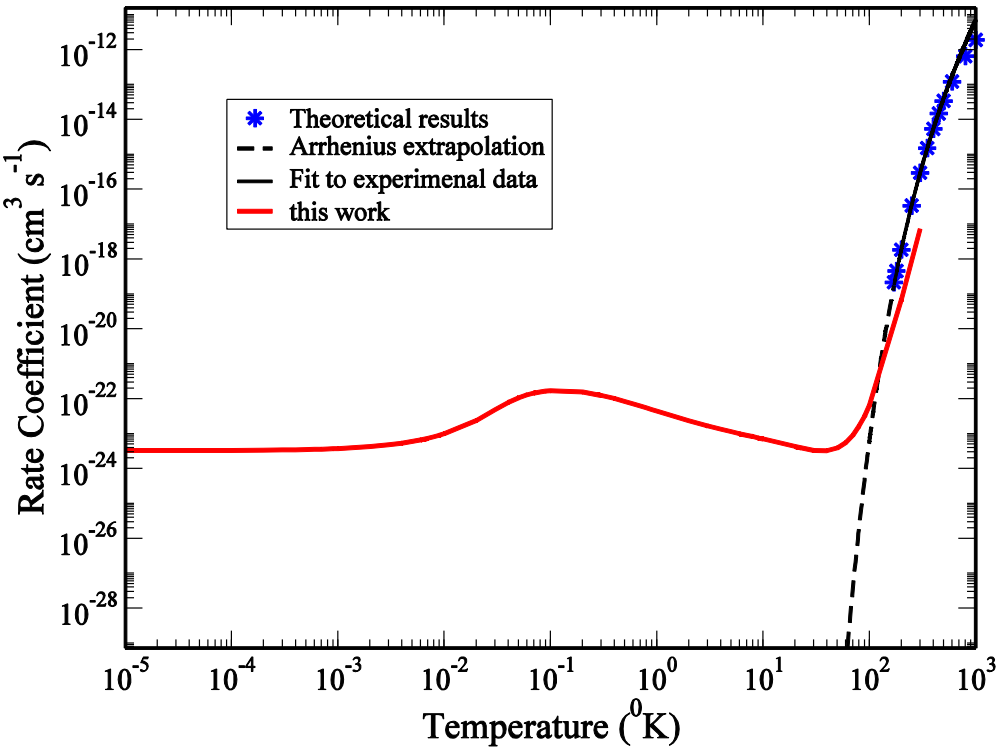

Figure 10: Temperature dependence of the rate coefficients of D + H_2 (v = *0*, j = *0*) → HD + H reaction. Experimental measurements and theoretical calculations and Arrhenius extrapolation at high temperature from Ref. [6] has been shown for comparison.

In general, temperature dependence rate coefficients of elementary reactions are explained by the Arrhenius theory of activated complex, $K_{Arr}(T) = Ae^{-B/T}$ where, A is the frequency factor and B represents the activation energy of the reaction [21]. At room temperature or higher, considering both A and B to be temperature independent, the linear extrapolation of experimental $lnK(T)\ Vs\ 1/T$ (Arrhenius plot) is often used to estimate rate coefficients at other temperatures. However, it is experimentally observed that for a wide range of temperature Arrhenius plot for many reactions are not straight line (curved) [22-24]. The curvature is generally accommodated in a modified form of Arrhenius equation, by introducing additional temperature dependence in the frequency factor A. But even the modified Arrhenius equation fails to explain the rate coefficients towards extremely low temperature and exact quantum mechanical treatment becomes necessary to understand the chemical reaction dynamics [25].

The temperature dependence of the rate coefficients at ultralow temperature limit completely disagreement with the famous Arrhenius law as shown in Figure 10. Arrhenius extrapolation of the available high temperature rate coefficients from Ref. [6] leads to vanishingly small values of the rate coefficient at ultracold temperature limit. To our understanding, Inclusion of these accurate rate coefficients for temperatures ≤ 10 K will lead to significant change in the low temperature cooling function of HD molecule which can be used for better modeling of the astrophysical processes of the early universe.

4.5 Dynamics of D + H_2 ($v, j = 0$) → HD (v', j') + H reaction in the thermal region (20-500 K)

At extremely low temperatures, H_2 molecule in ground state (v = 0; j = 0) predominantly contributes to the overall D + H_2(v, j) reaction. But, as the temperature is increased, contributions from higher rovibrational levels of H_2 (v = *0,1,. . . , j = 1,2,3, . . .*) become significant. Thus, obtaining state-to-state thermal rate coefficients are very expensive computationally and quickly becomes prohibitive for higher temperatures. The thermal reaction rate coefficients can be more efficiently calculated from the cumulative reaction probabilities, using the flux-flux correlation function method of Miller and coworkers [23,24], but contributions from individual initial levels are lost in that process. Since many initial rovibrational levels can contribute even at low temperatures, information on state-

specific reaction cross sections are important, particularly, for the intermediate temperature range to understand the non-Arrhenius behavior of the reaction rate coefficients. In this part, we have tried to bridge the gap between the extremely low to moderately low temperature range (1K–500 K) through full dimensional accurate state-to-state quantum mechanical calculations.

The state selected total reaction cross sections are shown in Figure 11 as function of collision energies of the individual rovibrational states of H_2 as indicated in the legends. The cross sections in Figure 11 have been summed over all the final states in the product arrangement (H + HD (v', j') whose energies are lower than the total energy. Contributions from all the higher partial waves (up to $J \sim 35$) are added cumulatively to estimate the individual state-selected reaction cross sections. The variation of $\sigma_{vj}(E_{vj}^c)$ with (E_{vj}^c) for different initial states have similar profiles; they exponentially increase with increasing kinetic energy, reaching ~$1a_0^2$ at high collision energies. It is expected, as the kinetic energy overcomes the potential barrier of the respective initial state, the reaction becomes classically allowed and the cross sections increase exponentially.

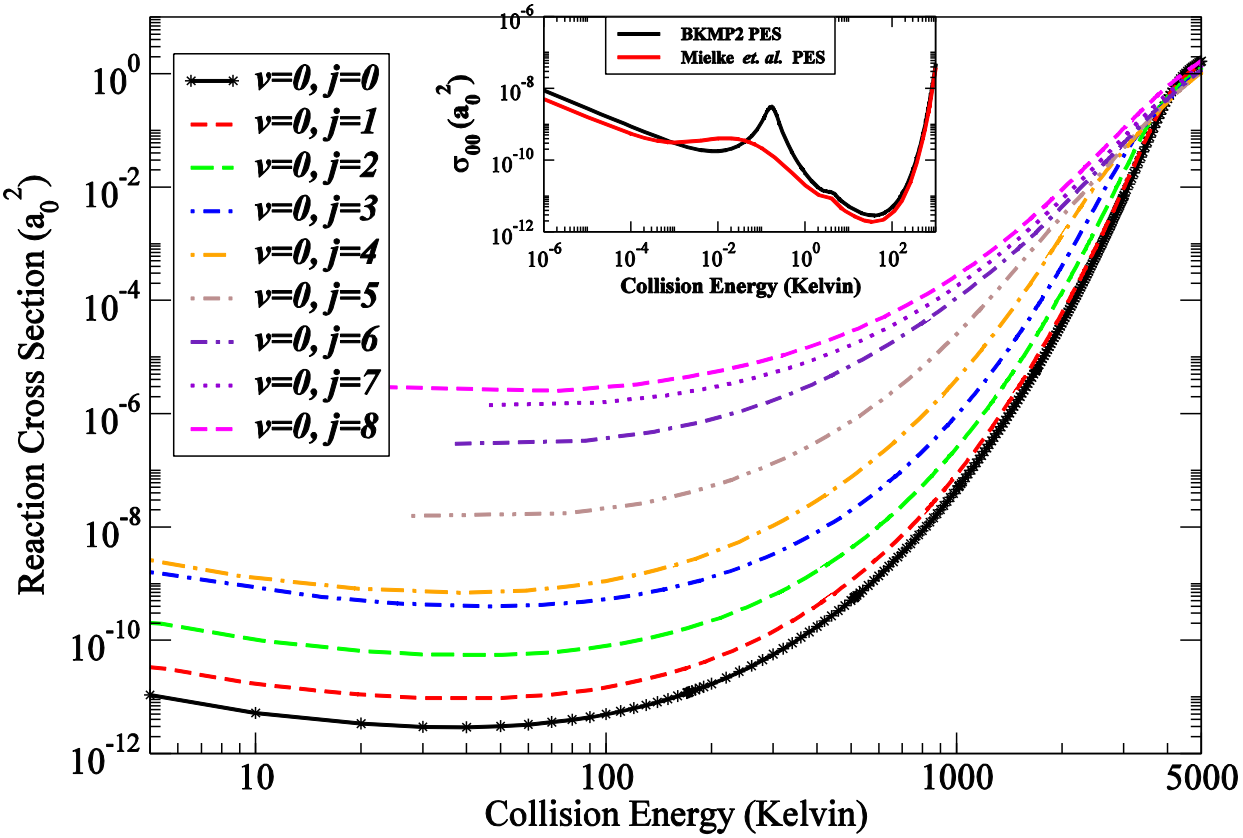

Figure 11: Collision energy dependence of reaction cross sections of D + H_2 (v; j) reaction. Initial rovibrational states are indicated in the legend. D + H_2 (v = 0, j = 0) reaction cross sections at ultralow collision energies calculated using BKMP2 [5] and Mielke *et al.* [15] PES are shown in the inset.

Due to the large energy barrier of reaction, the reaction cross sections are greatly reduced for the lower rovibrational states of H_2 molecule. For reactions starting from excited rovibrational states of H_2, quenching to lower states of D + H_2 ($v' \neq v, j' \neq j$**)** can be possible, but it is not considered for the present study.

The cross sections of D + H_2 (v = 0, j = 0) reaction for ultralow collision energies are shown in the inset of Figure 11. The reaction cross sections behave as $(E_{coll}^{vj})^{1/2}$ at ultralow collision energies and produce a straight line in the log-log plot. This simple power law behavior is in accordance with Wigner's threshold laws [18] and matches well with previous s-wave only calculations [9]. Reaction thresholds from the *p* and *d waves* (ℓ = *1* and *2*) appeared as small humps in the cross sections at $E_{coll}\sim$ 10^{-3} K and ~1 K. Here we note the difference between BKMP2 [5] and the Mielke *et al*. [15] PES in the ultralow collision energy range which gradually diminishes at higher collision energies.

We have chosen the initial collision energies carefully such that contributions from very low collision energies are included for the D + H_2 (v = 0, j = 0–5) initial states. Contributions from v = 1, j = 0, 1, 2 are also calculated in similar way to include in the overall reaction cross sections. Reaction cross sections and rate coefficients below 1 K for D + H_2 (v, j) reactions have been discussed in Section 4.2 [9, 19]. It is evident that, even with vanishingly small collision energies, the reaction can proceed through quantum mechanical tunneling. This is because the atoms and molecules have diffuse boundary (due to large de Broglie wave length) at low collision energies and the effective range of interaction increases with decreasing average velocity of the colliding species. For barrier dominated reactions, quantum mechanical tunneling is always theoretically present, but for D + H_2 reaction tunneling effect is more dominant because of the low reduced mass and high potential barrier of the system. At ultracold temperature limit, the scattering dynamics is purely governed by Wigner's threshold laws that produce power law relationships at ultralow collision energies [18].

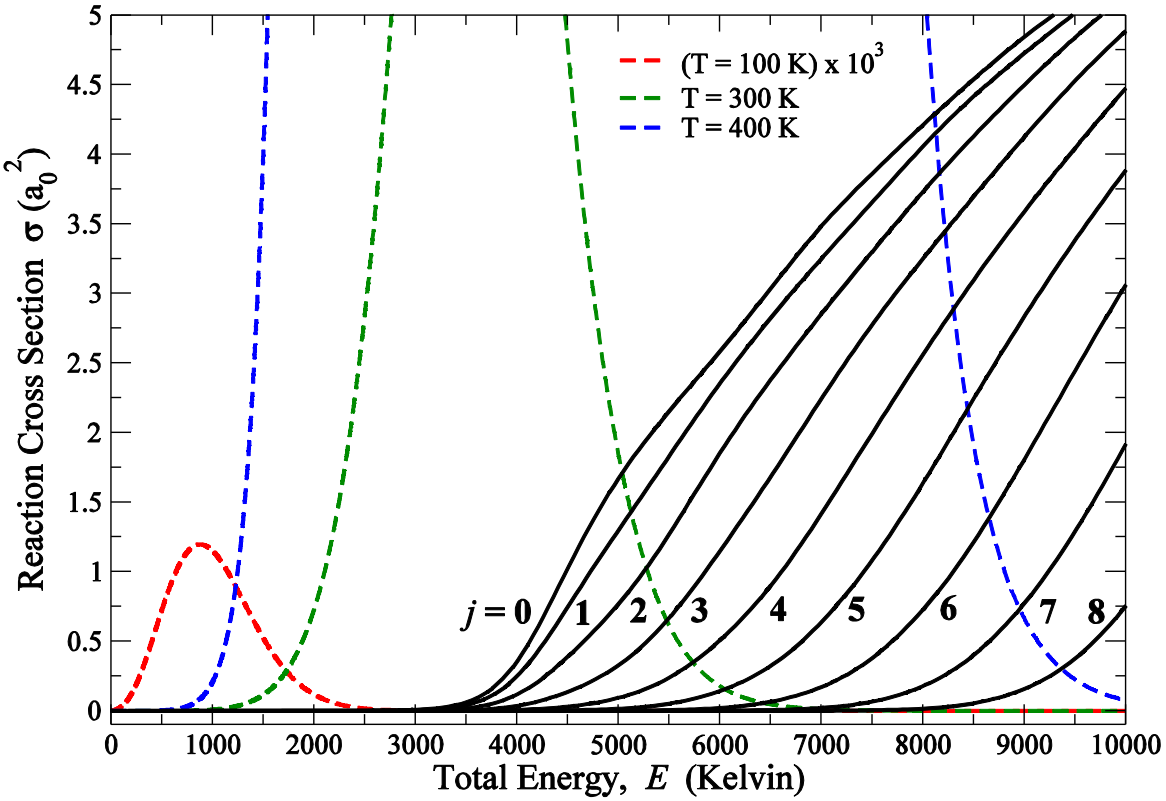

Figure 12: Same as Figure 11, total energy dependence of reaction cross sections of D + H_2 (v = *0*, j) reaction (in linear scale). The thermalization integrand, which is the energy distribution function times the energy-dependent cross section corresponding to T = 100 K, 300 K and 400 K are shown as dashed lines.

To have an overview of the individual rovibrational contributions to the overall reaction cross sections, we have analyzed the initial reaction cross sections as a function of the total energy of the reaction in Figure 12. The total energy is measured from the potential minimum of the D + H_2 (v = 0, j = 0) level and represented as $E = \varepsilon_{00} + E_{00}$. Reactions of D with higher rovibrational levels of H_2 starts to contribute as the total collision energy surpasses the corresponding channel threshold energies. At low temperatures, only slow or low kinetic energy collisions are dominant, but as the temperature is increased, high energy collisions start to contribute significantly. Thus, it is instructive to analyze the product of the reactive cross sections and Boltzmann distribution function, $E_{coll}^{vj}\exp(^{-E_{coll}^{vj}}/_{k_B T})$ to estimate the range of collision energies needed to calculate the rate coefficients for the temperature range of our interest. As shown in Figure 12, to obtain rate at T = 100 K we need to include cross sections starting from E_{coll} ~ 1 K to 2000 K (magnified 10^3 times in Figure 12) whereas to calculate rate at T = 400 K, we needed to calculate cross sections for $E_{coll} \sim 10^4$ K. Thus, calculation of cross sections for high collision energies requires inclusion of many partial

waves which makes this method computationally very expensive to estimate rate coefficients at higher temperatures.

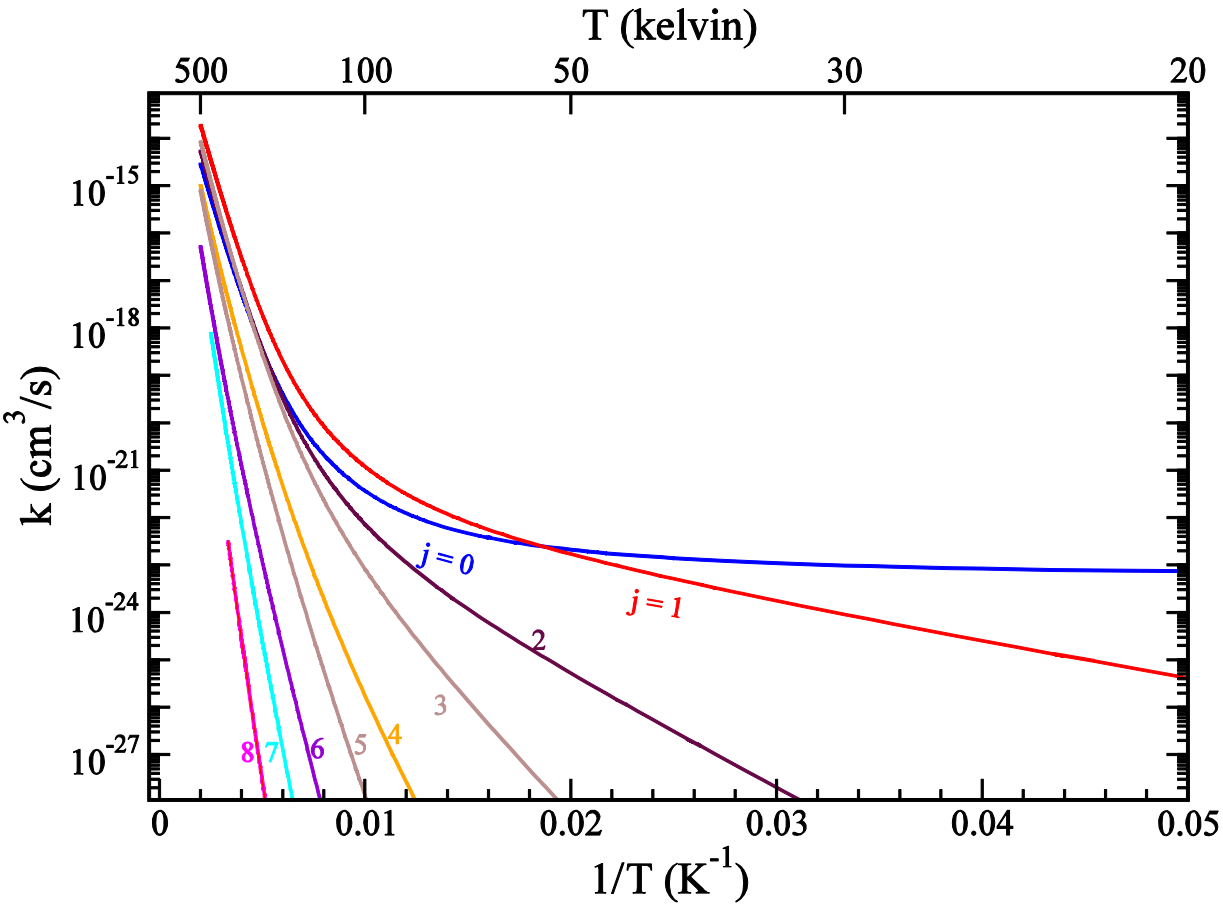

Figure 13: Arrhenius plot: the temperature dependence of the state-specific quantum mechanical rate coefficients for D + H_2 (v = 0, j = 0–8) reaction.

The rate coefficients calculated for different initial rovibrational levels have been shown in Figure 13 as usual Arrhenius representation. As we consider bulk phase experiment under equilibrium conditions, state selected rate coefficients are weighted by their relative populations. Relative populations are estimated from the Boltzmann factors $g(v,j) = \frac{\left(^{-\varepsilon_{vj}}/_{k_BT}\right)}{Q_{vj}}$, where $Q_{vj} = \sum_{v,j=even}^{\infty} \exp(^{-\varepsilon_{vj}}/_{k_BT}) + \sum_{v,j=odd} \exp(^{-\varepsilon_{vj}}/_{k_BT})$[28]. Additional degeneracy factor of 3 is included for odd rotational levels of H_2. Contribution from individual rovibrational levels are added to obtain the overall temperature dependent rate coefficients for the D + H_2 (v, j) reaction.

Here we note that, this work assumes full ortho–para interconversion at all temperatures; *i.e.*, we assume even and odd rotational states are freely interconvertible, but cooling within the ortho and para manifolds separately will be a better model for some physical processes [1, 29].

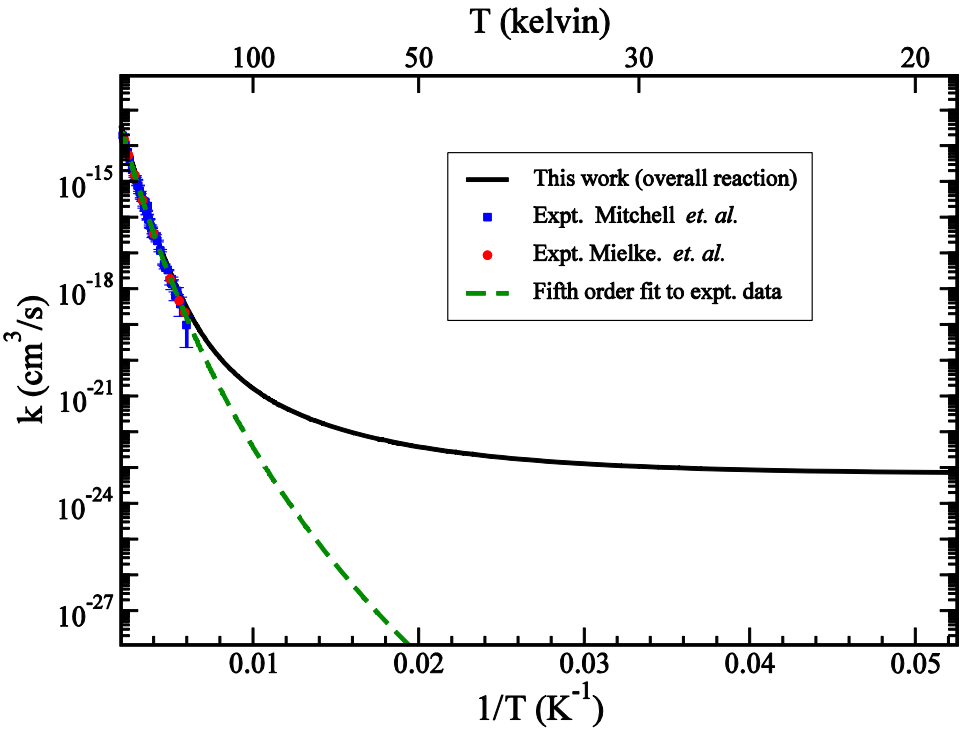

Figure 14: Same as Figure 13, overall thermal reaction rate coefficients along with available experimental results.

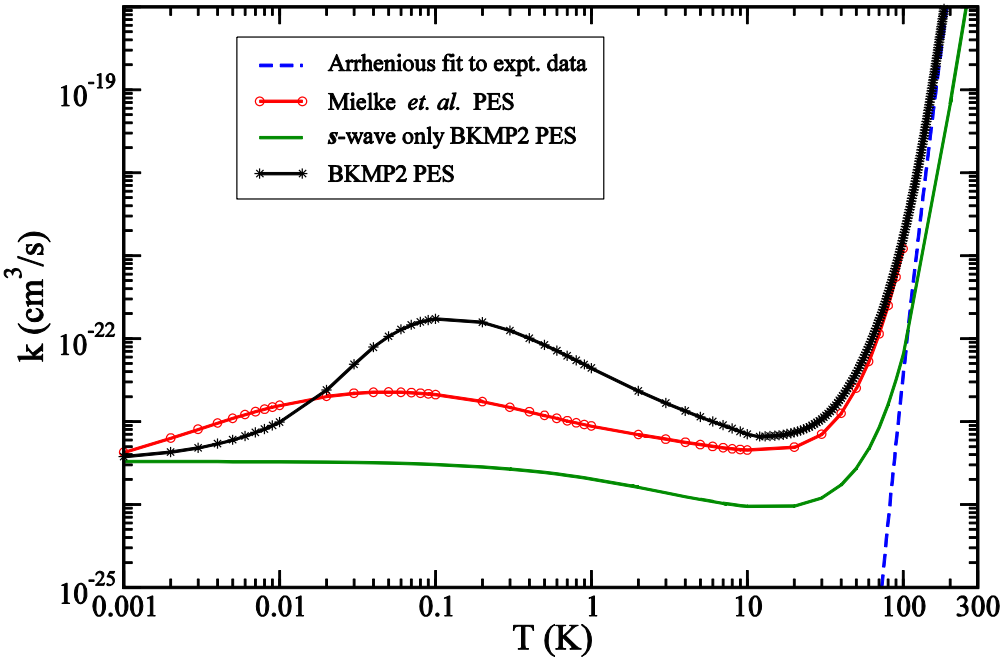

Figure 15: Overall temperature dependence of the thermal rate coefficients from ultracold to room temperature range using BKMP2 [5] and Mielke *et al.* [15] PES. Arrhenius fit to the experimental data from Ref. [6] and *s-wave* only rate coefficients from Ref. [9] are also shown for comparison.

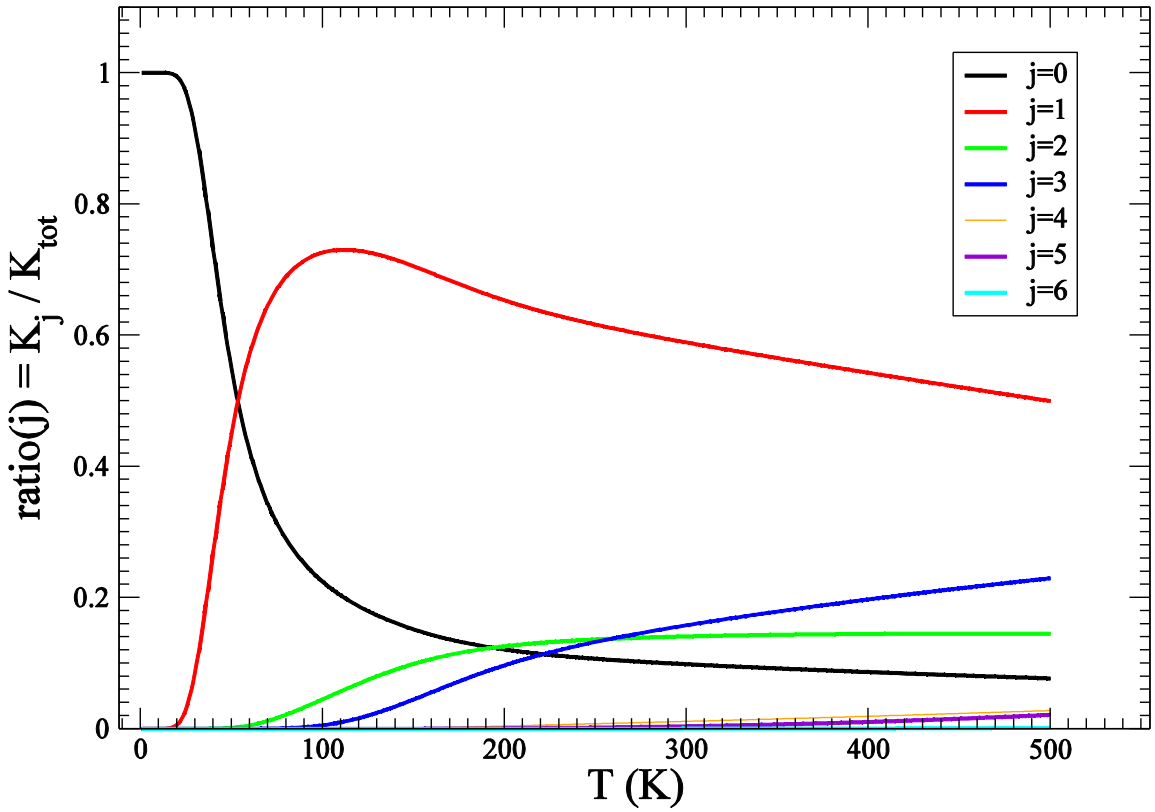

Figure 16: Fractional contribution of the individual rotational levels to the total reaction rate coefficients.

From Figure 13 it is evident that major contributions below T = 20 K are obtained from the v = 0, j = 0 and v = 0, j = 1 initial arrangements. Significant contribution from higher rotational levels are obtained above T = 50 K. Reaction starting from v = 1 (not shown in the figure) becomes significant only above T ~120 K. In Figures 14 and 15, we have compared the calculated rate coefficients with available experimental and theoretical results [6, 8, 13, 30]. Calculated rate coefficients agree well with the experimental results of Mitchell and Roy [8], Mielke *et al*. [6] and time-dependent wave packet calculations of Ghosal *et al*.[13] for temperature above ~170 K. This reaction had been also studied theoretically at temperatures much lower than 1 K and our calculations match well with previous reports [9, 10]. In the intermediate range, as the temperature is reduced, the rate coefficients obtained from exact QM calculations start to deviate from the extrapolated experimental data [6] and attend a near constant value at T ~ 10 K (as shown in Fig. 15). This deviation from the regular Arrhenius behavior is attributed to the increased quantum mechanical tunneling. As the temperature is reduced, due to large de Broglie wave length effective range of interaction between the colliding particles increases, which lead to increase in reaction cross sections. The cross section (σ) increases as $1/v$, thus, with decreasing temperature, the rate coefficients,

expressed as the average cross sections multiplied by the relative velocity of the colliding species, ($k = \langle \sigma . v \rangle$) becomes constant, as predicted by Wigner's threshold laws [18].

In order to analyze this major deviation from the Arrhenius behavior at lower temperature we have shown (in Figure 16) the fractional contributions of the individual rovibrational states to the overall rate coefficients. Up to T = 500 K collisions of D with H_2 in v = 0 and j = 0, 1, 2, 3 contribute significantly. The low temperature reaction (T < 20 K) is purely governed by collisions with D with H_2 in the rovibrational ground state, j = 2 and higher rotational levels start to contribute only above T > 50 K. Major contributions from odd rotational levels (j) are observed because of their rotational degeneracy factor of (2j + 1). Particularly, D + H_2 (v = 0, j = 1) dominates over all other rovibrational states and contributes ~50% to the overall reaction for the temperature range considered in the present study.

4.6 Conclusions

We have presented accurate time-independent quantum mechanical (TIQM) rate coefficients for the formation of ultracold HD molecules through D + H_2 (v, j)→ HD (v', j') +H reaction in the ultralow temperature regime. The dynamical parameters such as the state resolved integral cross sections between rotational (j) and vibrational (v) levels and corresponding rate coefficients are computed between temperature T = 10^{-8}K - 500K. It has been found that the exponential decrease of the rate coefficients with reducing temperature following Arrhenius' empirical equation is not valid at ultracold temperature limit. At lower temperatures, the rate coefficients become independent of temperature (constant) which is the consequence of Wigner's threshold law. Since the interaction of the atoms and molecules is very much sensitive to the potentials, occurrence of reactive resonances is very common. We have observed a resonance near ~10^{-2}K and discussed its origin. Finally, we have calculated the rate coefficients of both inelastic and reactive processes which are important for the calculation of the cooling functions and in understanding the evolution process.

4.7 References

[1] F. Lique, P. Honvault, A. Faure, Ortho–para-H_2 conversion processes in astrophysical media, International Reviews in Physical Chemistry 33 (2014) 125-149.

[2] D. Galli, F. Palla, The dawn of chemistry, Annual Review of Astronomy and Astrophysics 51 (2013) 163-206.

[3] C. Gay, P. Stancil, S. Lepp, A. Dalgarno, The highly deuterated chemistry of the early universe, The Astrophysical Journal 737 (2011) 44.

[4] S. Glover, T. Abel, Uncertainties in H_2 and HD chemistry and cooling and their role in early structure formation, Monthly Notices of the Royal Astronomical Society 388 (2008) 1627-1651.

[5] A.I. Boothroyd, W.J. Keogh, P.G. Martin, M.R. Peterson, A refined H_3 potential energy surface, The Journal of chemical physics 104 (1996) 7139-7152.

[6] S.L. Mielke, K.A. Peterson, D.W. Schwenke, B.C. Garrett, D.G. Truhlar, J.V. Michael, M.-C. Su, J.W. Sutherland, H + H_2 thermal reaction: a convergence of theory and experiment, Physical Review Letters 91 (2003) 063201.

[7] J. Michael, M.-C. Su, J. Sutherland, New Rate Constants for D + H_2 and H + D_2 Between 1150 and 2100 K, The Journal of Physical Chemistry A 108 (2004) 432-437.

[8] D. Mitchell, D.L. Roy, Rate Constants for the Reaction D + H_2 → DH + H at Low temperatures using ESR Detection, The Journal of Chemical Physics 58 (1973) 3449-3453.

[9] I. Simbotin, S. Ghosal, R. Côté, A case study in ultracold reactive scattering: D + H_2, Physical Chemistry Chemical Physics 13 (2011) 19148-19155.

[10] J. Hazra, B.P. Ruzic, J.L. Bohn, N. Balakrishnan, Quantum defect theory for cold chemistry with product-quantum-state resolution, Physical Review A 90 (2014) 062703.

[11] I. Simbotin, R. Côté, Effect of nuclear spin symmetry in cold and ultracold reactions: D+ para/ortho-H_2, New Journal of Physics 17 (2015) 065003.

[12] F. Lique, A. Faure, Communication: The rotational excitation of D_2 by H: On the importance of the reactive channels, AIP, 2012, pp. 031101.

[13] S. Ghosal, B.J. Rao, S. Mahapatra, Reactive chemical dynamics through conical intersections, Journal of Chemical Sciences 119 (2007) 401-407.

[14] R.S. Sutherland, M.A. Dopita, Cooling functions for low-density astrophysical plasmas, The Astrophysical Journal Supplement Series 88 (1993) 253-327.

[15] S.L. Mielke, B.C. Garrett, K.A. Peterson, A hierarchical family of global analytic Born–Oppenheimer potential energy surfaces for the H + H_2 reaction ranging in quality from double-zeta to the complete basis set limit, The Journal of chemical physics 116 (2002) 4142-4161.

[16] A.I. Boothroyd, W.J. Keogh, P.G. Martin, M.R. Peterson, An improved H_3 potential energy surface, The Journal of chemical physics 95 (1991) 4343-4359.

[17] I. Simbotin, S. Ghosal, R. Côté, Threshold resonance effects in reactive processes, Physical Review A 89 (2014) 040701.

[18] E.P. Wigner, On the behavior of cross sections near thresholds, Physical Review 73 (1948) 1002.

[19] R. Santosh, S. Ghosal, Quantum Mechanical Rate Coefficient of Formation of HD Molecule at Ultracold Temperatures: Its Importance in Interstellar Cooling, Journal of Atomic, Molecular, Condensate and Nano Physics; Vol 2, No 3 (2015).

[20] T. Yang, J. Chen, L. Huang, T. Wang, C. Xiao, Z. Sun, D. Dai, X. Yang, D.H. Zhang, Extremely short-lived reaction resonances in Cl + HD ($v = 1$)→ DCl + H due to chemical bond softening, Science 347 (2015) 60-63.

[21] K.J. Laidler, The development of the Arrhenius equation, Journal of Chemical Education 61 (1984) 494.

[22] D.G. Truhlar, A. Kohen, Convex Arrhenius plots and their interpretation, Proceedings of the National Academy of Sciences 98 (2001) 848-851.

[23] T. Takayanagi, Y. Kurosaki, Theoretical calculations of potential energy surface and thermal rate constants for the H (Mu) + F_2 reaction, The Journal of Physical Chemistry A 101 (1997) 7098-7104.

[24] C. Canepa, On the curvature in logarithmic plots of rate coefficients for chemical reactions, Chemistry Central Journal 5 (2011) 22.

[25] T. Miyazaki, Atom tunneling phenomena in physics, chemistry and biology, Springer Science & Business Media 2013.

[26] W.H. Thompson, W.H. Miller, On the "direct" calculation of thermal rate constants. II. The flux-flux autocorrelation function with absorbing potentials, with application to the O + HCl → OH + Cl reaction, The Journal of chemical physics 106 (1997) 142-150.

[27] H. Wang, W.H. Thompson, W.H. Miller, Thermal rate constant calculation using flux–flux autocorrelation functions: Application to Cl + H_2→ HCl + H reaction, The Journal of chemical physics 107 (1997) 7194-7201.

[28] G.G. Balint-Kurti, A. Palov, Theory of Molecular collisions, Royal Society of Chemistry 2015.

[29] S. Ionel, C. Robin, Effect of nuclear spin symmetry in cold and ultracold reactions: D + para/ortho-H_2, New Journal of Physics 17 (2015) 065003.

[30] Y.V. Suleimanov, R.P. de Tudela, P.G. Jambrina, J.F. Castillo, V. Sáez-Rábanos, D.E. Manolopoulos, F.J. Aoiz, A ring polymer molecular dynamics study of the isotopologues of the H + H_2 reaction, Physical Chemistry Chemical Physics 15 (2013) 3655-3665.

Chapter 5

Dynamics of H + HD ($v = 1, j = 0$) $\rightarrow$ H_2 ($v = v', j = j'$) + D reaction in the ultracold to thermal temperature limit

5.1 Introduction

Two small molecules, H_2 and HD, in their neutral and ionic forms have been found to be the most important interstellar coolants which helped to reduce the overall temperature of the early universe. To understand the evolution process, different research groups have studied the effectiveness of the cooling processes by considering hundreds of reactions between 16 species of neutral and ionic forms of H_2 and HD [1, 2]. Particularly, Glover *et. al*. have modelled the role of H_2 and HD molecules in the interstellar cooling by incorporating the rate coefficients of the collision process involving these molecules for a wide range of temperatures [3]. It has been found that the molecular HD is more effective coolant because of its intrinsic dipole moment and high reduced mass [4]. This is one of the reasons we have studied in detail the destruction of HD molecules through the reverse pathway of the D + H_2 reaction in the previous chapter.

Over the years, H + HD reaction has become a benchmark system as it is a simple system electronically and a benchmark prototype for a several theoretical studies. Early studies on H + HD reaction had been reported by Takayangi *et. al.* [5-7]. They have performed detailed investigation of D + H_2 and H + HD reactions to verify the Wigner's threshold law at low temperature and tested different potential energy surfaces for dynamical calculations available at that time. Quasiclassical trajectory calculations were performed by Hochman and Sato [8] using LSTH [9-11], DMBE [12], potentials and the dynamical outcomes were analyzed for H + HD, D + H_2 and H + D_2 reactions. Time dependent wave packet approach have been also employed to understand the transition state resonances considering dimensionality effects on H + HD, D + HD collisions [13]. Recently, the H exchange process in H + HD collisions has been studied by Balakrishnan *et. al*. considering geometric phase effects in the ultracold temperature regime [14, 15]. This reaction is also studied in thermal temperature regime [16, 17]. Scattering calculations were performed both theoretically and experimentally to understand the collisional events from moderate to thermal regime [18-23]. But, according to best of our knowledge, none of the previous studies have reported accurate rate coefficients for such a wide temperature range.

Based on our extensive literature search, it has been understood that the followings aspects of the H + HD ($v = 1, j = 0$) $\rightarrow$ H_2 ($v = v', j = j'$) + D reaction need more detailed investigation.

i) Effect of vibrational excitation of the reactant molecule on the overall reaction cross-sections and rate in the cold and ultracold regime.

ii) Comparative study of hydrogen exchange process with other possible reaction channels, such as quenching and the formation of H_2 molecule.

iii) Existence of virtual and/or bound states near the reaction threshold which generally leads to enhancement of the reaction cross sections.

iv) The effect of higher partial waves for higher temperatures/collision energies.

In this chapter, we have presented the dynamics of this reaction at the cold and ultra-cold temperature limit. We have also focused on the microscopic details to understand the effect of resonances due to various bound or quasi-bound states present in the potential energy surface.

5.2 Reactive scattering dynamics of H + HD reaction in the ultracold temperature limit.

For illustrative purpose, we have shown all the elastic and inelastic collision processes of the H + HD reaction in Figure 1. The inelastic processes can be of reactive or non-reactive type (quenching). In reactive collision, two types of reactive processes can occur, (a) formation of molecular hydrogen (H_2) and (b) hydrogen exchange reaction, where the hydrogen atom of the HD molecule is replaced by another hydrogen atom. Having more number of outgoing channels due to different arrangements, study of this reaction is more complex and challenging computationally compared to D + H_2 reaction.

We have also analyzed the threshold of the different vibrational and rotational levels and figured out that reaction between H + HD ($v = 0, j = 0$) is endo thermic in nature for ultralow energy collisions, so we have restricted our discussion on reactive scattering dynamics of H + HD ($v \geq 1, j = 0$) collisions.

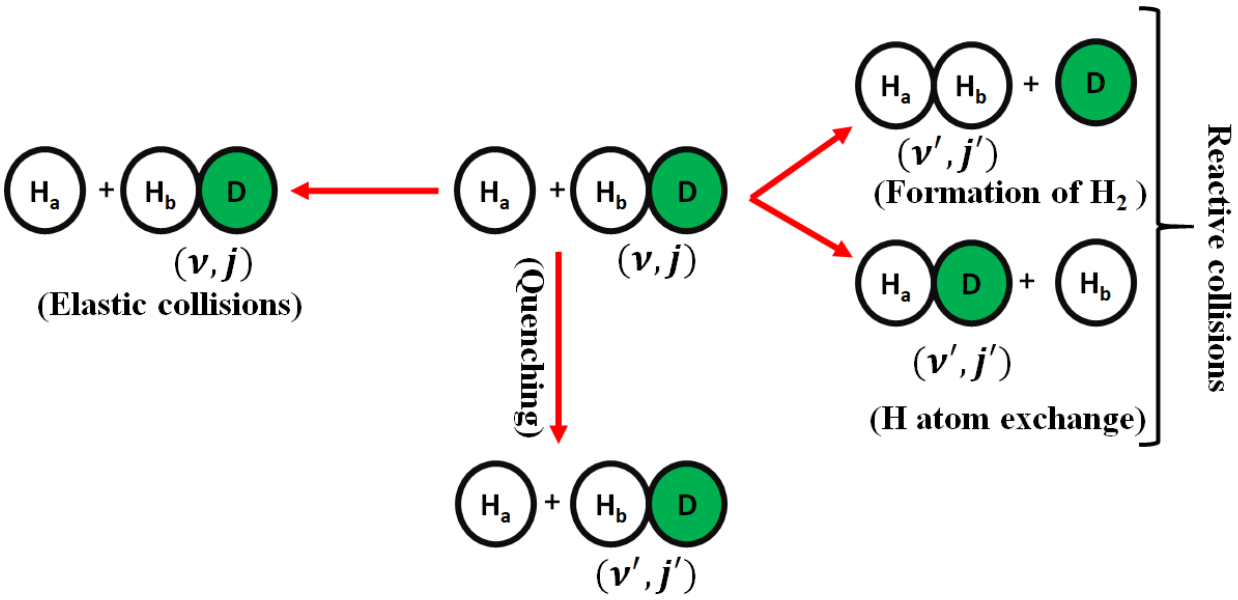

Figure 1(a): Elastic, quenching and reactive scattering events due to the collision of H and HD.

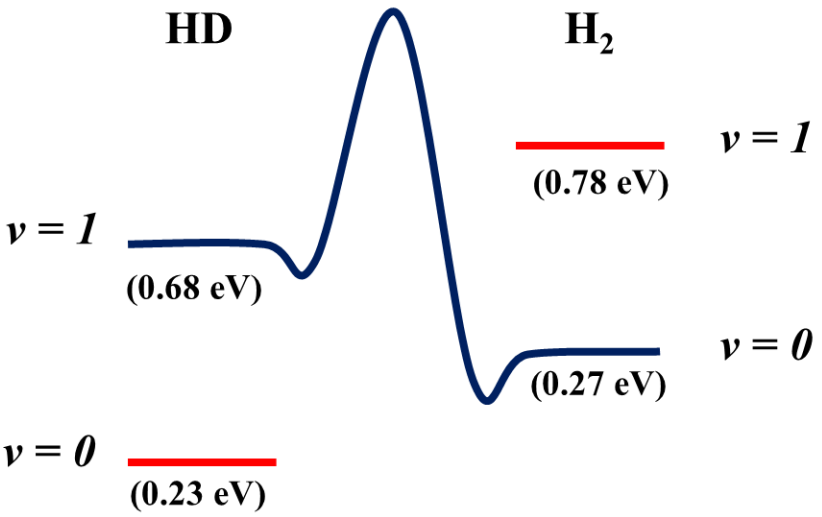

Figure 1(b): Comparison of the vibrational energy levels (threshold energies) of HD and H_2 molecule.

We have presented the cross sections for the reactive, quenching and exchange process of H + HD $(v, j) \rightarrow H_2$ + D reaction in Figure 2. Using the formalism described in chapter 2 for initial vibrational levels of HD molecule to v = 1, 2, 3, 4, 5, 6 and j = 0. Rotational quantum level was considered to be the minimum ($j = 0$) to avoid additional centrifugal potential barrier due to rotation of the higher rotational levels. To ensure convergence the cut-off energy (E_{max}) for the rovibrational basis sets is chosen to be 4.25 eV and all rovibrational

channels below E_{max} in the reactant and product arrangement are included in the dynamical calculations. The coupled equations are propagated up to $\rho_{max} = \sim 120\ a.u$ using small integration steps $d\rho = 0.002\ a.u.$ We have used the most recent Mielke *et. al.* PES for the present calculation [24]. According to our test calculations, these parameters are sufficient to achieve numerical convergence for studying reactive collisions for this reaction for H + HD (*v =1- 6, j=0*) reaction.

The reaction cross sections shown in Figure 2 are presented as a function of collision energy of the H + HD (*v*, *j*) initial states. The collision energies are scaled from the threshold energies of the respective initial channel. The total reaction cross sections are calculated from the ultra-low collision energy (~ 1μ K) regime to 4000K. A fine energy grid of 500 points is used to gather scattering information in the ultracold, intermediate and thermal energy range. For the cold (1K < T < 1mK) and ultra cold (< 1mK) collision energy regime, only *s-wave* scattering with total angular momentum *J = 0* is required to estimate the cross sections.

In order to understand the behavior of all the inelastic processes (reactive, H exchange and quenching from top to bottom), cross sections are presented in three panels as functions of collision energy of the initial colliding partners. It is evident from Figure 2 that low and ultralow energy collision cross sections are directly proportional to the energy of the initial vibrational quantum level. The cross sections can be distinguished for both the ultracold and thermal regimes. In the ultra low collision energy range, the cross sections behave according to the Wigner's threshold law *i.e*. reaction happens through quantum mechanical tunneling.

In Figure 2 we have shown the cross sections at collision energy of 1μK for H + HD (*v*, *0*) reaction. Collisions initiated from all these reactant states do not have sufficient energy to overcome the potential energy barrier and the product formation mostly occurs through quantum mechanical tunneling. Due to extremely low kinetic energy of collisional partners, transition from one state to other is difficult, but they can exchange their internal energy. Thus, the cross-sections for the lower vibrational states (v = 1 to v = 4) are dominated by the elastic collisions. As we go from lower vibrational states to the higher vibrational states of HD molecule, the elastic cross sections are diminished considerably and became lower than the inelastic process at $v \geq 6$.

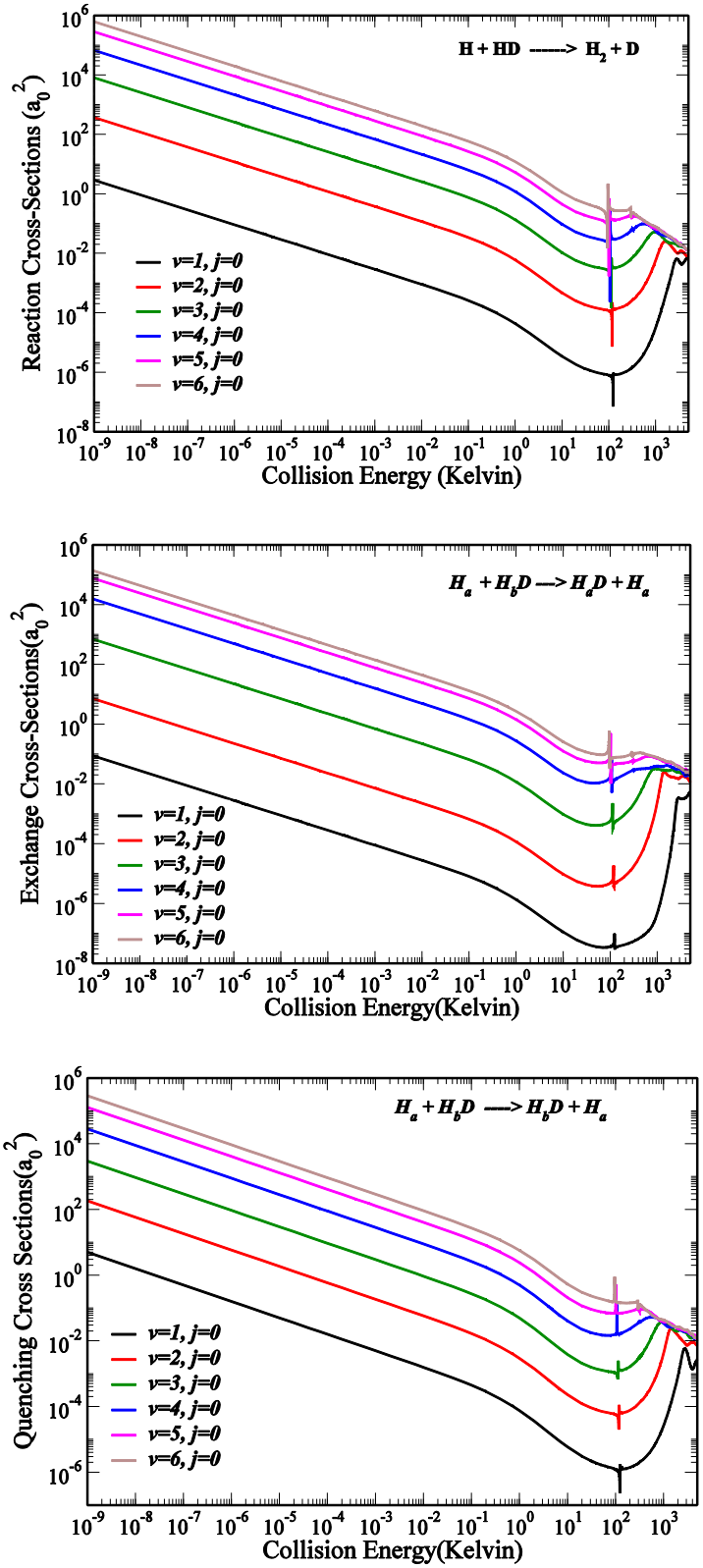

Figure 2: Computed cross-sections as a function of collision energy of the initial state of the interacting particles for the reactive, H exchange and quenching processes respectively (from top to bottom) as described in the Figure 1.

Elastic scattering cross sections manifest from the conservation of angular momentum of reacting species *i.e.* the rovibrational state of HD before and after the collision remains the same. Laser cooling technique is used to get the molecules at cold and ultracold temperatures. Thus, the elastic cross sections play the most crucial role in stabilizing the molecules with a desired quantum state at ultracold temperatures. In fact, the ratio between the elastic and inelastic cross sections becomes the most important. Inelastic cross sections have inverse relationship with the collision energies at ultracold temperature limit, on the other hand, according to Wigner's threshold law; elastic cross sections become constant at ultra-low collision energies.

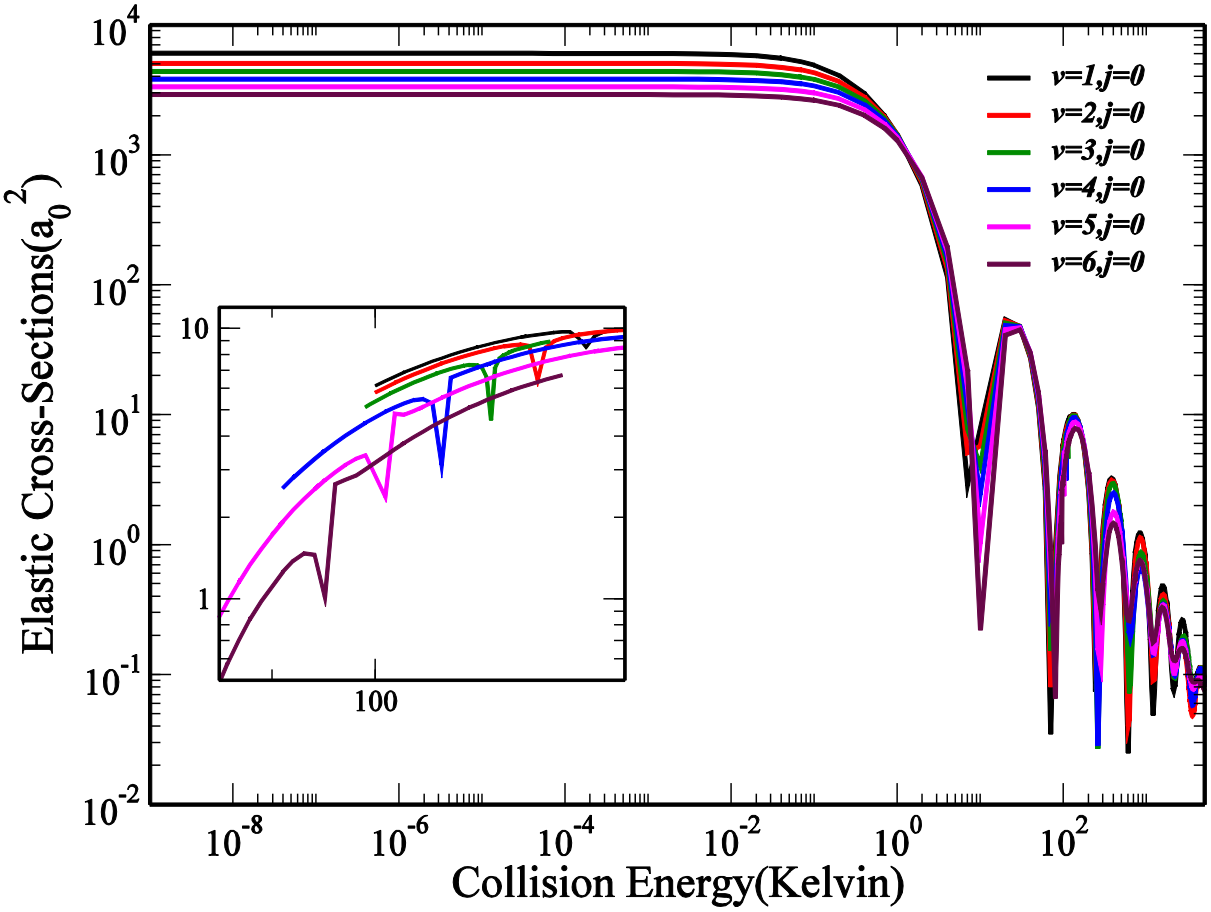

Figure 3: For different initial rovibrational channels of HD molecules, Elastic cross section is plotted as a function of Collision energy (Kelvin). Variation in the position of threshold resonance for different vibrational states have been shown in the inset.

The elastic cross sections from different initial rovibrational states have been shown in Figure 3. Elastic cross sections are calculated from the scattering length (a) which is real when only elastic scattering collisions may occur and complex in case of multichannel scattering.

$$\sigma_{el} = 4\pi|a|^2 = 4\,\pi\,(\,\alpha^2 + \beta^2)$$

Where $a = \alpha - i\beta$ is the *s-wave* scattering length.

For a given initial channel (v, j) in the entrance arrangement, the scattering length is extracted from the low k-expansion of the diagonal element of the *s-matrix*. $s_{avj,avj} = 1 - 2ia_{avj}k = 1 - 2\beta_{avj}k - 2i\alpha_{avj}k$, a is the entrance channel arrangement, v is the vibrational quantum state, j is the rotational quantum state and k is the momentum.

Collision energy dependent elastic cross-sections for the H + HD collisions of all initial states of HD ($v \leq 6$) give results that are nearly identical at energies above 1K which is unlikely in case of inelastic cross-sections. However, it is clear that in the subkelvin regime they differ significantly as shown in Figure 4. All these cross-sections were plotted by considering the contributions from *s-wave* but these oscillations generally lose its significance as higher partial waves start contributing.

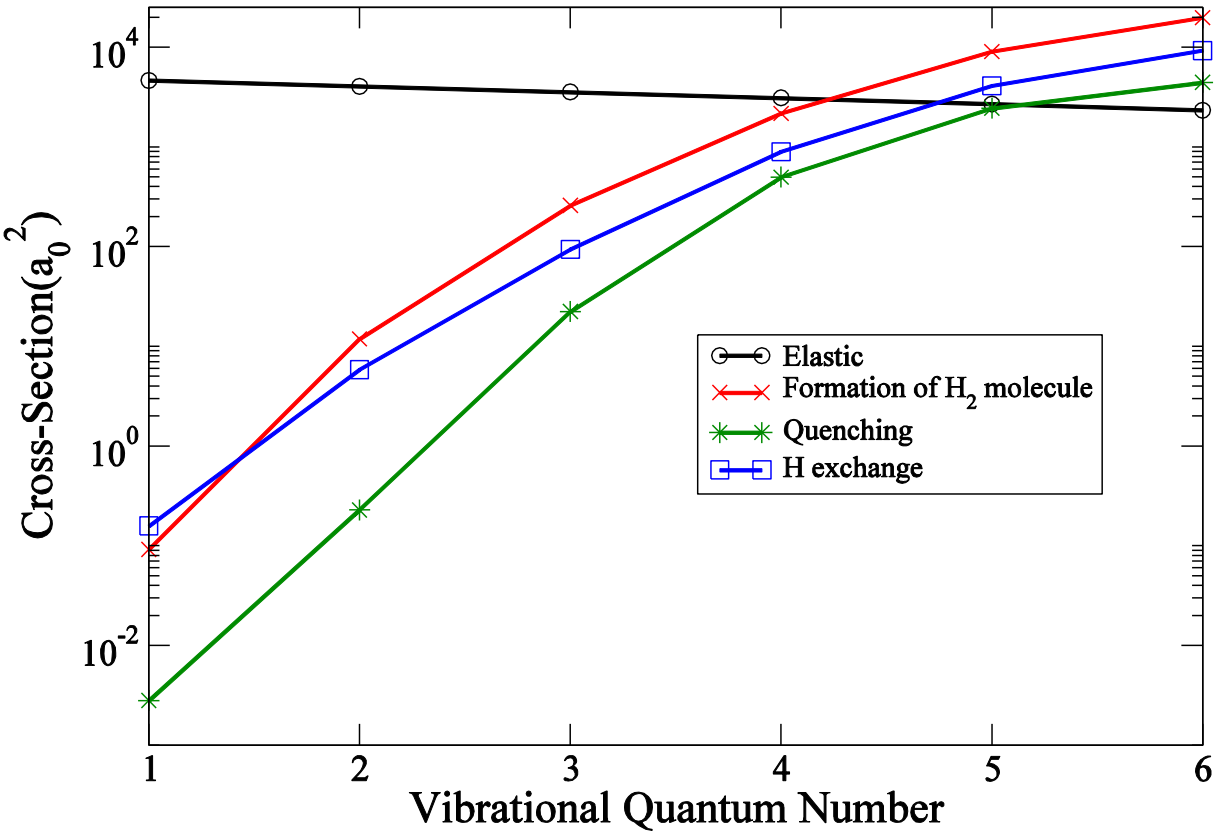

Figure 4: Effect of vibrational quantum number on the Cross-Sections from all the processes including elastic event.

All the inelastic processes, the H exchange, H_2 formation and the quenching are heavily suppressed for the lower vibrational states due to the potential energy barrier. Because of the long range interactions at this ultralow collision energy (10^{-6}K) of the colliding pairs, H exchange is favorable at v = 1. The potential barrier height is significantly lowered from the lower vibrational states to the higher vibrational states, thereby, significantly increasing the inelastic cross section as the reactant molecules can easily cross over the reaction barrier. This effect of barrier suppression on different inelastic processes are seen from v = 1 to v = 6. At $v \geq 2$, H_2 formation process is dominated over all other inelastic processes. It can be observed that for higher vibrational states ($v \geq 8$) the effect due to this repulsive barrier has been disappeared due to the higher initial threshold energies.

5.3 Rate coefficients in the ultracold temperature regime:

The temperature dependent rate coefficients for the reactive, quenching and hydrogen exchange processes are shown in Figure 4(a-c). Rate coefficients are calculated as the average product of the relative velocity of the colliding species and the corresponding cross sections ($K = < v_{rel}.\sigma >$).

The relative velocities are estimated from the Boltzmann distribution of the collision energies corresponding to the temperature T. At ultra-low temperatures (T ≤ 1mK), the relative velocity distribution is very narrow and the rate coefficients behaves according to the Wigner's threshold law. The rate coefficients corresponding to all the inelastic process attain constant value in the limit of zero temperature which is the consequence of inverse velocity ($1/k$) dependence of the corresponding cross-sections. The rate coefficient for the hydrogen exchange process is dominated at v = 1 over other inelastic processes (quenching and the formation of H_2 processes, according to Figure 4).

As the initial vibrational quantum level increases, barrier height of the reaction potential diminishes and the corresponding reaction rate would be faster. It can be seen from Figure 4(a-c) that the magnitude of rate coefficients is constant in the low temperature region which is in contrast to the usual Arrhenius behavior of the temperature dependence of the rate coefficients. At higher temperatures (T > 150K), the rate coefficients exponentially increase with temperature gradually behaving according to usual Arrhenius behavior.

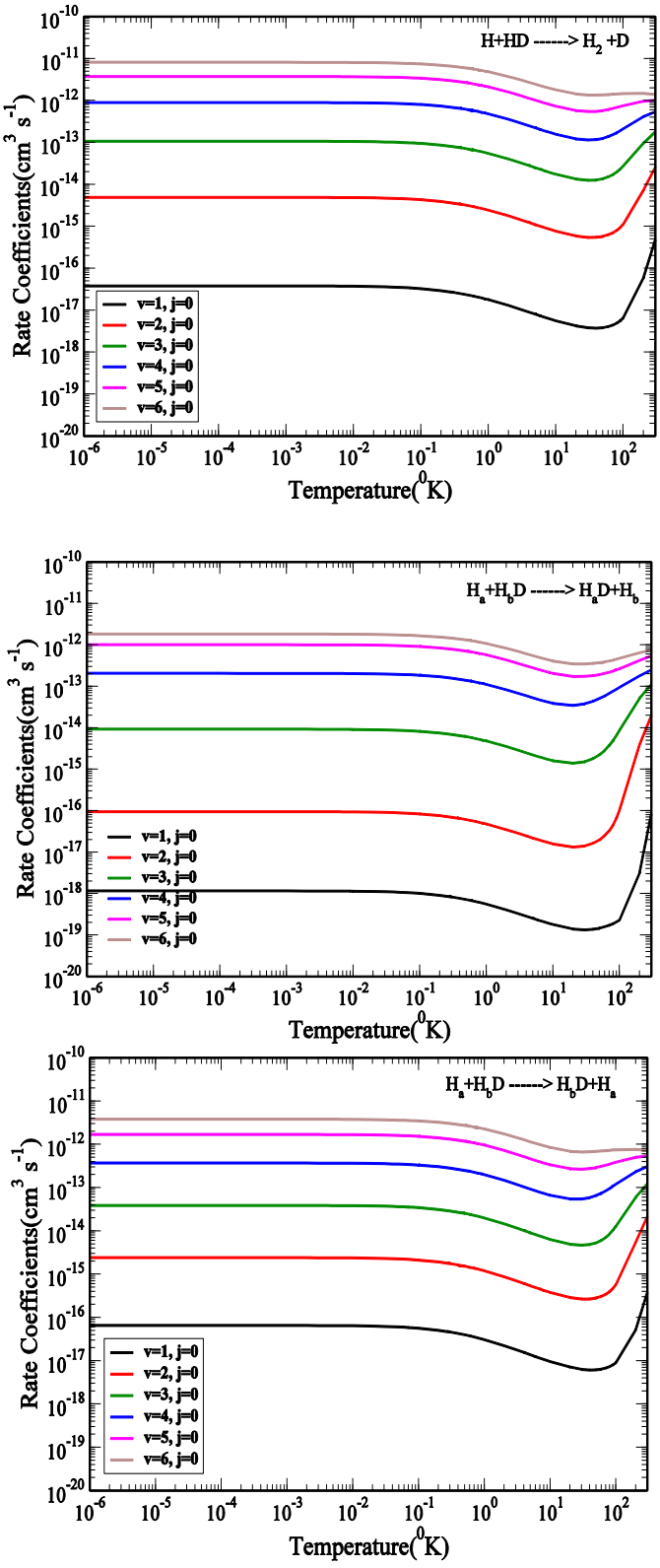

Figure 5: Temperature dependent rate coefficients of the reactive and non-reactive scattering of H+HD (v, j) reactions. Rate coefficients for all the process have been plotted as a function of temperature (similar to Figure 2).

5.4 Threshold resonances:

As it can be seen from Figure 6**,** Sharp resonance structures were observed in the elastic and all inelastic scattering cross sections of H + HD (*v*, *j*) reaction in the collision energy range of 120K-140K. These resonances appear due to the matching of the collision energy of the initial state with threshold of the next higher rotational levels of HD (*v*, *j* = 1, 2,….). From Figure 6, it is evident that the resonance peak shifts by ~5K towards lower collision energies with the increase in each initial vibrational quantum level. This manifests the anharmonic nature of the potential and the reduced gap between the rotational levels at higher vibrational levels.

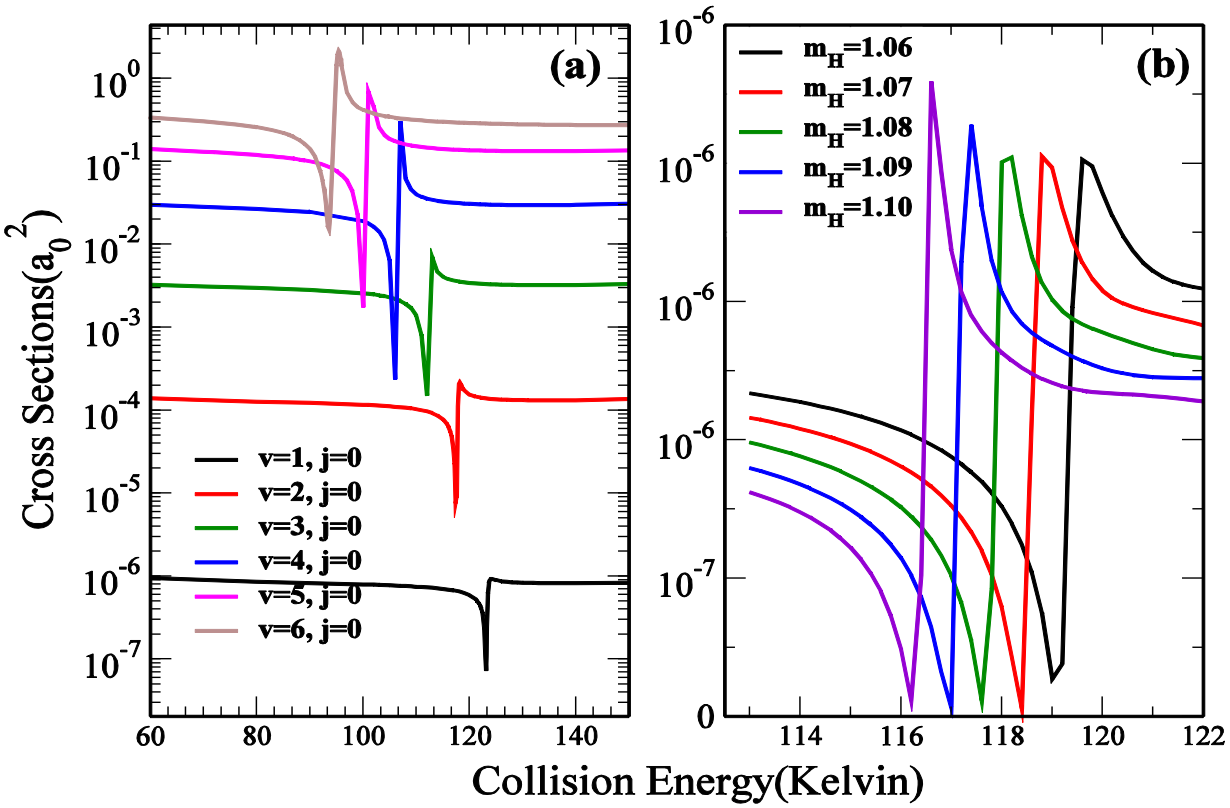

Figure 6: a) Represents the position of threshold resonance corresponds to each vibrational quantum number. b) Shows the conformation of threshold resonance with the change of mass of Hydrogen.

The origin of these resonances due to the presence of a quasi-bound state in the van der Waals well in the reactant arrangement. To verify this, we have performed a thought experiment by gradually modifying the energy of the quasi-bound state (if any) by changing the reduced mass of the colliding pairs [25]. We have varied the mass of hydrogens from m_H = 1.06 to m_H = 1.10 *a.u*) for this purpose. As the reduced mass of the system is increased, the energy difference between the rovibrational energy levels will be reduced which leads to the

shifts in the threshold energy. As observed in Figure 6(b), with increase in the mass of the hydrogen, the position of the peak towards lower kinetic energy, but there is no change in the intensity of the oscillation. This experiment clearly ruled out the possibility of any quasi-bound or virtual state very close to the reaction threshold and confirms the origin of these resonances purely from the crossover of the collision energy with the threshold of the higher rotational levels.

5.5 Connecting ultracold to thermal regime: Contribution of higher partial waves

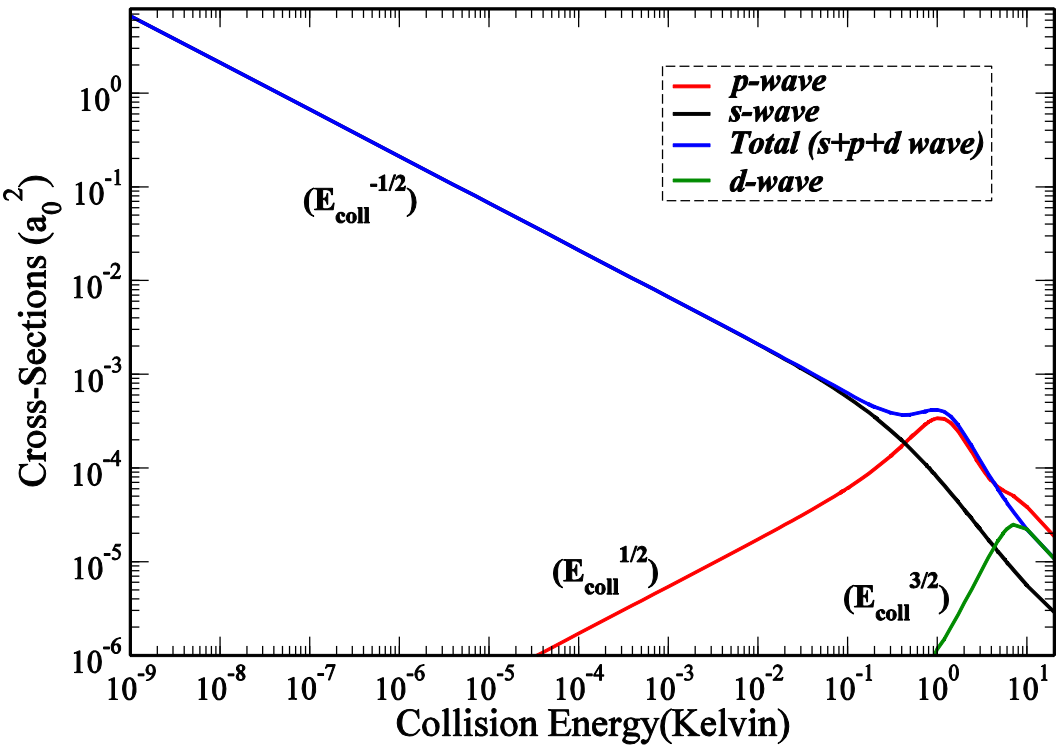

Figure7: Contribution from the individual partial waves (s, p, d waves) in the cold and ultra-cold regime.

In the cold and ultracold energies, we distinguish two different regimes of collision energy dependent reaction cross-sections. At $E_{coll} \leq$ 1mK, Wigner's threshold law obeyed followed by a gradual transition into the barrier dominated regime at higher collision energies. It can be clearly understood from Figure 7, that below ~1μK (10^{-9} eV), the reaction cross sections governed by purely *s-wave* (ℓ = 0) collisions but from 1 K onwards, higher partial waves started contributing.

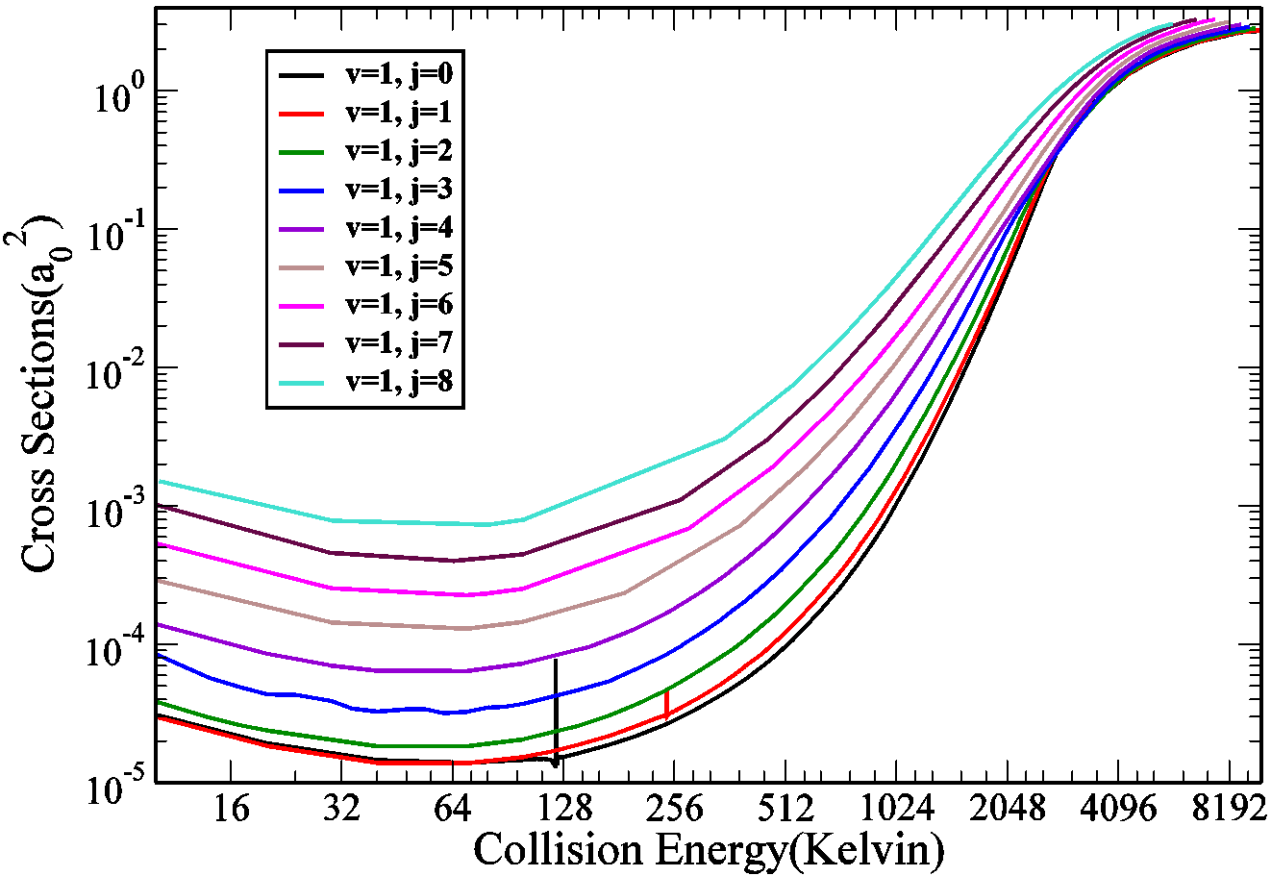

Figure 8: The initial state selected cross-sections: contribution of higher partial waves. Cross-sections as function of collision energy plotted for H + HD → H_2 + D (formation of H_2) reaction.

For calculating the cross-sections for the contribution of higher partial waves, we have taken the initial state selected channels of reacting molecules (HD) and all the product channels were summed up. Contribution of all the higher partial waves (upto $J \sim 45$) taken into account to estimate the individual reaction cross sections. Starting from $v = 1$, $j = 0$ to $v = 1$, $j = 8$, the variation of cross-section with the collision energies increases exponentially and reaches unity at high collision energies. There are two sharp peaks have been observed for $v = 1$, $j = 0$ and $v = 1$, $j = 1$. They are the signatures of threshold resonances as described in Figure 5. Since we have taken up to $J \sim 45$, the position of the peak is shifted by ~5K and for $j = 1$, it appeared at 256 K. These resonances are due the matching of collision energy with the threshold energy of $v = 1$, $j = 1$ and $v = 1$, $j = 2$.

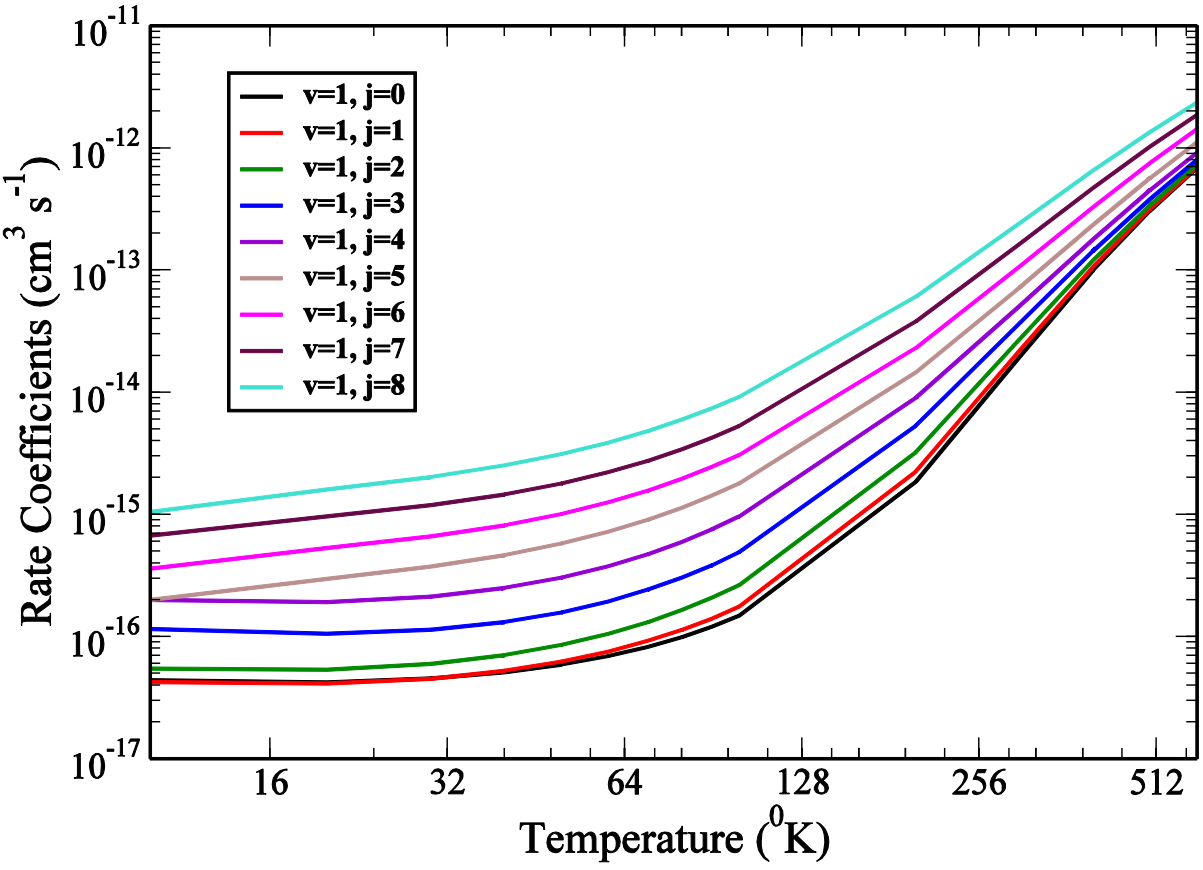

Figure 9: Rate coefficients ($cm^3\ s^{-1}$) are calculated as a function of temperature (^0K) for different rotational states.

The rate coefficients were calculated (Figure 8) for the reactive process (H_2 formation) considering different rotational levels of HD in a normal way as described in the ultra cold part of this chapter. From the Figure 7, it is clear that the *p-wave* starts contributing from 1mK and *d-wave* started contributing from 1K. So if we go beyond 1K, it is required to consider all the possible higher partial waves. Close observation at different collision energies tells that up to 500K, it is needed to consider 10-15 partial waves. For these calculations, the numerical parameters are the hyperradius $\rho_{max} = 50\ a.u,\ \Delta\rho = 0.01\ a.u, E_{max} = 3.00eV\ and\ j_{max} = 15$.

To calculate the rate coefficients particularly at 500K, we need to have the cross sections ranging from 1K to 10^4 K which has been conformed from the Boltzmann distribution (relative velocity distribution) of the reacting species. And also we did not average the contribution of all individual rotational levels as there are no experimental results available for overall rate coefficients of this reaction in the ultracold temperature limit.

In the high temperature regime (~ 500K), the converged results were obtained for J = 35 and since average value of $\sigma_{reactive} \cdot v_{rel}$ have been taken into account, all the sharp peaks were disappeared.

5.6 Conclusions

We have presented the dynamics of H + HD (v, j) reaction from the ultracold to the thermal temperature limit. Unlike H_2, HD molecule has some permanent dipole moment and because of its higher reduced mass, the ro-vibrational levels are closely spaced which makes it a better interstellar coolant. For the H + HD reaction, elastic, quenching, exchange and the formation of H_2 processes have been treated separately. The effect of higher rovibrational initial states on the dynamics is also analyzed and it has been found that the quenching process is more dominant over H exchange and the formation of H_2 in the ultracold regime.

5.7 References

[1] E. Ripamonti, The role of HD cooling in primordial star formation, Monthly Notices of the Royal Astronomical Society 376 (2007) 709-718.

[2] L. Pieri, G. Bertone, E. Branchini, Dark matter annihilation in substructures revised, Monthly Notices of the Royal Astronomical Society 384 (2008) 1627-1637.

[3] S.C.O. Glover, T. Abel, Uncertainties in H_2 and HD chemistry and cooling and their role in early structure formation, Monthly Notices of the Royal Astronomical Society 388 (2008) 1627-1651.

[4] R.V. Krems, Cold controlled chemistry, Physical Chemistry Chemical Physics 10 (2008) 4079-4092.

[5] T. Takayanagi, N. Masaki, K. Nakamura, M. Okamoto, S. Sato, G.C. Schatz, The rate constants for the H + H_2 reaction and its isotopic analogs at low temperatures: Wigner threshold law behavior, The Journal of Chemical Physics 86 (1987) 6133-6139.

[6] T. Takayanagi, K. Nakamura, S. Sato, Improved calculations of rate constants for the H + H_2 reaction and its isotopic analogs at low temperatures, The Journal of Chemical Physics 90 (1989) 1641-1643.

[7] T. Takayanagi, S. Sato, The bending-corrected-rotating-linear-model calculations of the rate constants for the H + H_2 reaction and its isotopic variants at low temperatures: The effect of van der Waals well, The Journal of Chemical Physics 92 (1990) 2862-2868.

[8] S. Hochman-Kowal, A. Persky, Quasiclassical trajectory study of the effect of rotation on reactivity for the reactions D + H_2, H + HD and H + D_2 on the LSTH and DMBE potential energy surfaces, Chemical physics 222 (1997) 29-41.

[9] B. Liu, Ab initio potential energy surface for linear H_3, The Journal of Chemical Physics 58 (1973) 1925-1937.

[10] D.G. Truhlar, C.J. Horowitz, Functional representation of Liu and Siegbahn's accurate abinitio potential energy calculations for H + H_2, The Journal of Chemical Physics 68 (1978) 2466-2476.

[11] D.G. Truhlar, C.J. Horowitz, Erratum: Functional representation of Liu and Siegbahn's accurate abinitio potential energy calculations for H + H_2, The Journal of Chemical Physics 71 (1979) 1514-1514.

[12] A. Varandas, A. Pais, A realistic double many-body expansion (DMBE) potential energy surface for ground-state O_3 from a multiproperty fit to ab initio calculations, and to experimental spectroscopic, inelastic scattering, and kinetic isotope thermal rate data, Molecular Physics 65 (1988) 843-860.

[13] A. Varandas, H. Yu, Dimensionality effects on transition state resonances for H + DH and D + HD reactive collisions, Journal of Molecular Structure: THEOCHEM 493 (1999) 81-88.

[14] J. Hazra, B.K. Kendrick, N. Balakrishnan, Geometric phase effects in ultracold hydrogen exchange reaction, Journal of Physics B: Atomic, Molecular and Optical Physics 49 (2016) 194004.

[15] J.F.E. Croft, J. Hazra, N. Balakrishnan, B.K. Kendrick, Symmetry and the geometric phase in ultracold hydrogen-exchange reactions, The Journal of Chemical Physics 147 (2017) 074302.

[16] B. Jayachander Rao, R. Padmanaban, S. Mahapatra, Nonadiabatic quantum wave packet dynamics of H + H_2 (HD) reactions, Chemical Physics 333 (2007) 135-147.

[17] T. Rajagopala Rao, B. Jayachander Rao, S. Mahapatra, Quantum nonadiabatic dynamics of hydrogen exchange reactions, Chemical Physics 365 (2009) 129-137.

[18] S.D. Chao, S.A. Harich, D.X. Dai, C.C. Wang, X. Yang, R.T. Skodje, A fully state- and angle-resolved study of the H + HD → D + H_2 reaction: Comparison of a molecular beam experiment to ab initio quantum reaction dynamics, The Journal of Chemical Physics 117 (2002) 8341-8361.

[19] S.A. Harich, D. Dai, X. Yang, S.D. Chao, R.T. Skodje, State-to-state dynamics of H + HD → H_2 + D at 0.5 eV: A combined theoretical and experimental study, The Journal of Chemical Physics 116 (2002) 4769-4772.

[20] S.A. Harich, D. Dai, C.C. Wang, X. Yang, S.D. Chao, R.T. Skodje, Forward scattering due to slow-down of the intermediate in the H + HD → D + H_2 reaction, Nature 419 (2002) 281.

[21] J. Jankunas, M. Sneha, R.N. Zare, F. Bouakline, S.C. Althorpe, Hunt for geometric phase effects in H + HD → HD(v', j') + H, The Journal of Chemical Physics 139 (2013) 144316.

[22] A.I. Boothroyd, W.J. Keogh, P.G. Martin, M.R. Peterson, A refined H_3 potential energy surface, The Journal of Chemical Physics 104 (1996) 7139-7152.

[23] S.L. Mielke, B.C. Garrett, K.A. Peterson, A hierarchical family of global analytic Born–Oppenheimer potential energy surfaces for the H + H_2 reaction ranging in quality from double-zeta to the complete basis set limit, The Journal of Chemical Physics 116 (2002) 4142-4161.

[24] S.L. Mielke, B.C. Garrett, K.A. Peterson, A hierarchical family of global analytic Born–Oppenheimer potential energy surfaces for the H + H_2 reaction ranging in quality from double-zeta to the complete basis set limit, The Journal of chemical physics 116 (2002) 4142-4161.

[25] I. Simbotin, S. Ghosal, R. Côté, Threshold resonance effects in reactive processes, Physical Review A 89 (2014) 040701.

Appendix

Computational Investigation on the Mechanism of *n*-BuLi Triggered phospha-Brook Rearrangement

(Mecahnistic Study)

A.1 Abstract

The mechanism of *n*-BuLi triggered phospha-Brook rearrangement has been explored using density functional theory (DFT) calculations. The results indicate facile formation of Li-atom stabilized five-member cyclic transition state, leading to excellent catalytic effect of *n*-BuLi in trace amount, even for less reactive carbonyl compounds. The rate coefficients calculated using transition state theory matched well with the experimentally observed time taken for completion of the reactions.

A.2 Introduction

The Phospha-Brook rearrangement, an intramolecular transfer of a phosphoryl group from carbon to oxygen atom, exhibits versatile applications in the C-C bond forming reactions [1-7]. This rearrangement is commonly used to synthesize highly functionalized phenanthrene derivatives [8], β-amino acid derivatives [9] and enantioselective [10] phosphates compounds. Base catalyzed reaction of diethyl phosphite with carbonyl compounds through phospha-Brook rearrangement is a popular way towards synthesis of organophosphate compounds (eq. 1).

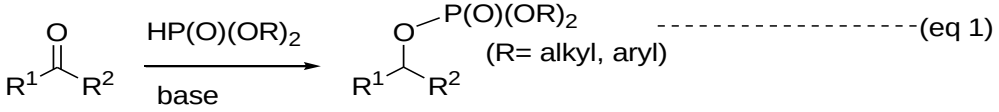

Different bases such as NEt_3, NaH, K_2CO_3 KO^tBu, and DBU were individually examined in literature [7-11]. Our communication [12] on *n*-BuLi triggered phospha-Brook rearrangement to prepare organophosphate compounds (Scheme 1) is promising because of its wide range of application (including both activated and inactivated allylic/naphthylic carbonyl compounds), mild conditions (room temperature), requirement of catalytic amount of base (~0.1 equiv) and

excellent yield of the product. Higher reactivity of the electron-deficient carbonyl compounds suggests a possible formation of a carbanion like intermediate for this reaction.

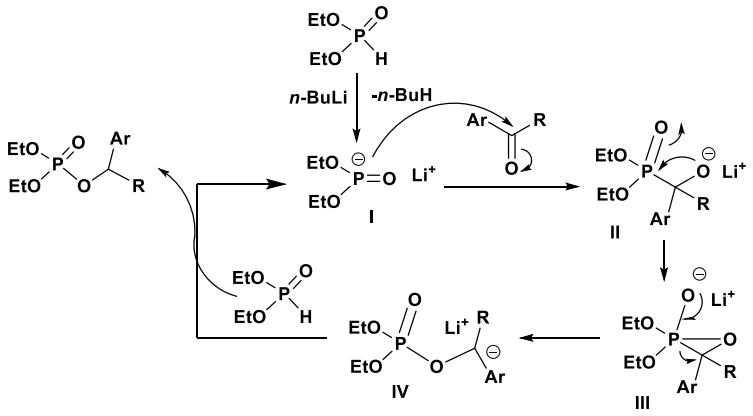

Scheme 1: Proposed mechanism of n-BuLi triggered phospha-Brook rearrangement as in Ref.[12].

Based on earlier literature reports, it was proposed that this reaction is triggered by *n*-BuLi to form an activated Li-diethyl phosphite, which consequently reacts with a carbonyl compound to form the active intermediate **II** (Scheme 1). The reactive species **II** (Scheme 1) spontaneously undergoes phospha-Brook rearrangement through the formation of a three-member cyclic transition state **III** (Scheme 1), resulting in formation of carbanion intermediate carbanion **A**. This step was considered to be the rate determining step for the whole process [12]. However, in contrast to the other literature reports, favourable reaction of less reactive acetophenone in presence of trace amount of *n*-BuLi appeared quite surprising to our understanding. This exceptionally good catalytic efficiency of *n*-BuLi motivated us to investigate the role of Li^+ in phospha-Brook rearrangement.

The transition states having fleeting existence (zero life time) are often difficult to identify experimentally. However, they can be characterized theoretically by analysing the saddle points on multidimensional potential energy surface of the reaction. Although, there are a few theoretical investigations [13, 14] on Brook rearrangement, such studies on phospha-Brook rearrangement are mostly inadequate. Herein, we present a comprehensive investigation on the mechanistic pathway of n-BuLi-triggered phosphate formation from diethyl phosphite and carbonyl compounds using density functional theory (DFT).

A.3 Computational Details

All calculations have been performed using Gaussian 09 software suite of programs [15]. In order to have a good starting point, we have optimized the structures of all the reactants, products, intermediates and the transtion states using B3LYP/6-31G (d, p) level of theory without any symmetry constrains. We have reconfirmed the structures using other density functionals and higher basis sets with diffuse functions *e.g.* 6-31+G (d, p).A comprehensive table of the calculated activation energies and other thermodynamic parameters using M06/6-31+G (d, p) and B3LYP/6-31+G (d, p) level of theory has been included in the following table.

System	**Activation Energy(E_a) (Kcal/mol)**		**Free Energy change($\Delta G^{\#}$) (Kcal/mol)**		**Rate Coefficients(s^{-1})**		Reaction Time
	B3LYP	**M06**	**B3LYP**	**M06**	**B3LYP**	**M06**	
4-Methyl benzaldehyde	33.93	30.65	47.30	45.24	1.34×10^{-22}	4.24×10^{-21}	~ 4 h
Benzaldehyde	32.76	29.02	46.04	42.28	1.10×10^{-21}	6.33×10^{-19}	~ 4 h
4-Chloro benzaldehyde	24.90	15.86	18.46	30.34	1.80×10^{-1}	3.53×10^{-10}	~ 15-20min
4-Methyl acetophenone	23.79	18.41	37.28	32.39	2.90×10^{-15}	7.00×10^{-11}	~ 4 h
Acetophenone	22.43	16.9	35.39	30.75	6.98×10^{-14}	1.78×10^{-10}	~ 4 h
4-Chloro acetophenone	14.97	2.79	29.60	18.00	1.23×10^{-9}	3.96×10^{-1}	~ 15-20min

Table 1: Comparison of thermal rate coefficients using B3LYP and M06 different functionals.

The optimized structures are confirmed as minimum energy conformations from the real (positive) frequencies and the transition states are identified with a single imaginary frequency vibrational mode along the reaction coordinate. Mathematically, for a transition state, the second derivate of the potential energy should be positive for all nuclear coordinates except the reaction coordinate which represents a maximum along that particular direction. This fact is manifested as an imaginary (negative) frequency along the reaction coordinate.

n-BuLi is generally unstable and explosive in nature in its pure form. Hence, a trace amount (~1%) of *n*-Hexane has been used to dissolve the *n*-BuLi during the experiment. For this reason, we have considered *n*-Hexane as a primary solvent (dielectric constant, ε=1.8819) in our theoretical calculations. We have used the integral equation formalism of the polarizable continuum model (IEF-PCM) [16] which is the default Self Consistent Reaction Field (SCRF) method in G09 software.

A.4 Results and discussion

Based on current DFT calculations, we have proposed that the *n*-BuLi catalyzed reaction of diethyl phosphite with carbonyl compounds proceeds through a two-step process (Scheme 2). The first step, a reaction between the activated Li-diethyl phosphite with carbonyl compound, takes place *via* two possible transition states (**TS1a** or **TS1b**) resulting the intermediate carbanion **A** (see Scheme 2). Although Li^+ ions tend to form complexes with higher coordination numbers, all our theoretical attempts to optimize a possible transition state with higher coordination number of Li were unsuccessful. We have tried with multiple ketones as ligating centre but failed to optimize those large structures. Most likely, such complex formation is completely redundant in the presence of trace amount of non-polar solvent (*e.g.* *n*-hexane in the present study, with no coordinating atom), thus, we have restricted our discussion considering Li having maximum coordination number of two (II) in this report.

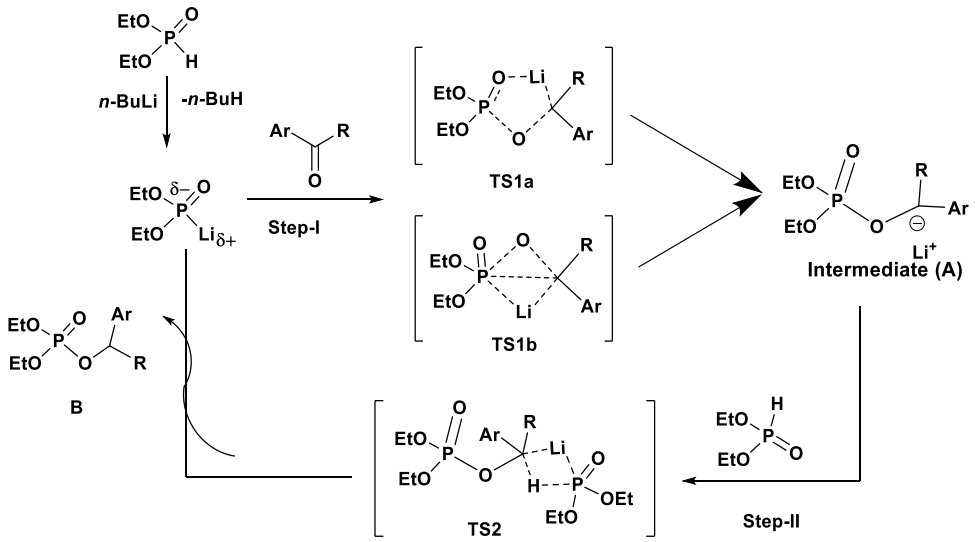

Scheme 2. The plausible mechanistic pathway of the n-BuLi catalyzed reaction of Acetophenone (R=-CH_3) and diethyl phosphite.

The geometry optimized structures of **TS1a** and **TS1b** for the reaction of acetophenone and diethylphosphite are shown in Figure 1a and Figure 1b, respectively. In the second step, the carbanion **A** undergoes proton exchange with another diethyl phosphite molecule to form organo-phosphate **B** (see Scheme 2), leading to regeneration of Li-diethyl phosphite, which again participates in the reaction cycle. A four-membered cyclic transition state (**TS2**) with C-Li-P-H linkage has been identified for this proton transfer step. Geometrically optimized structure of **TS2** for the reaction of acetophenone and diethylphosphite is shown in Figure 1c.

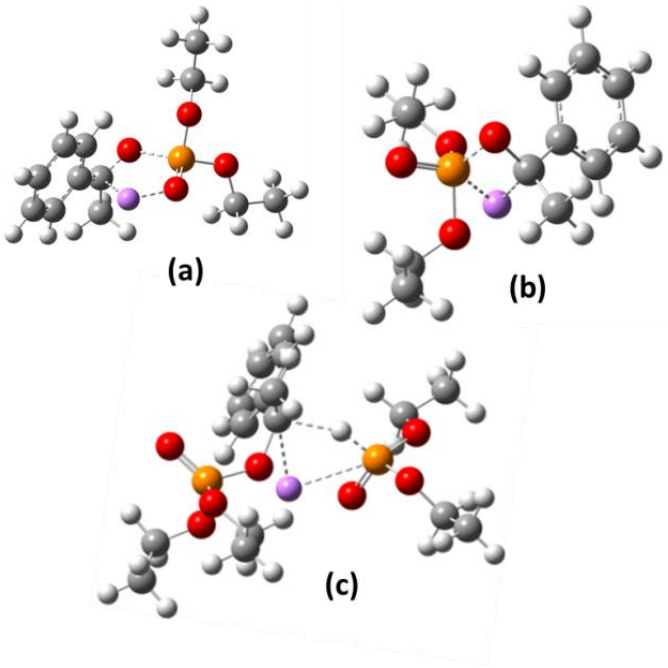

Figure 1: Geometry optimized structures of the transition states (a) **TS1a**, (b) **TS1b** and (c) **TS2** for the reaction of acetophenone and diethyl phosphite in the presence of n-BuLi as mentioned in Scheme 2. (Color: C-grey, O-red, P-orange, Li-pink and H-white)

In search for an appropriate justification for the formation of transition states **TS1a** and **TS1b**, a detailed scrutiny of the geometrically optimized structure has been carried out.

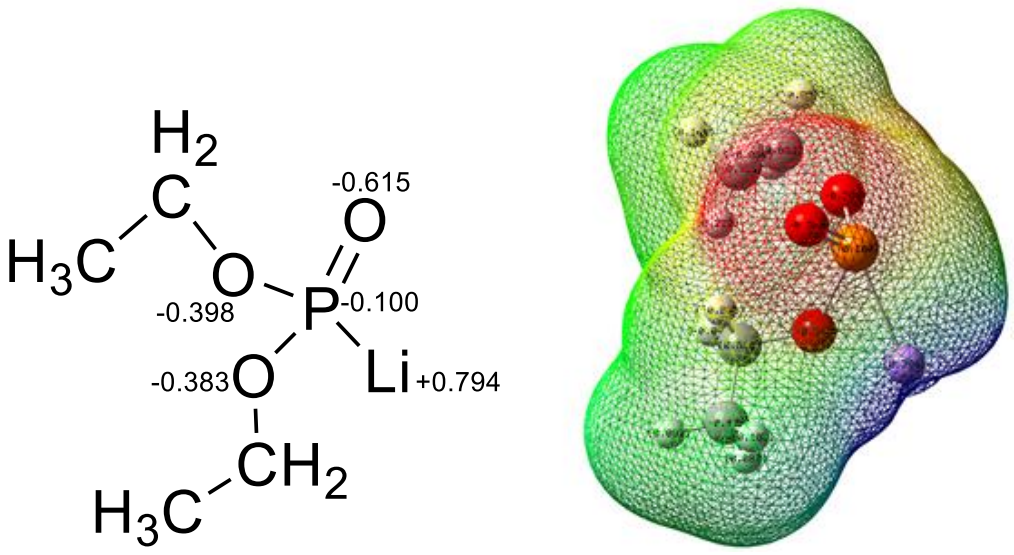

Figure 2: Electrostatic potential charges & surface (ESP charges). (Calculated using the method implemented in Gaussian 09[1] using 6-31G (d, p) basis set. For the illustration purpose, the charges on Hydrogen and the carbon have been omitted. The Mullikan charge on P indicates the nucleophilic nature of P center (-0.1).)

The complete ionization of Li atom from Li-diethyl phosphite should lead to the formation of **TS1a** with a puckered five-member ring structure having P—O—C—Li—O linkage, where no direct interaction between carbonyl C and P is observed. The imaginary frequency of vibration for **TS1a** indicates the formation of the P—O—C linkage. Consequently, the strained structure of **TS1a** spontaneously rearranges to form a firm P—O—C bond with the Li^+ ion stabilizing the negative charge on the carbon atom.

On analysing the electrostatic potential (ESP) of Li-diethyl phosphite, it was evident that the electron density on the phosphorus is delocalized on the surrounding oxygen atoms (Figure 2) referring the P···Li bond might have some partial covalent character. Thus, the addition of an aldehyde or ketone to the Li-diethyl phosphite moiety can favour the formation of two new bonds between P···O and Li···C leading to the four-membered transition state (**TS1b**). In the optimized structure of **TS1b**, the Li atom acts as a bridge between the C and P atom. Therefore, the carbonyl C atom is unable to approach much closer to the P atom, resulting in a very week nonbonding interaction between the carbonyl C and P atoms. The imaginary frequency vibrational mode in **TS1b** depicts the transfer of Li atom from P towards C, as P and C moves away from each other. The existence of such transition state structures **TS1a** and **TS1b** are confirmed for both electron–deficient and electron-rich aldehydes and ketones.

It is noteworthy that, considering the polarity of simple carbonyl compounds used in this reaction, the first step of the phospha-Brook rearrangement seems the addition of the anion of phosphite to the carbonyl carbon, which was proposed earlier [12].

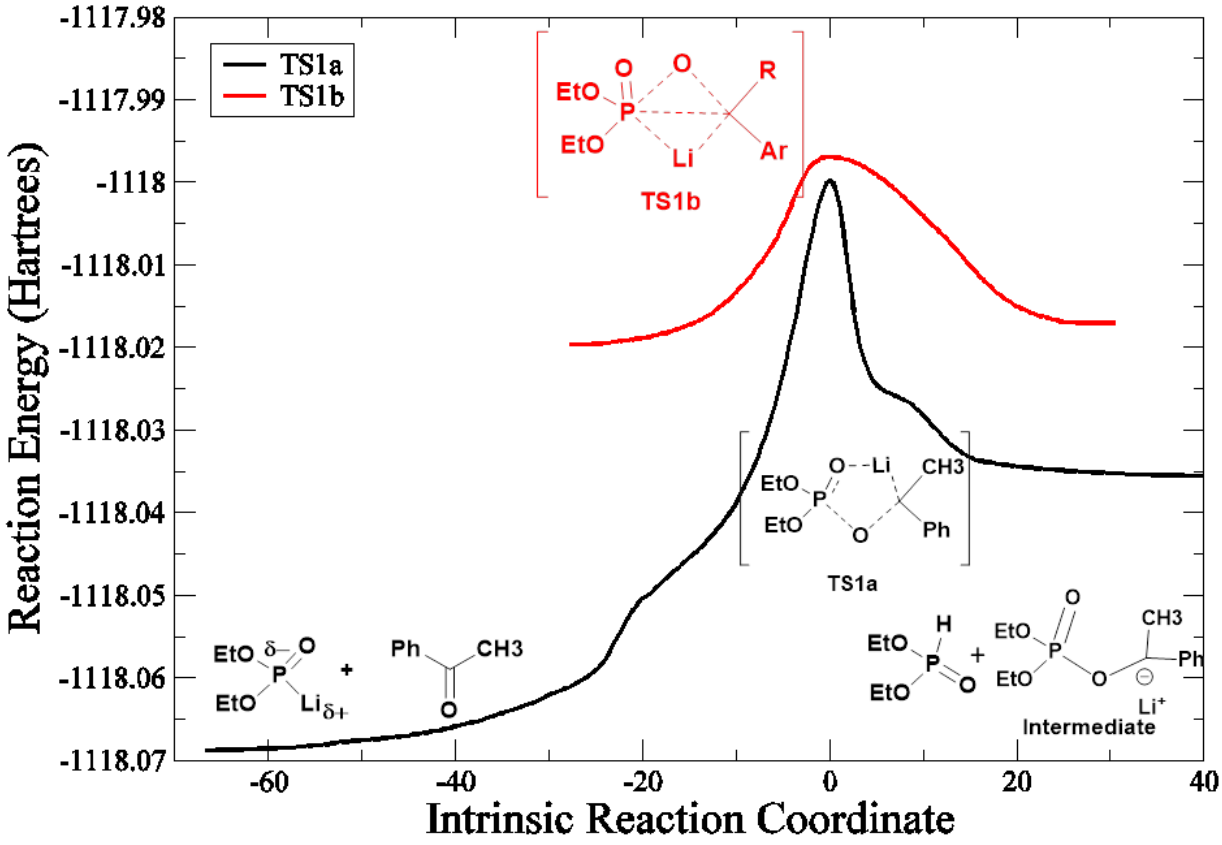

Figure 3: Intrinsic reaction coordinate (IRC) for the reaction of Li-diethyl phosphate with Acetophenone.

But further calculations on intrinsic reaction coordinate (IRC) scan to identify the minimum energy pathway connected to the transition states, we found only **TS1a** leads to the formation of carbanion intermediate **A.** The rearrangement of both transition state **III** (Scheme 1) and **TS1b** (Scheme 2) do not lead to the formation of carbanion intermediate **A**, which could be experimentally isolated for the reaction of carbonyl compounds containing electron withdrawing substituents such as, fluoroarene or trifluroarene, which provides significant stability to the intermediate **A** (Figure 3). Therefore, we have considered the formation of **TS1a** as the rate determining step for this reaction.

The energy profile for the complete reaction was derived from the thermodynamic parameters obtained from the DFT calcaulations. The relative changes in the free energies between the reactants, transition states, intermediates, and products formed during the course of the reaction have been determined and presented in the energy profile diagram in Figure 5. Considering the formation of **TS1a** as the rate determining step, we have calculated the rate

coefficient, which is expected to correlate with the overall kinetics of the reaction. From transition state theory,[17] the rate coefficients (*k*) can be calculated as,

$$\boldsymbol{k} = \frac{\boldsymbol{K_B\, T}}{\boldsymbol{hc^o}} \boldsymbol{e}^{\frac{-\Delta \boldsymbol{G}^{\#}}{\boldsymbol{RT}}} \qquad \text{(Eq. 2)}$$

Where, $\Delta \boldsymbol{G}^{\#}$ is the change in the free energy from reactants to the rate determining transition state $\boldsymbol{c^0}$ is initial concentration, and *T* is temperature considering $\boldsymbol{c^0} = \boldsymbol{1}$ and *T*=298.15 K, rate coefficients are calculated for substituted aldehydes and ketones and listed in Table 2..

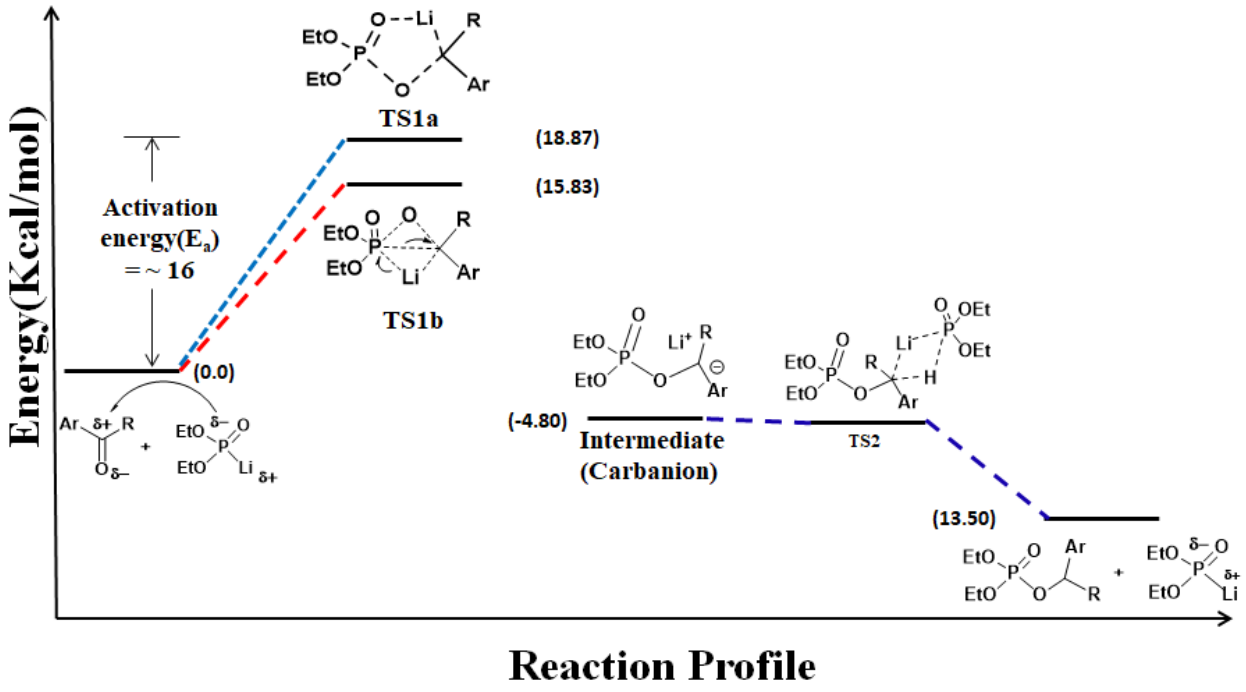

Figure 1: The energy profile diagram for the reaction of acetophenone and diethyl phosphite in the presence of n-BuLi using B3LYP/6-31G(d,p) level of method.

Usually, the presence of electron withdrawing or releasing substituents adjacent to the carbonyl group has crucial control on the electrophilicity and polarizability of the carbonyl group resulting in faster/slower rate of the reaction, which is exponentially related to the $\Delta \boldsymbol{G}^{\#}$ of these reactions. For phospha-Brook rearrangement, the carbonyl compounds containing electron withdrawing (*p*-chloro) group reasulted in faster kinetics compared to those having electron releasing (*p*-methyl) substituents. A good corelation was observed between the calculated rate coefficients and the actual time taken for the completion of the reaction for both the aldehyde and ketone reactants (see Table 2)

Entry	Substrate	Activation Energy (E_a)	Free Energy ($\Delta G^{\#}$)	Rate coefficients (s^{-1})	Reaction Time (from Ref. 16)
1	4-Methyl Benzaldehyde	27.91	40.51	1.24×10^{-19}	~ 4h
2	Benzaldehyde	27.1	39.65	5.33×10^{-19}	~ 4 h
3	4-Chloro Benzaldehyde	14.15	27.17	7.45×10^{-8}	~ 15-20min
4	4-Methyl Acetophenone	16.9	30.52	2.62×10^{-12}	~ 4 h
5	Acetophenone	15.84	29.24	2.27×10^{-11}	~ 4 h
6	4-Chloro Acetophenone	11.08	25.14	2.31×10^{-8}	~ 15-20min

Table 2: Calculated Activation energies, Free energies and the rate coefficients of reaction between Li-diethyl phosthate and substituted aldehydes and ketones with the same level of method. Activation energy and Free energies were given in Kcal/mol.

A.5 Conclusions

We have analyzed the catalytic efficiency of *n*-BuLi in the formation of organophosphates using diethylphosphite and carbonyl compounds applying DFT calculations. The computational results suggested two possible transition states, out of which, Li^+ ion stabilized five-member cyclic transition state (**TS1a**) is found to be the rate determining step.The reaction rate coeffiecients has been calculated for the reaction involving diversely substituted (electron withdrawing and electron releasing) carbonyl compounds. A good corelation has been observed between the theoretical rate coefficients and the actual time taken for completion of the reactions. We hope that the insight gained in this study will be helpful for further experimental studies in this area.

6. A.6 References

[1] M. McLaughlin, Suzuki-Miyaura Cross-Coupling of Benzylic Phosphates with Arylboronic Acids, Org. Lett. 7 (2005) 4875-4878.

[2] C.C. Kofink, P. Knochel, Synthesis of functionalized diarylmethanes via a copper-catalyzed cross-coupling of arylmagnesium reagents with benzylic phosphates, Org. Lett. 8 (2006) 4121-4124.

[3] S.-H. Kim, R.D. Rieke, Benzylic Manganese Halides, Sulfonates, and Phosphates: Preparation, Coupling Reactions, and Applications in Organic Synthesis, J. Org. Chem. 65 (2000) 2322-2330.

[4] A. Kondoh, M. Terada, Bronsted Base Catalyzed [2,3]-Wittig/Phospha-Brook Tandem Rearrangement Sequence, Org. Lett. 15 (2013) 4568-4571.

[5] A. Sokolsky, A.B. Smith, Validation of Diethoxyphosphonate as an Effective Agent for Charge Transfer in Anion Relay Chemistry (ARC), Org. Lett. 14 (2012) 4470-4473.

[6] G. Pallikonda, M. Chakravartya, Benzylic Phosphates in Friedel-Crafts Reactions with Activated and Unactivated Arenes: Access to Polyarylated Alkanes, J. Org. Chem. 81 (2016) 2135-2142.

[7] A. Kondoh, M. Terada, Bronsted base-catalyzed [small alpha]-oxygenation of carbonyl compounds utilizing the [1,2]-phospha-Brook rearrangement, Organic Chemistry Frontiers 2 (2015) 801-805.

[8] A. Kondoh, T. Aoki, M. Terada, Synthesis of phenanthrene derivatives by intramolecular cyclization utilizing the [1,2]-phospha-Brook rearrangement catalyzed by a Bronsted base, Chem. - Eur. J. 21 (2015) 12577-12580.

[9] A. Kondoh, M. Terada, Bronsted base-catalyzed three-component coupling reaction of α-ketoesters, imines, and diethyl phosphite utilizing [1,2]-phospha-Brook rearrangement, Org. Biomol. Chem. 14 (2016) 4704-4711.

[10] M. Hayashi, S. Nakamura, Catalytic Enantioselective Protonation of α-Oxygenated Ester Enolates Prepared through Phospha-Brook Rearrangement, Angewandte Chemie International Edition 50 (2011) 2249-2252.

[11] S. Protti, M. Fagnoni, Phosphate esters as "tunable" reagents in organic synthesis, Chem. Commun. (Cambridge, U. K.) (2008) 3611-3621.

[12] G. Pallikonda, R. Santosh, S. Ghosal, M. Chakravarty, BuLi-triggered phospha-Brook rearrangement: efficient synthesis of organophosphates from ketones and aldehydes, Tetrahedron Letters 56 (2015) 3796-3798.

[13] Y. Orimoto, K. Naka, K. Takeda, Y. Aoki, Ab initio MO study on [3 + 2] annulation using [small beta]-phenylthio-acryloylsilanes with alkyl methyl ketone enolates and its through-space/bond interaction analysis, Organic & Biomolecular Chemistry 3 (2005) 2244-2249.

[14] A.M. Rouf, B.O. Jahn, H. Ottosson, Computational Investigation of Brook-Type Silabenzenes and Their Possible Formation through [1, 3]-Si→ O Silyl Shifts, Organometallics 32 (2012) 16-28.

[15] M.J. Frisch, G.W. Trucks, H.B. Schlegel, G.E. Scuseria, M.A. Robb, J.R. Cheeseman, G. Scalmani, V. Barone, B. Mennucci, G.A. Petersson, H. Nakatsuji, M. Caricato, X. Li, H.P. Hratchian, A.F. Izmaylov, J. Bloino, G. Zheng, J.L. Sonnenberg, M. Hada, M. Ehara, K. Toyota, R. Fukuda, J. Hasegawa, M. Ishida, T. Nakajima, Y. Honda, O. Kitao, H. Nakai, T. Vreven, J.A. Montgomery, J.E. Peralta, F. Ogliaro, M. Bearpark, J.J. Heyd, E. Brothers, K.N. Kudin, V.N. Staroverov, R. Kobayashi, J. Normand, K. Raghavachari, A. Rendell, J.C. Burant, S.S. Iyengar, J. Tomasi, M. Cossi, N. Rega, J.M.

Millam, M. Klene, J.E. Knox, J.B. Cross, V. Bakken, C. Adamo, J. Jaramillo, R. Gomperts, R.E. Stratmann, O. Yazyev, A.J. Austin, R. Cammi, C. Pomelli, J.W. Ochterski, R.L. Martin, K. Morokuma, V.G. Zakrzewski, G.A. Voth, P. Salvador, J.J. Dannenberg, S. Dapprich, A.D. Daniels, Farkas, J.B. Foresman, J.V. Ortiz, J. Cioslowski, D.J. Fox, Gaussian 09, Revision C.01, Wallingford CT, 2009.

[16] D.M. Chipman, Reaction field treatment of charge penetration, J. Chem. Phys. 112 (2000) 5558-5565.

[17] A.D. McQuarrie, J.D. Simon, Physical Chemistry: a molecular approach, University Science Books1997.

Future Perspective

In the view of astrophysical conditions of the early universe, the initial phase of the universe dominated by more number of ions compared to the neutral molecules. In comparison to the neutral systems, ions can interact from longer distance due to the difference in the long-range polarization forces. Since we have mainly focused on the atom-diatom neutral reactions in this thesis, the following ion-molecule reactions can be studied in future.

$$H^+ + H_2 \rightarrow H_2^+ + H$$

$$D + H_2^+ \rightarrow HD + H^+$$

$$H^+ + HD \rightarrow H_2^+ + D$$

$$H + HD^+ \rightarrow H_2^+ + D$$

$$H^+ + D_2 \rightarrow HD + H^+ \textit{ etc.}$$

Hydrogen is most abundant species in the universe. Thus, reactions involving its ions have lot of astrophysical importance. We also need to consider the reaction between the corresponding negative ions. Because of the strong attractive forces between reacting species, optimization of the numerical parameters (as discussed in chapter 3) would be more critical.

One has to calculate reaction probabilities, cross sections, and rate coefficients *etc.*, using accurate quantum mechanical treatment. For all these reactions, the main objectives would be to study the effect of rovibrational excitation of target diatomic molecular ions, existence of short-lived resonances and most importantly, estimation of accurate rate coefficients ranging from ultracold to thermal temperature regime.

Reactions involving the ions may not have reaction barrier. For this reason, the reactive scattering code *ABC* has to be tested and substantial changes might be required to treat barrierless reactions. Further, obtained results have to be compared with the available experimental data. Once the dynamical observables are calculated, one can combine them with their abundance to calculate the cooling functions as a further step to model the evolution process.

List of publications

1) **S. Ranga, S. Ghosal**, Accurate quantum mechanical rate coefficients for D + H_2 (v, j) reaction: from ultracold to thermal temperature limit, *Computational & Theoretical Chemistry*, 69-73(1102), 2017.

2) **Ranga Santosh**., Subhas Ghosal, Quantum Mechanical Rate Coefficient of Formation of HD Molecule at Ultracold Temperatures: It's Importance in Interstellar Cooling. *Journal of Atomic, Molecular, Condensate and Nano Physics, 2*(3), 179-186, 2015.

3) **Ranga Santosh**, Subhas Ghosal, Dynamics of H + HD (v=1, j=0) → H_2 +D reaction from ultracold to thermal temperature regime. (Manuscript under communication)

4) **Ranga Santosh**, Subhas Ghosal, A mechanistic investigation of role of Li in a phospha-Brook rearrangement. (under review)

5) **Ranga Santosh**, Subhas Ghosal, Study of the convergence of numerical parameters on D + H_2 reaction and its isotopic substitutions (under communication)

6) Gangaram Pallikonda, **Ranga Santosh**, Subhas Ghosal, Manab Chakravarty, BuLi-triggered phospha-Brook rearrangement: efficient synthesis of organophosphates from ketones and aldehydes, *Tetrahedron Letters*, 56, 10, 3796-3798, 2015.

7) Yadagiri Thigulla, **Santosh Ranga**, Subhas Ghosal, Jayanthi Subbalakshmi and Anupam Battacharya, One-Pot Two Step Nazarov-Schmidt Rearrangement for the Synthesis of Fused δ-Lactam Systems, *Chemistry Select*, 2, 9744-9750, 2017.

List of conferences attended

1) A national conference Convergence of Chemistry and Materials (CCM-2017) held at BITS-Pilani Hyderabad Campus.

2) The Eighth edition of Asia-Pacific *Conference* of Theoretical and Computational Chemistry (*APCTCC* 8), from 15th to 17th of December, *2017 and presented a poster entitled* **"Dynamics of H + HD (v=1, j=0) → H2 +D reaction from ultracold to thermal temperature regime".**

3) A national conference 16th Theoretical Chemistry Symposium (TCS), University of Hyderabad, 14-15 the December 2016 and presented a poster entitled **"Theoretical investigation of H+HD and D+H_2 reactions from ultracold to thermal temperature regime"**

4) Attended and presented a poster entitled with "**Electronic, redox and spectroscopic properties of various M-BChls: A computational study"** in a national conference on "new frontiers in chemistry from fundamentals to applications" in BITS-Pilani, Goa Campus, during 18-19 December, 2015.

5) Attended and presented a poster entitled with **"Slow Reactive collisions of H+HD: A Quantum Mechanical approach"** in International Conference on Nascent Developments in Chemical Sciences: Opportunities for Academia-Industry Collaboration in BITS-Pilani, Pilani Campus, Rajasthan, during October 16-18, 2015.

6) Attended and presented a poster entitled with **"Mechanistic Investigation of phospha-Brook Rearrangement": A DFT Study** in 10th Mid-year CRSI Symposium, in NIT-Trichy. During July, 23-25, 2015.

Biography of Mr. Ranga Santosh

Mr.Ranga Santosh has completed his bachelor's degree from Kakatiya University, Warangal. He has received master's degree from Osmania University, Hyderabad. He has joined in Nizam College as a teacher in the department of chemistry for undergraduate, M.Sc students and has 3 years of teaching experience. He has joined for Ph.D in theoretical chemistry at BITS-Pilani Hyderabad Campus, under the supervision of Dr. Subhas Ghosal in the year 2013. His research interest includes understanding the behavior of atoms/molecules in the ultracold regime, studying the reaction mechanism and also molecular modeling *etc.*

Biography of Dr. Subhas Ghosal

Dr Ghosal has worked on understanding the mechanism and dynamics of elementary chemical reactions using first-principle quantum mechanical techniques for more than ten years. His research towards the formation of polar molecules at ultracold temperature (below 1miliKelvin) using photoassociation laser pulses and understanding of resonance enhancement of reaction rate coefficients in extreme ultra-low temperature conditions have got significant attention in recent years.

From BITS Pilani Hyderabad Campus, Dr. Ghosal has recently completed a major research project in the field of ultracold collisions. The main focus of this project was to develop suitable computer programs to study the electronic structure and the quantum reaction dynamics of elementary reactions of astrophysical interest. He is also a dedicated teacher innovating new teaching methodologies for undergraduate and postgraduate courses in BITS Pilani Hyderabad Campus for past six years.

List of Contributions:

- Study of chemical reaction dynamics to understand the electronic and spectroscopic properties of elementary reactions.
- Understanding the formation of ultracold molecules using photoassociation laser pulses.
- Effect of threshold resonances to reactive processes at ultracold temperature limit.
- Understanding reaction mechanism of organo-phosphorous compounds using density functional theory